EFFECT OF PARTICLE SIZE ON RESISTANCE TO CHLORIDE FOR HYDRODECHLORINATION OF TRICHLOROETHYLENE IN WATER

A THESIS SUBMITTED TO
THE GRADUATE SCHOOL OF NATURAL AND APPLIED SCIENCES
OF
MIDDLE EAST TECHNICAL UNIVERSITY

BY

SELİN KARAHAN

IN PARTIAL FULFILLMENT OF THE REQUIREMENTS
FOR
THE DEGREE OF MASTER OF SCIENCE
IN
CHEMICAL ENGINEERING

AUGUST 2022

Approval of the thesis:

EFFECT OF PARTICLE SIZE ON RESISTANCE TO CHLORIDE FOR HYDRODECHLORINATION OF TRICHLOROETHYLENE IN WATER

submitted by **SELİN KARAHAN** in partial fulfillment of the requirements for the degree of **Master of Science** i**n Chemical Engineering, Middle East Technical University** by,

Prof. Dr. Halil Kalıpçılar
Dean, Graduate School of **Natural and Applied Sciences** _____

Prof. Dr. Pınar Çalık
Head of the Department, **Chemical Engineering** _____

Assist. Prof. Dr. Gökhan Çelik
Supervisor, **Chemical Engineering, METU** _____

Examining Committee Members:

Assoc. Prof. Dr. Bahar İpek Torun
Chemical Engineering, METU _____

Assist. Prof. Dr. Gökhan Çelik
Chemical Engineering, METU _____

Assist. Prof. Dr. Harun Koku
Chemical Engineering, METU _____

Assist. Prof. Dr. Zafer Say
Material Science and Nanotechnology Eng., TOBB ETÜ _____

Assist. Prof. Dr. Zeynep Tutumlu
Material Science and Nanotechnology Eng., TOBB ETÜ _____

Date: 23.08.2022

I hereby declare that all information in this document has been obtained and presented in accordance with academic rules and ethical conduct. I also declare that, as required by these rules and conduct, I have fully cited and referenced all material and results that are not original to this work.

Name Last name: Selin Karahan

Signature:

ABSTRACT

EFFECT OF PARTICLE SIZE ON RESISTANCE TO CHLORIDE FOR HYDRODECHLORINATION OF TRICHLOROETHYLENE IN WATER

Karahan, Selin
Master of Science, Chemical Engineering
Supervisor: Dr. Gökhan Çelik

August 2022, 114 pages

Contamination of groundwater by chlorinated compounds is an important environmental hazard to humanity because worldwide drinking water demand is generally supplied by groundwater. Chlorinated pollutants, especially trichlorethylene (TCE), are released to the environment due to its frequent use in industrial applications. This highly toxic chemical poses a serious threat to human health and the environment. In this regard, cleaning of groundwater from TCE is of great importance.

Catalytic hydrodechlorination (HDC) is a desirable approach for remediation of water contaminated with chlorinated compounds. It is an elimination-based catalytic remediation technique where toxic chlorinated compounds in water are transformed to chloride-free hydrocarbons with hydrogen over a catalyst. Studies conducted so far have concluded that platinum (Pt) and palladium (Pd)-based catalysts show high catalytic activity for HDC of chlorinated compounds. However, during HDC, the overall performance of the catalyst is mainly affected by (i) adsorption of the reactants and the reaction medium on catalyst surface, (ii) simultaneous reactions including dechlorination, hydrogenation, and hydrodechlorination, and (iii) inhibition due to the unavoidable reaction product HCl. Of particular note is the

inability of HCl to desorb from the active sites that leads to complete loss of the catalytic activity and irreversible catalyst deactivation by the chloride poisoning. This effect, however, could be alleviated by catalysis engineering.

In this study, the objective is to undertake an approach to investigate the effect of particle size of Pt nanoparticles (Pt NPs) on resistance to chloride poisoning for HDC of TCE in water. Although there are existing studies which examined particle size effect on catalytic activity, studies on HCl inhibition are scarce. By fine-tuning the particle size distribution of catalysts, the inhibition problem of HDC catalysts can be circumvented.

The study includes synthesizing Pt nanoparticles with three different particle sizes (3.0, 5.8 and 60.9 nm) by colloidal synthesis method, performing activity experiments in a semi-batch reactor, carrying out characterization studies and performing kinetic measurements. The results demonstrate that Pt NPs were synthesized successfully as evidenced by transmission electron microscopy. For 20 ppm initial TCE concentration, almost 100% conversion was achieved in all experiments. As expected, the fastest reaction kinetic was observed at the smallest particle size. Rate constants were found as 4.2 h^{-1}, 1.3 h^{-1} and 0.4 h^{-1} for Particle size 1 (small), 2 (medium) and 3 (large), respectively. The initial turnover frequency (TOF) was calculated based on initial rate and molar concentration of Pt in the batch reactor. TOF data (0.077 (Particle 1), 0.023 (Particle 2) and 0.007 (Particle 3) mol TCE/(mol Pt.s)) decreased with increasing particle size. The highest resistance to chloride poisoning were also observed at the smallest particle size. The heat and mass transfer limitations were also investigated. Kinetic experiments performed within the scope of this study revealed insight into structure sensitivity of reactions involved in HDC of TCE in water at atmospheric conditions.

Keywords: Hydrodechlorination, Trichloroethylene, Platinum, Water, Catalysis

ÖZ

SUDAKİ TRİKLOROETİLEN HİDRODEKLORİNASYONU İÇİN PARÇACIK BOYUTUNUN KLORÜR DİRENCİNE ETKİSİ

Karahan, Selin
Yüksek Lisans, Kimya Mühendisliği
Tez Yöneticisi: Dr. Gökhan Çelik

Ağustos 2022, 114 sayfa

Yeraltı suyunun klorlu bileşiklerle kirlenmesi, insanlık için önemli bir çevresel tehlikedir, çünkü dünya çapında içme suyu talebi genellikle yeraltı sularından karşılanmaktadır. Klorlu kirleticiler, özellikle trikloretilen (TCE), endüstriyel uygulamalarda sık kullanılması nedeniyle çevreye salınmaktadır. Bu son derece toksik kimyasal, insan sağlığı ve çevre için ciddi bir tehdit oluşturmaktadır. Bu bakımdan yeraltı sularının TCE'den temizlenmesi büyük önem taşımaktadır.

Katalitik hidrodeklorinasyon (HDC), klorlu bileşiklerle kirlenmiş suyun iyileştirilmesi için arzu edilen bir yaklaşımdır ve sudaki toksik klorlu bileşiklerin bir katalizör üzerinde hidrojen ile klorür içermeyen hidrokarbonlara dönüştürüldüğü eliminasyon bazlı katalitik iyileştirme tekniğidir. Şimdiye kadar yapılan çalışmalar, platin (Pt) ve paladyum (Pd) bazlı katalizörlerin, klorlu bileşiklerin HDC'si için yüksek katalitik aktivite gösterdiği sonucuna varmıştır. Bununla birlikte, HDC sırasında, katalizörün genel performansı esas olarak (i) reaktanların ve tepkime ortamının katalizör yüzeyinde adsorpsiyonundan, (ii) klorsuzlaştırma, hidrojenasyon ve hidrodeklorinasyon dahil olmak üzere eşzamanlı tepkimelerden ve (iii) kaçınılmaz tepkime ürünü HCl nedeniyle oluşan inhibisyondan etkilenir. HCl'nin

aktif bölgelerden desorbe edilememesi, katalitik aktivitenin tamamen kaybına ve klorür zehirlenmesi ile geri dönüşümsüz katalizör deaktivasyonuna yol açar. Ancak bu etki, kataliz mühendisliği ile hafifletilebilir.

Bu çalışmadaki amaç, sudaki TCE'nin HDC'si için Pt nanopartiküllerin (NP) partikül boyutunun klorür zehirlenmesine karşı direnç üzerindeki etkisini araştırmaktır. Partikül boyutunun katalitik aktivite üzerindeki etkisini inceleyen mevcut çalışmalar olmasına rağmen, HCl inhibisyonu ile ilgili çalışmalar azdır. Katalizörlerin parçacık boyutu dağılımına ince ayar yaparak, HDC katalizörlerinin inhibisyon sorunu aşılabilir.

Çalışma, kolloidal sentez yöntemi ile üç farklı partikül boyutuna sahip Pt nanopartiküllerin (3.0, 5.8 ve 60.9 nm) sentezlenmesini, yarı kesikli reaktörde aktivite deneylerinin yapılmasını, karakterizasyon çalışmalarının yapılmasını ve kinetik ölçümlerin yapılmasını içermektedir. Sonuçlar, transmisyon elektron mikroskobu ile kanıtlandığı gibi Pt NP'lerin başarılı bir şekilde sentezlendiğini göstermektedir. 20 ppm başlangıç TCE konsantrasyonu için tüm deneylerde neredeyse %100 dönüşüm elde edildi. Beklendiği gibi, en hızlı reaksiyon kinetiği en küçük parçacık boyutunda gözlenmiştir. Partikül büyüklüğü 1 (küçük), 2 (orta) ve 3 (büyük) için reaksyion hız sabitleri sırasıyla 4.2 h^{-1}, 1.3 h^{-1} ve 0.4 h^{-1} olarak bulunmuştur. Başlangıç katalitik döngü frekansı (TOF), kesikli reaktördeki başlangıç hızı ve Pt molar konsantrasyonuna dayalı olarak hesaplanmıştır. TOF verileri (0.077 (Partikül 1), 0.023 (Partikül 2) ve 0.007 (Partikül 3) mol TCE/(mol Pt.s)) partikül boyutunun artmasıyla azalmıştır. Klorür zehirlenmesine karşı en yüksek direnç de, en küçük parçacık boyutunda gözlenmiştir. Isı ve kütle transferi sınırlamaları da araştırılmıştır. Bu çalışma kapsamında gerçekleştirilen kinetik deneyler, atmosferik koşullarda sudaki TCE'nin HDC'sinde yer alan reaksiyonların yapı duyarlılığına dair bir fikir ortaya koymuştur.

Anahtar Kelimeler: Hidrodeklorinasyon, Trikloroetilen, Platin, Su, Kataliz

To my precious family…

ACKNOWLEDGMENTS

To begin with, I would like to present my sincere gratitude to my supervisor, Assist. Prof. Dr. Gökhan Çelik, for his guidance, continuous support and encouragement throughout my thesis study. Thanks to his patience and wisdom, I completed my research and tried to do my best.

I would like to thank Assoc. Prof. Dr. Bahar İpek Torun, Assist. Prof. Dr. Harun Koku, Assist. Prof. Dr. Zafer Say and Assist. Prof. Dr. Zeynep Tutumlu for serving on my jury. Their recommendations and inputs were invaluable.

I would like to thank Chemical Engineering Department and the instructors for their education and limitless information about chemical engineering discipline.

I would like to thank to METU Chemical Engineering Department and METU Central Lab personnel for my characterization results.

I would like to say my special thanks to all the Laboratory of Advanced Catalysis Engineering and Kinetics (LACEK) group members. I warmly thank the postdoctoral researchers of our lab, Dr. Asmae Bouziani and Dr. Hamdiye Ece for their guidance. I also express my special gratitude to my lab mates; Almira Çaldıklıoğlu, Candan Karaeyvaz, Arzum Ceren Aydoğdu, Enes Akyıldız, Iqtidar Ali Khan and Uğur Sökmen, for their help and contribution. I have learned many things from them. There have been times in these last 3 years that I have seen them more than my family and they have become my other family here. We had very good times together, their endless friendship and support taught me many valuable things.

I would like to thank my dear colleagues Merve Sarıyer, Seda Sivri, Çağla Bozcuoğlu, Asena Kızıl and Azad Yılmaz for their friendship and support. They made my last three years unforgettable.

I would also like to say a big thank you to Başak Tekin and Cemre Ünal, who were always there for me in all those METU years with their endless support and love. I feel very lucky to have them in my life.

I am fortunate to have my dearest friends who always supported me. I would like to thank to Ezgi Kürtül and İlayda Kavruk for their love, support and encouragement for all these years, thank you sisters. It has been fifteen years, and I know that we will always be there for us no matter what happens. They are my past and my future.

Last, but not least, I would like to thank my precious parents, Nermin and Gökhan Karahan, my lovely sister Pelin Karahan and my family elders for their endless love, trust and unconditional support throughout my entire life. They were always there whenever I needed them. I cannot express my gratitude for them with words. I am dedicating this thesis to them. They have always stood behind me and supported all my decisions. They are the greatest chance of mine, thank you.

TABLE OF CONTENTS

LIST OF TABLES

TABLES

LIST OF FIGURES

FIGURES

LIST OF ABBREVIATIONS

ABBREVIATIONS	DEFINITION
CFC	Chlorofluorocarbon
CHC	Chlorinated Hydrocarbon
DCE	1,2-Dichloroethane
EPA	Environmental Protection Agency
HDC	Hydrodechlorination
HRTEM	High Resolution Transmission Electron Microscopy
NP	Nanoparticle
PDMS	Polydimethylsiloxane
PGMs	Platinum Group Metals
TA	Tannic Acid
TCE	Trichloroethylene
TEM	Transmission Electron Microscopy
TGA	Thermogravimetric Analysis
TOF	Turnover Frequency
TON	Turnover Number
TPO-MS	Temperature Programme Oxidation-Mass Spectroscopy
TTCE	Tetrachloroethylene
UV-Vis	Ultraviolet-Visible Spectroscopy
VOC	Volatile Organic Compound
XPS	X-Ray Photoelectron Spectroscopy

LIST OF SYMBOLS

SYMBOLS	DEFINITION	UNIT
a	Deactivation parameter	-
a_{GL}, a_S	Specific areas for gas-liquid interface and catalyst solid in overall batch reactor liquid volume	m^2/g or m^{-1}
$C_{L,i}$, C_{liq}, C_S	Concentrations of TCE in liquid phase at gas liquid interface, in liquid bulk, and at catalyst surface	ppm or M
C_p	Specific heat capacity	kJ/mol/K
$C_{TCE,0}$	Initial TCE Concentration	ppm or M
D_{TCE}	Diffusivity of TCE in water	cm^2/s
H	Henry's Law Constant	mol/L/bar
H_{rxn}	Enthalpy of reaction	kJ/mol
k	Rate constant based on a unit volume of reacting fluid	h^{-1}
k'	Rate constant based on unit mass of solid in fluid-solid system	$L/g_{Pt}/min$
k"	Rate constant based on unit interfacial surface in two fluid systems	$L/m_{surf\ Pt}{}^2/min$
k_d	Rate constant for the deactivation of catalyst	h^{-1}
k_G, k_{GL}, k_{LS}	mass transfer coefficients for gas, gas-liquid, and liquid-solid	m/s
N_A	Moles A formed	mol
P_g, $P_{g,i}$	partial pressures of TCE in gas bulk and gas film at gas-liquid interface	bar or atm
R	mean radius of catalyst particle	nm or m

Re	Reynolds number	-
S	Surface of catalyst	m^2
Sc	Schmidt number	-
Sh	Sherwood number	-
T_{ad}	Adiabatic temperature rise	K
TOF_0	Initial turnover frequency	$mol_{TCE}/mol_{Pt}/s$
V	Volume of fluid	L
W	Weight of catalyst	g
W_S	mass fraction of catalyst with respect to total liquid	g_{Pt}/g_{liq}
X_{TCE}	TCE conversion	-
$X_{TCE, \infty}$	TCE conversion at time is infinity	-

GREEK SYMBOLS	**DEFINITION**	**UNIT**
ρ_{liq}	density of liquid	g/cm^3
ρ_p	density of catalyst particle	g/cm^3

CHAPTER 1

INTRODUCTION

1.1 Groundwater Pollution due to Trichloroethylene

Water is a substance that affects all biological life and human activities. However, very few of the water resources on Earth are usable and drinkable. As shown in Figure 1.1, 97.5% of water resources in the world is salty and therefore not suitable for industrial and agricultural use. 2.5 % of water resources is fresh. However, 69.5% of the fresh-water resources are not suitable because they are found as ice field at the poles [1], [2]. For this reason, groundwater is used all over the world as a fresh water source. That is, water need is generally provided from groundwater resources. Unfortunately, groundwater is quickly affected by pollutants and becomes unsuitable and unsafe for humans. Therefore, groundwater pollution has attracted the attention of public due to its widespread use as drinking water. In this respect, cleaning of groundwater is of great importance.

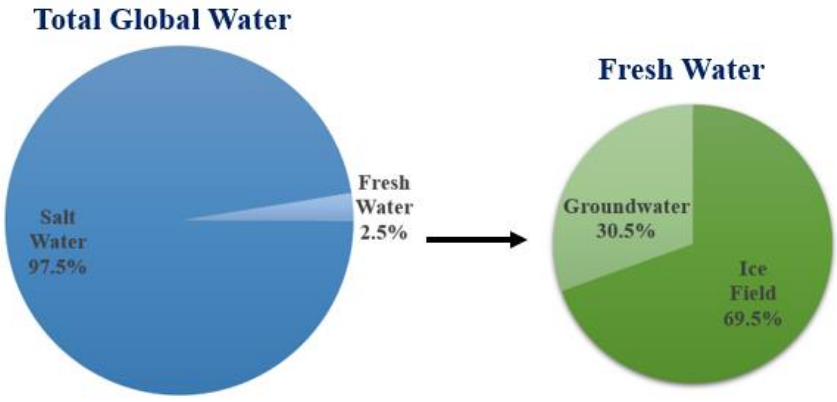

Figure 1.1 Total global water and fresh water, data taken from [1], [2]

Many sources such as storage tanks, septic systems, chemicals, and uncontrolled hazardous wastes cause groundwater pollution. In contaminated groundwater, hazardous volatile organic compounds (VOCs) are commonly observed. The most frequently detected harmful compounds among these VOCs are chlorinated chemicals [3]. Chlorinated organic compounds have been widely used in a variety of industrial applications; however, they have negative effects on the environment and human health. For example, chlorofluorocarbons (CFCs) which are widely used as refrigerants cause ozone depletion. Chlorinated hydrocarbons (CHCs) which are neurotoxins are used as heat transfer fluids and metal degreasers [4].

Among these chlorinated hydrocarbons, trichloroethylene (TCE), also known as trichloroethene, is a chlorinated chemical that is usually found at high concentrations in water [5]. The Environmental Protection Agency (EPA) allows the maximum contaminant level to be 0.005 ppm in groundwater, and maximum contaminant level goal for TCE is zero [6]. The chemical structure of TCE is shown in Figure 1.2.

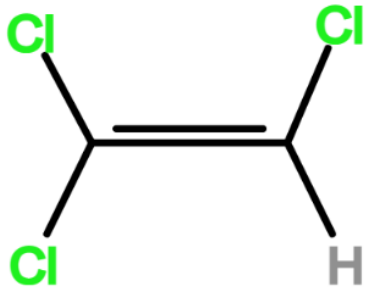

Figure 1.2 Chemical structure of trichloroethylene (TCE)

TCE is a colorless and non-flammable liquid. It is hazardous to both human health and the environment. EPA states that it can cause kidney and liver cancer. It also has an impact on the central nervous system, the male reproductive system, and the immune system [6], [7]. As can be seen in Table 1.1, TCE was listed as 16th the most hazardous chemical according to the Agency for Toxic Substances and Disease Registry's. Furthermore, vinyl chloride, a byproduct of natural environmental degradation of TCE, is ranked as 4th the most hazardous chemical [8], [9].

Table 1.1 Priority list of hazardous substances, data taken from [8]

Rank	Substance	Rank	Substance
1	Arsenic	**16**	**Trichloroethylene**
2	Lead	17	Dieldrin
3	Mercury	18	Chromium, Hexavalent
4	**Vinyl Chloride**	19	Phosphorus, White
5	Polychlorinated Biphenyls	20	Chlordane
6	Benzene	21	DDE, P, P'-
7	Cadmium	22	Hexachlorobutadiene
8	Polycyclic Aromatic Hydrocarbons	23	Coal Tar Creosote
9	Benzo (A) Pyrene	24	Aldrin
10	Benzo (B) Fluoranthene	25	DDD, P, P'-
11	Chloroform	26	Benzidine
12	DDT, P, P'-	27	Aroclor 1248
13	Aroclor 1254	28	Cyanide
14	Aroclor 1260	29	Aroclor 1242
15	Dibenzo (A, H) Anthracene	30	Aroclor

TCE is widely used in industry as a metal degreaser and cleaning agent, and it is released to the environment during its use. The primary sources of contamination include improper disposal of metal degreasing plant process water and industrial charges [10]. Furthermore, because TCE is very volatile compound, handling of TCE is difficult [7], [10]. Therefore, when considering these problems, the treatment of waste TCE should be considered.

1.2 Remediation Methods for Removal of TCE from Groundwater

TCE and other chlorinated chemicals have been traditionally removed from groundwater using some remediation technologies, including air stripping, activated carbon adsorption, biological treatments, chemical treatment by oxidation and

reduction. These technologies can be classified into two types: elimination-based and recovery-based (Figure 1.3). In elimination-based remediation methods, hazardous compounds are eliminated and converted to benign compounds in a single unit without a need for further treatments. In recovery-based remediation methods, contaminants are transferred from groundwater to another media where further treatments are needed [11]–[15].

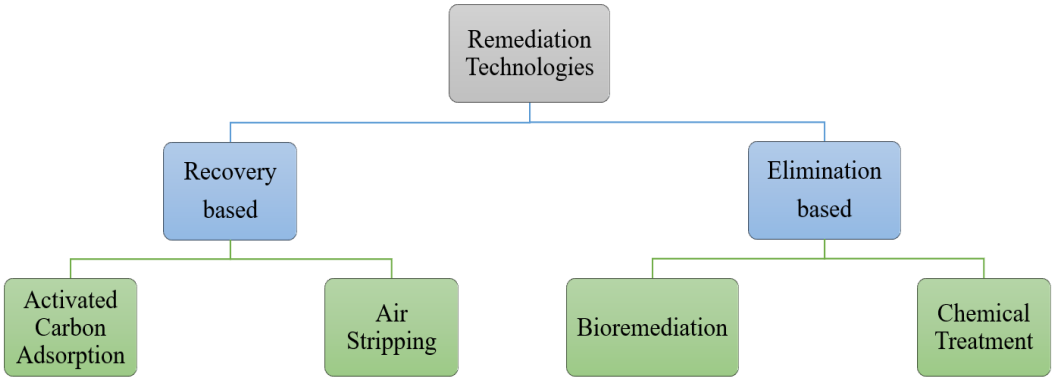

Figure 1.3. Classification of remediation technologies

1.2.1 Elimination-based Remediation Technologies

Elimination-based remediation approaches include biological and chemical treatments (based on oxidation and reduction). During biological groundwater remediation (bioremediation), microorganisms are utilized to remove toxins in groundwater. Microorganism-produced enzymes can decompose chlorinated chemicals and convert them into harmless species. This is very attractive process, however, this process and its efficiency are highly dependent on growth rate of microorganisms [13]. Thus, it is a long and slow process. Furthermore, undesirable chemicals such as chlorine-based compounds may remain after treatment.

Chemical treatment by oxidation & reduction is another elimination-based remediation approach. Combustion of chloride-containing substances results in the formation of chloride-free chemicals. Nonetheless, this combustion procedure needs high temperature because chlorinated chemicals are non-flammable. This makes the

entire process energy demanding. Furthermore, the production of more hazardous byproducts such as Cl_2 has been observed [16], [17].

1.2.2 Recovery-based Remediation Technologies

Air stripping and activated carbon adsorption are two main examples for recovery-based remediation procedures. Air stripping involves flushing chlorinated chemicals in groundwater with a flow of hot air. TCE's strong vaporization propensity makes air stripping easier, but at large concentrations, TCE can produce a dense bottom layer that is more difficult to remove using air stripping [11], [12]. The cost of pumping and heating hot air is a significant component of the entire cost [13]. High tendency of TCE to vaporize makes air stripping easier. However, pumping and heating of hot air constitute major part of the overall cost.

Hazardous substances are adsorbed and subsequently transported to another media by desorption in the adsorption process utilizing activated carbon. Adsorption-based remediation methods are widely established. However, this process is generally followed by a thermal incineration at very high temperatures. Thermal destruction of chlorinated compounds requires temperatures above 1000 ^{o}C because of their stable molecular nature [18]. The disadvantages of this technique include the regeneration of spent adsorbents and the replacement of the adsorbent, and this makes the process economically unfeasible [16].

There are various shortcomings with remediation approaches for removing chlorinated compounds from groundwater. Advantages and disadvantages of these technologies are summarized in Table 1.2. These techniques are generally unfeasible and inefficient due to low remediation kinetics, high media regeneration/replacement costs, and high energy inputs due to high working temperatures. Furthermore, some of the techniques' on-site applicability is restricted, and the formation of additional harmful compounds has been reported [11]–[15], [19].

Table 1.2 Comparison of remediation technologies

Remediation Technology	**Advantages**	**Disadvantages**
Air Stripping	• Commonly used & well studied	• Recovery-based technique • An expensive process • "Pump and treat" method
Activated Carbon Adsorption	• Well-developed and simple operations	• Regeneration of the spent adsorbent is needed • Replacement of the adsorbent media is needed. • Recovery-based technique • "Pump and treat" method
Bioremediation	• Destruction-based remediation technique	• Degradation of TCE is not always complete • Slow kinetics • Reactor cleaning is necessary
Chemical Treatment	• Destruction-based remediation technique	• Formation of more toxic chemicals during incineration • Requires high energy inputs for combustion.

While environmental standards are strict and environmental awareness is critical, there is a definite need for an effective and practical remediation technology to remove chlorinated chemicals from groundwater. The method should be:

i. environmentally friendly (minimum toxin production),
ii. economically feasible (rapid reaction rate at low temperature and pressure),
iii. efficient (complete destruction of reactants with high conversion and selectivity).

The suggested technology is catalytic hydrodechlorination (HDC), which has been used to remove chlorinated chemicals at ambient conditions.

CHAPTER 2

LITERATURE REVIEW

This chapter explains the background information of the present study, and consists of eight parts: hydrodechlorination of trichloroethylene, shortcomings that hydrodechlorination catalysts face, protection strategies, effect of particle size, platinum-based catalysts, catalyst synthesis (impregnation and colloidal Slot-Geuze method) and the focus of the study.

In Section 2.1, definition of hydrodechlorination, practicability of these reactions and hydrodechlorination of trichloroethylene are explained.

In Section 2.2, problems leading to deactivation of the catalysis used in the hydrodechlorination reaction are described.

In Section 2.3, strategies used to prevent deactivation and to improve the deactivation resistance are explained.

In Section 2.4, based on the purpose of this study, particle size effect as a design parameter on resistance to deactivation is described.

In Section 2.5, platinum metal properties, advantages of platinum and synthesis techniques of platinum are explained.

In Section 2.6 and 2.7, selected synthesis methods are described. Incipient wetness impregnation technique for supported platinum on alumina, modified colloidal Slot-Geuze method for unsupported platinum nanoparticles are selected.

In Section 2.8, the focus of this study is explained.

2.1 Hydrodechlorination of Trichloroethylene

Hydrodechlorination (or hydrodehalogenation) is an elimination-based remediation method that catalytically converts chlorinated chemicals to halogen-free (or less halogenated) hydrocarbons and hydrogen chloride. Hazardous chlorinated pollutants are transformed to ecologically benign species such as hydrocarbons and hydrochloric acid. This study was done focusing on HDC of TCE (C_2HCl_3), and its corresponding reaction scheme is shown in Equation 2.1. As it can be seen, ethane (C_2H_6) and hydrogen chloride (HCl) are major products of this reaction [9], [17], [20]. It is an exothermic reaction.

$$C_2HCl_3 + 4H_2 \rightarrow C_2H_6 + 3HCl \qquad \Delta H_{rxn,298\ K} = -309\ kJ/mol \qquad (2.1)$$

HDC of chlorinated compounds utilizing catalysts has received a lot of interest from researchers because it is an effective and promising remedial strategy. There are various benefits to catalytic reduction of chlorinated chemicals with HDC over traditional remediation approaches. Firstly, HDC is an effective method because a variety of chlorinated substances including hydrocarbons and chlorophenols may be successfully hydrodechlorinated over catalysts at mild conditions [20]–[22]. Secondly, it is an environmentally clean method since complete removal of chlorinated compounds is achievable without the formation of hazardous species such as Cl_2. A treatment approach that produces additional harmful species, such as combustion or incineration, defeats the goal of the remediation system. Thirdly, HDC is an economically feasible method because it may be performed at ambient temperature without the requirement for high temperatures (above 150 ^oC). Compared to other remediation technologies, HDC can save a significant amount of energy. Thanks to fast kinetic of HDC reactions, on-site remediation is achievable [17], [23].

For many years, researchers have been studying the catalytic reduction of chlorinated compounds utilizing hydrogen as an electron donor. Research emerged in the early 1990s reported that HDC was very effective and feasible catalytic application compared to existing treatment options [24]–[26]. For example, Kovenklioglu et al. [24] indicated that a palladium-based catalyst was extremely effective in HDC of chlorinated compounds in aqueous phase at ambient temperature and near atmospheric pressure with hydrogen gas. Then, Reinhard and co-workers verified this for the HDC of tetrachloroethylene (TTCE) [17].

In time, many investigations on HDC in the aqueous, organic, and gas phases have been undertaken. Metals such as Pd, Pt, Rh, Ru, Ni, Mo, and V have been evaluated for HDC of chlorinated ethenes on various supports such as alumina, silica, carbon and zeolite [27]–[30]. There are simultaneous reactions including hydrogenation, hydrodechlorination, and dechlorination so selection of metal and support is critical.

Ordonez and Diez's group have done research on the catalytic activity and stability of Pd supported by Al_2O_3 on HDC of chlorinated compounds. In one of their early investigations in 2000, eight different commercial catalysts were investigated for catalytic activity on HDC of tetrachloroethylene and TCE, including noble metals such as Pd, Pt, Rh, and Ru supported on either alumina or activated carbon. The reaction was carried out in gas phase at 50 bar and 300 °C. High conversion rates of greater than 90% were observed with Pt and Pd based catalysts. Generally, successful results were obtained with precious metal-containing catalysts however low catalytic activities were also observed with catalysts containing Ni and Mo [27]. Following that, the same research group conducted a follow-up investigation on Pt, Pd and Rh supported on alumina with a 0.5% metal loading for HDC of TTCE in a continuous fixed bed reactor at 250 °C and 5 bar. As shown in Figure 2.1, the maximum yield was achieved with 0.5% Pd/Al_2O_3 catalysts, while 0.5% Pt/Al_2O_3 and 0.5% Rh/Al_2O_3 catalysts deactivated with time [29], [30]. TGA, TPO-MS, and XPS characterization studies demonstrated that the most likely cause of deactivation is the production of chloride-containing carbonaceous deposits. Carbon formation was linked to HCl generation because of the HDC reaction. Experiments with external

HCl addition revealed that raising the HCl content in the reactor improved deactivation [31]. When compared to other catalysts, Pd-based catalysts deactivate the least.

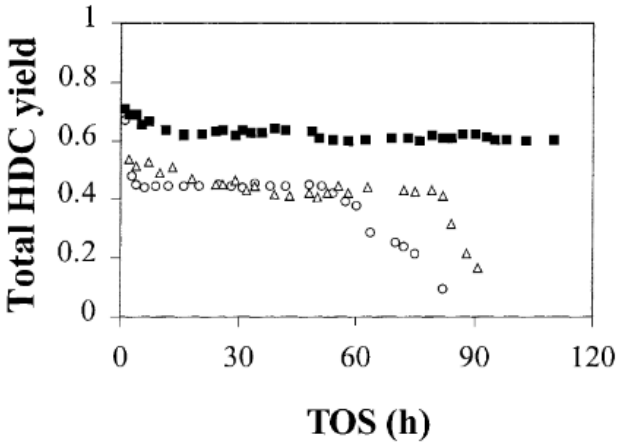

Figure 2.1 Evolution of the total hydrodechlorination yield (moles of ethane formed per mole of TTCE fed to the reactor) with time-on-stream for Pd/Al_2O_3 (black square), Pt/Al_2O_3 (circle), and Rh/Al_2O_3 (triangle) catalysts [30]

The bimetallic catalysis technique has improved catalytic activity and stability. Early attempts to use bimetallic catalysts in HDC of TTCE reveal that vanadium modified Pt/Al_2O_3 enhanced deactivation resistance at 250°C up to 85 hours, despite the development of insignificant quantities of carbonaceous deposits [32]. As another bimetallic example, Nutt and his colleagues developed a palladium on gold nanoparticles for HDC of TCE, and it exhibited the greatest reaction rate in the literature. The bimetallic Pd on Au catalyst outperformed Pd nanoparticles, Pd/Al_2O_3, and Pd/carbon in terms of catalytic activity [9], [33]. Pd-Au catalyst achieved 70 times the catalytic activity of Pd/Al_2O_3 on a per Pd atom basis [33]. According to these reports from the same study group, there is a synergistic interaction between Au and Pd in which Au stabilizes Pd atoms at metallic state, resulting in better catalytic activity than monometallic catalysts with no such stabilizing effects [34], [35].

While it is unknown how HDC occurs on a catalyst surface, a Langmuir - Hinshelwood mechanism may be speculated to involve a sequence of chlorine removal and hydrogen addition stages after TCE and H_2 molecules bond to the surface (Figure 2.2). TCE adsorbs to the metal surface at presumably designated active sites, while H_2 dissociatively adsorbs as surface H atoms. These surface species then react with one another via hydrogenolysis surface reaction steps to create progressively dechlorinated surface species (DCE isomers and vinyl chloride) until surface-bound ethene is formed. After that, ethane is formed by hydrogenating ethene, which desorbs into the aqueous phase [11].

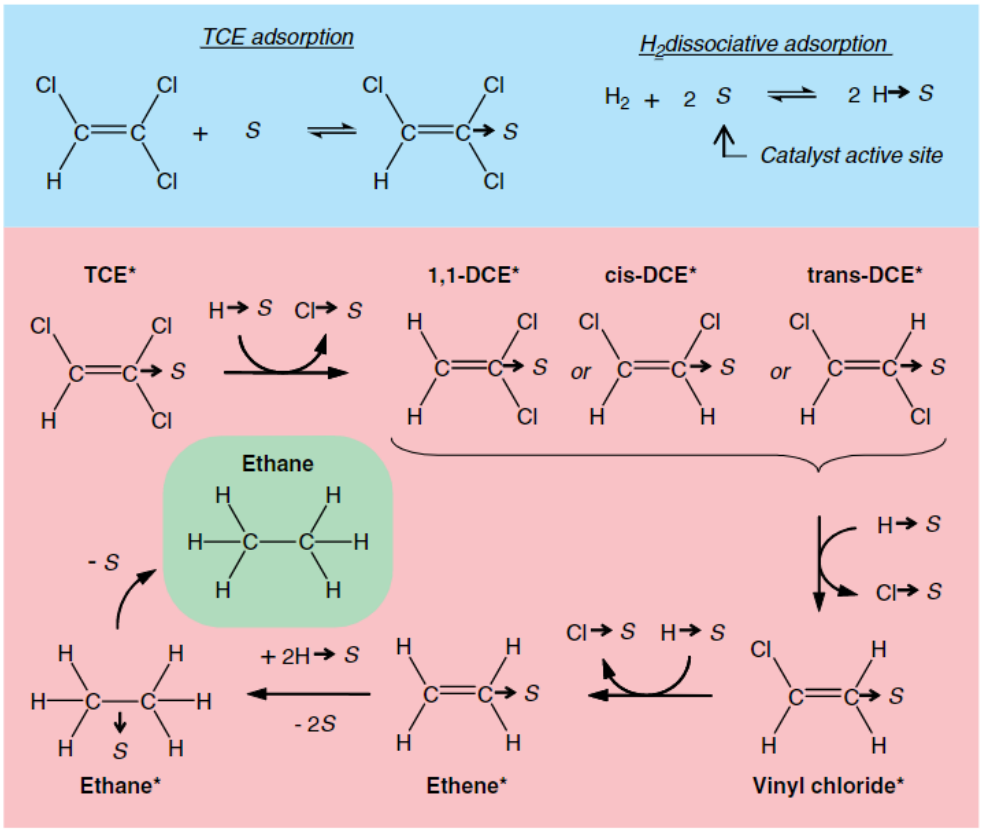

Figure 2.2 Proposed reaction mechanism for TCE HDC. The 'S' represents an active site somewhere on the metal surface [11]

2.2 Shortcomings that Hydrodechlorination Catalysts Face

Although HDC has significant benefits over traditional approaches, catalysts of HDC reaction suffers from several phenomena. When actual groundwater including sulfur, chlorine, carbonate, nitrate and nitrite species is used in these studies, the catalytic activity of catalysts falls dramatically. These groundwater species are either poisoning the active metal or competing for adsorption on the active site, reducing catalytic activity [14]. Aside from groundwater treatment systems, wastewater treatment systems had similar deactivation concerns. Indeed, the poisoning can be more severe due to the presence of several organic and inorganic elements that interact with the water remediation catalyst, complicating the catalytic treatment [36]. The deactivation of the catalyst is an important consideration for HDC processes, and it highly depends on the type of metal, type of support and operating conditions [27]–[29], [37].

Metal sintering, leaching of the active metal, carbon formation on active sites and HCl-induced metal-chlorine interactions were observed to have a negative influence on the catalytic activity of HDC catalysts [30], [31], [38]–[40]. Metal sintering occurred in several of the situations where deactivation was seen, and the particle size of the active metal increased due to agglomeration. However, among the possible deactivation modes above, metal sintering seems to take place less likely due to low operating temperatures. In HDC studies where metal sintering was observed, minimum operating temperatures were around 225-300 ^{o}C [41]–[43].

Leaching of the active metal from supports catalysts is an on-going problem of liquid phase operations [44], [45]. During HDC reactions, the unavoidable reaction product HCl decreases the pH of the reaction solution and acidic sites were formed. Yuan and Keane investigated the HDC of chlorophenols in a semi-batch aqueous-phase slurry reactor. On post-reaction samples, Pd-Cl bonding was found, and approximately 20% of the active catalyst leached from the solid catalyst. They reported up to 40% Pd leaching from supports including carbon and alumina [46], [47]. Metal leaching and metal-chloride interactions are more severe in Pd/Carbon

than in Pd/Al_2O_3. Although Yuan and Keane said that Pd leaching is not substantial throughout the process and cannot be the primary method of deactivation, such large metal leaching percentages are expected to cause major difficulties, particularly on an industrial scale. Leaching in a batch reactor may not be a major problem and may not alter the catalytic performance significantly if the leached metal has a considerable activity towards HDC of TCE. In a flow reactor, however, leached metal is flushed away from the reactor, resulting in constant loss of the active metal. As a result, HCl-induced leaching is one of the most critical issues with liquid phase HDC. Furthermore, chlorides in the concentration range of 0-0.02 M Cl^- had no effect on the catalytic activity of Au-Pd based bimetallic catalysts. The commercial catalyst Pd/Al_2O_3 deactivated in the similar concentration range. The increased chloride tolerance was due to Au-Pd interactions [48].

Under hydrogen rich environment, formation of carbon on the active sites may lower the catalytic performance. Leaching and carbon formation on active sites are related to each other. The increased acidity of the surface aided in the production of carbonaceous compounds on the catalyst. For example, Lopez et al. (2006) studied similar phenomena in TTCE HDC and discovered that HCl-induced carbon accumulation was the primary cause of deactivation [41]. The same research group investigated HDC of chlorinated ethylenes in time on stream tests. A direct relationship was discovered between carbon deposition and the ease of deactivation. The interaction of Cl^- species with the surface under HDC conditions may encourage coke production, according to the authors [30]. Characterization studies also verified the formation of carbon [41]. In another study, Pt/Al_2O_3 and vanadium modified Pt/Al_2O_3 bimetallic catalyst were tested for HDC of TTCE [32]. Although the bimetallic catalyst showed improved resistance to deactivation, formation of carbonaceous deposits on both catalysts were observed.

Catalyst deactivation because of chloride species has been observed in gas-phase and liquid-phase reactions. In a typical HDC reactor, there are two types of chloride species: groundwater reaction product Cl^- and dissolved salt Cl^- at high concentrations. HCl has been shown to inhibit catalytic activity on a variety of

catalysts, including Ni-based catalysts [28], metal sulfides [49], and noble metal-containing catalysts such as Pd and Pt [50], [51]. It has been claimed that HCl was reversibly adsorbed on the active surfaces, reducing catalytic activity [50], [51].

Apart from these deactivation modes, metal-supported catalysts are extremely sensitive to sulfur forms, including HS^-, SO_4^{2-}, SO_3^{2-}, SO^{2-}, and readily deactivate based on exposure time, sulfur species concentration, and concentration type [52]. These species are produced as a result of sulfur-containing discharges and bacterial activity, particularly anaerobic bacterial respiration. Sulfate concentrations in groundwater have been measured as high as 710 ppm [53]. Even ppm concentrations of these compounds are sufficient to deactivate the catalyst.

Carbonate (CO_3^{-2}, HCO_3^-), nitrate (NO_3^-), and nitrite (NO_2^-) species may impair the water remediation catalyst's effectiveness. Although the impacts of these anions are not as harmful as the effects of chlorine and reduced sulfur species, catalytic activity has been observed to diminish in many circumstances [17].

Nitrates in drinking water can be converted using hydrogen and a palladium-based catalyst. However, when the amount of hydrogen available is low, nitrate removal techniques are preferred. As a result, under our reaction circumstances, if sufficient hydrogen is available, hydrogen is likely to be employed for chlorinated compound removal rather than nitrate removal [17].

2.3 Protection Strategies

To alleviate the negative effects of chloride interactions, some ways to developing deactivation-resistant catalytic systems have been reported in the literature [54]. For reducing deactivation effects caused by HCl production is to neutralize it by adding base-containing solutions to the reaction mixture. Yuan and Keane conducted chlorophenol HDC in an aqueous-phase batch reactor by adding numerous inorganic bases to the starting reaction solution, including NaOH, LiOH and KOH [47], [55]. By adding base to the reaction solution, catalytic activity increased in a pH-

dependent manner. The increase in catalytic activity was attributed to the inhibition of neutralizing HCl. Catalytic activity rises after NaOH addition if the final reaction solution is somewhat acidic or neutral owing to HCl neutralization.

One relevant question is if cations were used in conjunction with OH anions to reduce the inhibitory effect when the base solution was introduced. The kind of cation had an influence on the activity of the Pd/Carbon catalyst, but not on the Pd/Al_2O_3 samples. The qualities of supports are likewise altered by base addition. Base addition enhanced the basicity of the Ru/Carbon samples, according to Velis et al. (1999). Given that the acidity of the support can cause carbon deposition on active metals, adding a base to the original starting solution can also inhibit carbon formation. It should also be noted that, while NaOH addition helps to decrease HCl deactivation effects, raising groundwater pH with NaOH has practical implications in groundwater applications [56]. However, if the resultant solution is mildly basic or basic, catalytic activity reduces because the basic reaction environment inhibits reactant adsorption on the catalytic surfaces. When considering huge quantities of polluted water streams, changing the pH of groundwater by external addition of NaOH may raise concerns about the operation's sustainability and applicability in groundwater applications [54], [57]. Another method for controlling solution pH is to utilize buffer solutions to keep the environment non-acidic during the process. However, it is critical to ensure that buffer solutions do not interfere with catalytic activity [37], [58].

In another approach, novel catalytic systems were designed to develop the resistance of deactivation and considered as a solution in inhibition situations. Hydrophobic materials were utilized as a support to protect the active metals from anionic species found in groundwater. Reinhard's research group was the first to employ hydrophobic materials in water abatement. They changed the sample's hydrophobic characteristics by synthesizing materials with varied Si/Al ratios, as samples with different Si/Al ratios display varying degrees of hydrophobicity. The hydrophobic materials were referred to as "protected samples."

The highest performing catalyst for HDC of 1,2-dichlorobenzene was palladium on hydrophobic zeolite Y, which was evaluated alongside conventional supports. Sulfite protection was obtained with a loss of 60% of pristine catalytic activity. These findings were notable since silica and alumina-based samples deactivated fully within a few minutes [19]. Further testing of the zeolite-Y over a prolonged length of time yielded comparable findings, with maintained efficiency observed. However, authors found that the reactor bed should be regenerated on a regular basis to eliminate H_2S produced by sulfate reducing bacteria [59]–[61].

Kopinke et al. (2010) coated Pd particles with the silicone-based chemical polydimethylsiloxane (PDMS) to protect them from soluble species such as anionic, cationic, and non-ionic surfactants that can be harmful. Because of its high diffusivity and thermal stability, PDMS was explored as a coating polymer. Surfactants induce modest loss in catalytic activity in non-coated materials, according to activity tests. Coating the catalyst with PMDS polymers improved its resistance to ionic poisons such as bisulfides [60]. More recent study from the same research group has showed that the silicone covering of the catalyst experiences silicone hydrolysis reactions as a result of HCl produced as a byproduct of the reaction. Furthermore, covering the catalyst retained some of the HCl generated within the coated matrix, which was ascribed to a portion of the deactivation. The reaction's aggressive effects on HCl precluded its long-term usage [61]. Comandella et al. (2016) evaluated the coated catalyst's long-term HDC. They pointed out that when the sample was coated with PDMS or the catalyst was put in a membrane reactor, there is an unavoidable loss of catalytic activity [62].

Nutt et al. designed bimetallic palladium on gold (Pd-Au) nanoparticles with a Pd-shell/Au-core structure to improve catalytic activity by using Pd in various ways [9]. Room temperature and 1 bar were chosen as experimental conditions. Palladium nanoparticles (Pd NPs), Palladium on alumina support (Pd/Al_2O_3), palladium on carbon support (Pd/Carbon) and bimetallic palladium on gold nanoparticles (Pd/Au NPs) were tested. The Turkevich-Frens (citrate reduction) technique was used to create Au NPs with a diameter of around 20 nm, and Pd metal was deposited using

Pd chloride salt and ascorbic acid reducing agent. The NPs showed high TCE HDC reaction rate constants (Figure 2.3); the most active composition had a first-order rate constant (943 $L/g_{Pd}/min$) that was >10, >70, and >2000 times greater than monometallic Pd NPs, Pd/Al_2O_3, and Pd black, respectively. That is, it was reported that Pd on Au bimetallic nanoparticles are more active than others. However, they also stated that the 20 nm Au NPs are too large for practical applications in terms of wasted gold particles. So, they decided to synthesize smaller particles.

In their next work, they developed this by synthesizing 4 nm particles [33]. Operating conditions are same as previous study. The Slot-Geuze (citrate/tannic acid reduction) process was used to create Au NPs with a diameter of around 4 nm, and Pd metal was deposited using Pd chloride salt and H_2 gas reducing agent. And as a result, they found that smaller particle sizes have more activity. They also state that the optimum activity for different particle sizes is at different Palladium metal contents.

With comparison of the results of these studies with Figure 2.3, the blue square is for 20 nm and the red triangle is for 4 nm. The smaller NPs produced were more catalytically active, with the most active composition (13 wt% Pd) being twice as active as the 20 nm NPs with 1.9 wt% Pd (Figure 2.3(a)) [11]. The two reaction rate-Pd content 'volcano' curves revealed that the 4 nm and 20 nm NPs had two distinct optimal Pd metal contents that resulted in maximal activity. By altering the x-axis to Pd surface coverage, the curves might be replotted. Figure 2.3(b) demonstrates that the data points lie on a single curve, which leads to many conclusions. One is that catalytic activity is very sensitive to a quantitative property of the bimetal structure, namely the Pd surface coverage. Second, the most active catalyst is 4 nm AuNPs with 70% Pd coverage. Third, 70% Pd coverage may be optimal for TCE HDC activity, at least for Au particle sizes ranging from 4 to 20 nm.

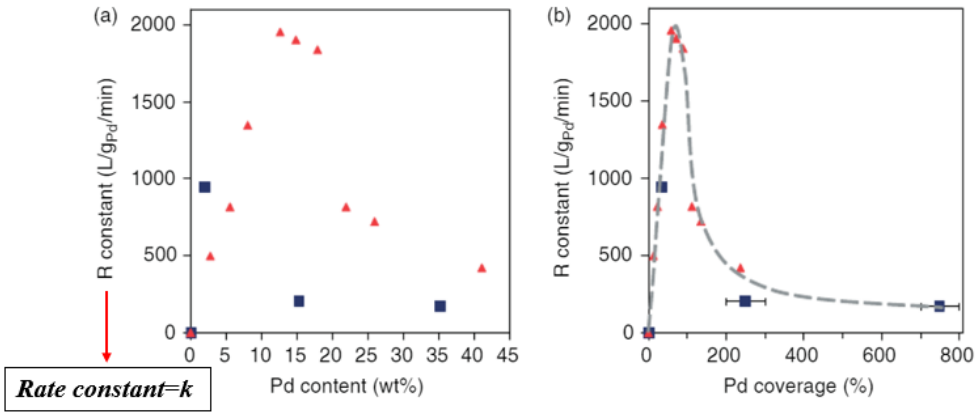

Figure 2.3 Reaction constants for Pd-on-Au NPs prepared with 20 nm (blue squares) and 4 nm (red triangles) Au NPs, plotted as a function of (a) Pd weight content and (b) Pd surface coverage [11]

They stated that bimetallic catalysts have much higher activity, selectivity, and/or deactivation characteristics than monometallic catalysts. Gold has long been thought to be a catalytically inert material; however it has been shown to improve the catalytic characteristics of Pd in a variety of chemical processes, including gas-phase HDC of chlorofluorocarbons, hydrodesulfurization, and the synthesis of vinyl acetate monomer (an industrial-scale reaction) [11].

One challenge in bimetallic catalysis research is the lack of control over the metallic nanostructure during synthesis. Pd-Au bimetallic catalysts are traditionally made by depositing Au and Pd salt species onto a support material (e.g., alumina, silica, and carbon), which are subsequently transformed into nanometer-sized metallic domains using gas-phase heat treatment. These domains can vary in size, but more problematically, they can vary in composition.

As a result of these studies, it can be thought that particle size effect is important for efficiency and protection of catalysts. Synthesizing small nanoparticles would be better for more efficient use of the precious metals. Initial activity for HDC is clear, however, resistance to deactivation is unknown in these studies. In this study, we want to investigate the effect of particle size of catalysis as a design parameter.

2.4 Effect of Particle Size

Surface catalyst phenomena is dependent on some factors such as particle size and surface area. To save precious metal, catalyst designers aim to distribute metal particles finely since only surface atoms play role in catalysis. It has long been noted that raising the metal dispersion (or lowering the particle size) can change the reaction rate per surface atom of the catalyst metal (usually referred to as the turnover number, TON) for particular reactions. The TON might rise, decrease, reach a maximum, or remain constant (Figure 2.4) [63]. Catalytic reactions that vary the TON with metal dispersion are referred to be *structure sensitive*, whereas those that do not vary with dispersion are referred to as *structure insensitive*. Understanding structure sensitivity can assist in design of catalysts, allowing control over mechanisms, activity and selectivity.

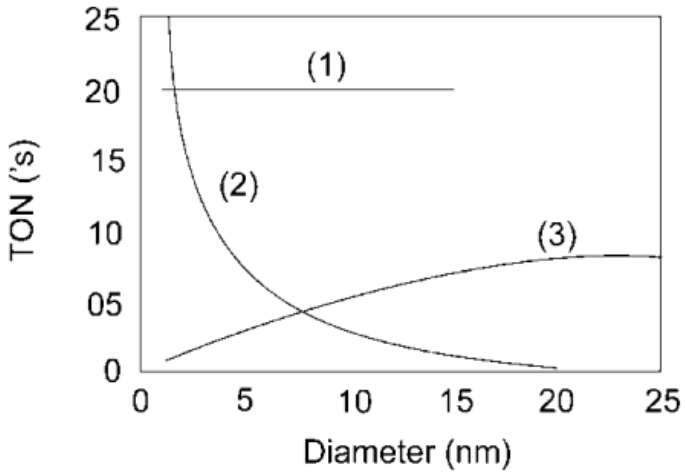

Figure 2.4 The three different kinds of structure sensitivity-particle size relationships plotted as turnover number versus particle size [63]

Che and Bennett [64] have provided a detailed overview of size effects in catalysis. Some distinguishing characteristics emerge from the survey. In general, hydrogenation processes are thought to be structure insensitive. It is the instance of benzene hydrogenation on a Pt/SiO_2 catalyst, as shown by curve (1) in Figure 2.4.

Curve (2) represents ethane hydrogenolysis on a structure-sensitive Rh/SiO_2 catalyst. As particle size decreases, the TON increases by roughly two orders of magnitude. In the final example, curve (3), which corresponds to CO hydrogenation on Ru/Al_2O_3, resulting in methane and water, the TON reduces as the cluster size decreases. In the final example, it can be seen that the size impact is noticed from very large cluster sizes in some circumstances, correlating to a decrease in activity when clusters get smaller. Size effects can also be seen in selectivity (the preference for one product over others generated by the reaction). This final stage is critical for industrial processes. Both activity and selectivity frequently vary with metal dispersion.

The apparent sensitivity of a reaction to the structure of a catalyst is measured experimentally by monitoring the rate of reaction over a series of catalysts with variable particle size (preferably with catalysts whose particle size is monodisperse) [65], [66].

Reducing metal particle size to the nanoscale range has been proposed as a feasible method of improving catalyst performance. The increase in catalytic activity has been linked to:

i. an increase in metal surface area,
ii. higher dispersion of metal particles which increases the exposed surface-active sites
iii. less mass transfer restriction.

As mentioned above, the most common problem for HDC of TCE reaction is deactivation by HCl, which is the unavoidable reaction product. If HCl poisoning in this reaction is structure sensitive, deactivation can be prevented by designing stable catalysts.

2.5 Platinum-based Catalysts

Group VIIIB metals, especially Pt, Pd and Rh, are well-known catalytic materials for hydrodechlorination of halogenated organic compounds. They can catalyze HDC reactions at mild temperatures (20-30 ^{o}C) and atmospheric pressure (1 atm). However, rhodium is thought to deactivate quickly owing to hydrogen chloride poisoning [29].

HDC of TCE process has some consequent chloride removal reactions. Substances such as 1,2 dichloroethene (C_2HCl_3), vinyl chloride (C_2H_3Cl) and ethylene (C_2H_4) may be formed in these reactions (Equations 2.2, 2.3 and 2.4). That is, incomplete HDC results in formation of chemicals that are more toxic than TCE. In this part, Pd and Pt have another advantage. As an advantage over other chemical transformation approaches, they convert TCE into ethane without the formation of vinyl chloride and other chlorinated intermediates [9], [20], [67]. Vinyl chloride (C_2H_3Cl) is much more dangerous than TCE and is even more carcinogenic. Therefore, avoiding this substance formation is important for safety.

$$C_2HCl_3 + H_2 \rightarrow C_2H_2Cl_2 + HCl \quad (2.2)$$

$$C_2H_2Cl_2 + H_2 \rightarrow \mathbf{C_2H_3Cl} + HCl \quad (2.3)$$

$$C_2H_3Cl + H_2 \rightarrow C_2H_4 + HCl \quad (2.4)$$

Palladium catalysts were generally the most active with conversions up to 100% and strong selectivity. Nonetheless, they deactivated quickly and severely. Pt is often claimed to be less active than Pd, with low conversion values, it is more stable as an advantage [68]. Although there are many studies with Pd in the literature, HDC reactions with Pt-based catalysts are very few. As another advantage, Pt is a relatively cheaper metal than Pd. Although there is not much difference for lab-scale experiments, this advantage will work when it is considered on an industrial scale. Considering these parameters, this study was carried out with Pt-based catalysis.

Platinum ranks 72nd among the chemical elements found in the Earth's crust. Platinum (atomic number 78) may be found in the center of the periodic table. Its close neighbors include iridium, osmium, palladium, rhodium, and ruthenium, which are together known as the platinum group metals (PGMs). They're widely recognized for their catalytic characteristics, which allow them to assist speed up chemical processes without altering themselves. Platinum's catalytic characteristics have been known since the 1820s, when German scientist Johann Wolfgang Döbereiner (1780-1849) discovered them.

Platinum is heavy, soft, malleable (simple to work—only silver and gold are easier to form), and ductile (easy to pull into wires), with a relatively high melting point (1770°C or 3220°F). Because it is so inert chemically, it is frequently referred to as a noble metal. It does not even react with oxygen in the air, thus it does not rust or tarnish. It's also fairly resistant to acid damage [69].

There are many synthesis techniques for catalysts. Although no single approach is better to the others, one method may be more advantageous than another depending on the final use of the catalyst and the instrumentation available [70]. Commonly used synthesis techniques can be listed as follows:

- Low-temperature Chemical Precipitation
- Colloidal
- Sol-gel
- Impregnation
- Microemulsions
- Electrochemical
- Spray Pyrolysis
- Vapor Deposition

In this study, two types of Pt-based catalysis, supported and unsupported, were synthesized. Impregnation was used for supported Pt on alumina and Colloidal Slot-Geuze method was used for unsupported Pt nanoparticles.

2.6 Impregnation

This process begins by impregnating a prepared support with a metal salt solution. During drying, the solvent is eliminated via evaporation. When the amount of solution used matches to the pore volume of the support, the procedure is known as incipient-wetness impregnation or dry impregnation. When there is little or no interaction between the precursor and the support, this technique is utilized [64]. The necessary amount of metal salt is dissolved in enough water to just fill the pore volume of the support using this procedure. The most common way, however, is to add solvent to support from an excess solution slurry. This technique is known as wet impregnation [71].

Following the impregnation stage, the catalyst precursor must be reduced to its metallic state by a reduction step. Because particle size is controlled after the impregnation stage, the type of the support is critical. $Na_2S_2O_3$, $NaBH_4$, $Na_4S_2O_5$, N_2H_4, and formic acid are common liquid phase reducing agents. H_2 is the most common gas phase reducing agent [70].

The most frequent platinum precursors used for impregnation are chloride salts; nevertheless, it has been suggested that the metal chloride salts may cause chloride poisoning, which may impair the catalytic activity of the particles. Metal sulfite salts, metal carbonyl complexes, and metal nitrate salts have been used instead of chlorine to avoid chlorine toxicity [70], [72].

The impregnation approach is a relatively green way of catalyst synthesis. The benefits include technological simplicity, cheap cost, and repeatable metal loadings. Reduction processes occur at moderate or room temperatures, decreasing energy usage, and organic solvents are avoided by utilizing aqueous media. The disadvantages of the impregnation technique stem from the use of liquid solutions as the processing medium. Particles in solution can easily agglomerate.

2.7 Colloidal Slot-Geuze Synthesis Method

Gold sols are made by condensing metallic gold from a supersaturated solution formed by the reduction of Au^{3+}, which is normally in the form of gold trichloride. This approach can produce homodisperse gold sols with average particle sizes greater than 12 nm. Smaller markers are often required for high resolution research. Preparation procedures for sols with smaller particles, on the other hand, are far less acceptable in terms of reproducibility, particle size control, and homodispersity.

To address these flaws, Slot and Geuze [73] investigated the reaction conditions for sol formation that used a combination of tannic acid (TA) and citrate (C) as reducing agents. This method is described for preparing colloidal gold nanoparticles in any size (Figure 2.5). They can make these TA-C sols homodisperse by using the proper conditions.

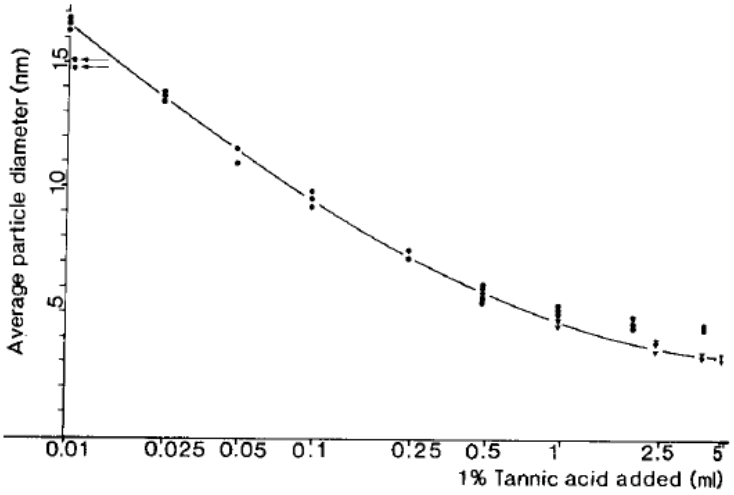

Figure 2.5 The influence of the TA concentration during gold sol formation on the size of the gold particles [73]

For preparation of 100 mL of colloidal gold sol, two solutions were made. While first solution contains 1 mL of 1% $HAuCl_4$ in 79 mL distilled water, second solution which is called as reducing mixture, consists of 4 mL 1% trisodium citrate dihydrate, 0 to 5 mL of 1% tannic acid, 25 mM potassium carbonate (same volume as 1% TA) and distilled water to bring the total volume of second solution up to 20 mL.

To compensate for the acidifying impact of TA, carbonate was added. When 0.5 mL or less of 1% TA was added, the pH change was minimal, and carbonate was not added. On a hot plate, both solutions were heated to 60 ^{o}C. The reducing solution was then immediately added to the first solution while stirring. After mixing of solutions, a sudden color change is observed, and sol formation is complete. It is then heated until boiling. After an overnight aging procedure, the sol becomes ready. Average particle diameter is found by using electron microscopy.

Citrate responds slowly, whereas TA reacts quickly. As a result, in the small size range, when an excess of TA is employed, the reduction is virtually entirely accomplished by TA. In the higher size range, insufficient TA is supplied, allowing the citrate to take over and complete the reduction. In such range, it appears that particle size is still determined by TA concentration. The temperature was crucial during the preparation procedure. The sols become heterodisperse at higher temperatures. Larger gold particles were produced when the reaction temperature was reduced. Temperatures around 60 ^{o}C gave the best results in this regard.

In the study of bimetallic Pd on Au NPs (Nutt et al.), they used this method for both metals during the catalysis synthesis and achieved a successful result. In this study, the applicability of this method for Pt was also considered for noble catalysts with similar properties, and this method was modified for Pt.

2.8 Focus of the Study

Although HDC is still economically competitive with alternative remediation technologies like as air stripping and activated carbon adsorption, catalyst deactivation difficulties are preventing HDC from being commercialized and fully utilized. As a result, rather than improving intrinsic catalytic activity, there is a clear need for research to focus on catalyst deactivation [36], [62]. As a result, our study has concentrated on building a novel catalytic water treatment system with increased deactivation resistance.

The focus of this study is investigating the effect of particle size on chloride resistance as a design parameter and determination of structure sensitivity of HDC of TCE using Pt NPs.

CHAPTER 3

EXPERIMENTAL PROCEDURE

This chapter explains the experimental systems used in this study. The research plan consists of four parts:

i. Synthesis of platinum on alumina supported catalyst with incipient wetness impregnation
ii. Synthesis of platinum nanoparticles with modified colloidal Slot-Geuze method
iii. Catalyst characterization
(Transmission electron microscopy and UV-Visible Spectroscopy)
iv. Aqueous phase catalytic activity experiments
(Description of the system and HDC of TCE catalytic activity testing in batch and semi-batch modes)

3.1 Synthesis of Platinum on Alumina Supported Catalyst

3.1.1 Chemicals

The following chemicals are used to synthesize supported platinum on alumina (Pt/Al_2O_3).

i. Platinum (II) Acetylacetonate ($Pt(C_5H_7O_2)_2$), (Sigma-Aldrich 15170-57-7)
ii. Aluminum Oxide (Al_2O_3) NanoArc (nonporous), (Alfa Aesar 1344-28-1)
iii. Absolute Acetone (CH_3COCH_3), (Sigma-Aldrich, 67-64-1)

3.1.2 Synthesis Procedure

Platinum on alumina (Pt/Al_2O_3) was synthesized by incipient wetness impregnation technique (dry impregnation). In this synthesis, platinum (II) acetylacetonate, NanoArc aluminum oxide and acetone were used as a metal salt, support, and solvent, respectively. The metal loading was selected as 1 wt% Pt. 6 mL of acetone was added to 20.2 mg of metal salt, and solution was mixed for 2 minutes. Small drops of this solution were added to the support intermittently. It was an important point that two drops do not get in one spot. Then, it was mixed with the glass baguette. As the mixture was dried, impregnation was continued until the solvent-metal salt solution was consumed. Finally, when the process was finished, it was put into the oven at 100 °C for drying.

After the prepared mixture was taken out of the oven, it was observed that its color turned from yellow to gray. Then calcination and reduction were performed. The calcination was carried out under static air at 300 ^oC for 2 hours. The reduction was carried out under H_2/Ar flow at 450 ^oC for 5 hours. Synthesis procedure is shown in Figure 3.1.

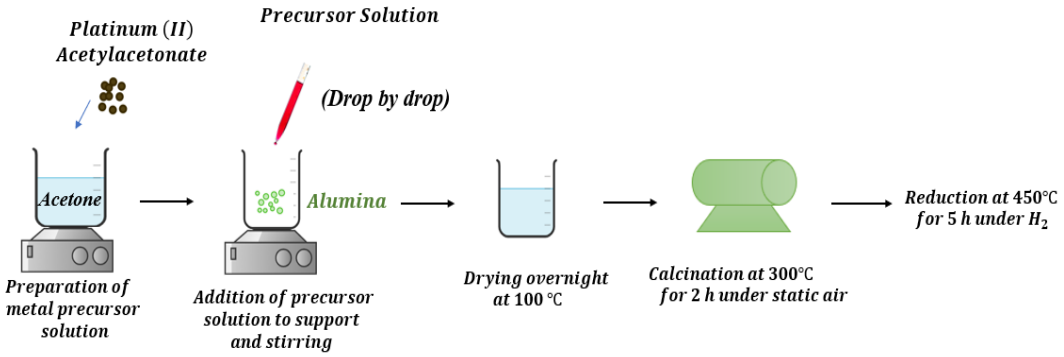

Figure 3.1 Incipient wetness impregnation synthesis for Pt/Al_2O_3 catalyst

3.2 Synthesis of Platinum Nanoparticles

3.2.1 Chemicals

The following chemicals are used to synthesize platinum nanoparticles (Pt NPs).

i. Chloroplatinic acid (H_2PtCl_6) 8 wt. % solution in water, (Sigma-Aldrich 16941-12-1)
ii. Ultrapure water, (Middle East Technical University, Department of Chemical Engineering)
iii. Tannic acid ($C_{76}H_{52}O_{46}$), (Sigma-Aldrich 1401-55-4)
iv. Potassium Carbonate (K_2CO_3), (Merck, 584-08-7)
v. Trisodium Citrate Dihydrate ($C_6H_5Na_3O_7.2H_2O$), (ISOLAB, 6132-04-3)

3.2.2 Synthesis Procedure

Platinum nanoparticles (Pt NPs) with three different particle sizes were synthesized by modifying the method reported by Slot and Geuze [73]. For smallest particle, a platinum salt solution was prepared by diluting 144 μL chloroplatinic acid, H_2PtCl_6, in 79.9 ml of ultrapure water as a first solution (Appendix A). A second solution containing 0.0456 g trisodium citrate dihydrate, 0.05 g tannic acid and 0.018 g potassium carbonate dissolved in 20 ml of ultrapure water was prepared.

Both solutions were stirred while being heated to 60 ^oC. Once this temperature was reached, the second solution was added to the first solution; an immediate color change (from yellow to brown) was observed, indicating end of the sol formation. The solution was then heated and left to boil for 25 min, and then removed from the heat source. The resulting sol was cooled to room temperature and aged overnight. The day following, water was added so that the final solution volume is 100 ml. The final fluid had a dark brown color, indicating reduction of Pt. Synthesis procedure is shown in Figure 3.2.

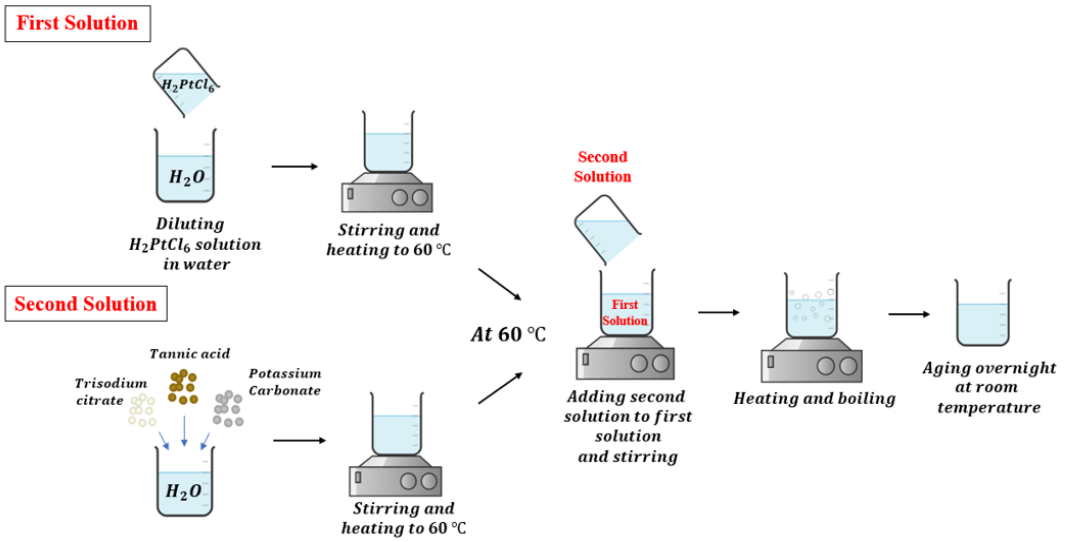

Figure 3.2 Colloidal Slot-Geuze synthesis method for Pt NPs

Larger Pt NPs were similarly prepared but no potassium carbonate was used, and concentration of tannic acid in the second solution was changed. For second particle, the second solution was prepared by using 0.005 g tannic acid, 0.0456 g trisodium citrate dihydrate and 20 mL water. For largest particle, the second solution was prepared by using 0.001 g tannic acid, 0.0456 g trisodium citrate and 20 mL water.

3.3 Catalyst Characterization

3.3.1 Transmission Electron Microscopy (TEM)

Particle size of platinum nanoparticles (Pt NPs) was analyzed using high resolution transmission electron microscopy (HRTEM) images collected using a JEOL JEM 2100F HRTEM (Central Laboratory – METU) operating at 200 kV. Pt NPs were deposited onto CF200-Cu carbon film grid. The suspended samples in distilled water were mixed in an ultrasonic cleaner for 60 minutes, then a drop was dropped on the grid with a micropipette and left to dry for at least one night. Particle size distribution measurements were made using the *ImageJ* program.

3.3.2 Malvern Particle Size and Concentration Analyzer

Particle size and concentration of Pt NPs were also analyzed using particle size and concentration analyzer (Malvern Panalytical Ultra Pro). Refractive index (n=2.32) and absorption (k=4.16) values of Pt were entered into the software of the device for the analysis of Pt NPs. The device is in Middle East Technical University, Department of Chemical Engineering.

3.3.3 Ultraviolet-Visible Spectroscopy (UV-Vis)

Pt NP sols were analyzed through ultraviolet-visible absorption spectroscopy (Shimadzu UV-2550). Spectra of the NP sols were collected between wavelengths of 230 and 730 nm. Quartz cuvettes (Hellma Analytics) with a path length of 1 cm were used. The device is in Middle East Technical University, Department of Chemical Engineering.

3.4 Aqueous Phase Catalytic Activity Experiments

3.4.1 Description of the System

An aqueous phase reactor system capable of running liquid phase reactions at atmospheric pressure was built to perform the proposed experiments. The reactor can be operated as a batch or semi-batch reactor.

The system is composed of syringe injector port, chloride detector (Hanna Instruments HI 4107), heater & stirrer (IKA C-MAG HS 7), two contact thermometer connections (one from heater, one from chloride detector), a quartz gas dispenser, a glass reactor (volume=800 ml) as well as valves and tubes.

The reactor is continuously stirred at 750 rpm to ensure good mixing of the reactants to obtain uniform temperature and concentration distribution. It was operated under ambient conditions (1 atm, 30 ^{o}C).

No uncontrolled temperature and pressure increase is expected during HDC of TCE. Leak checks were performed during the setup of experimental system and no leak was observed in the lines as well as the reactor components.

Before H_2 introduction to the reactor, a flushing step with Ar for 30 minutes were performed to ensure that no oxygen is left in the gas phase as well as in the liquid phase. In addition, the reactor assembly was always kept in a fume hood to increase the safety of operation.

HDC of TCE catalytic activity experiments were performed in batch mode as well as semi-batch mode. A schematic of reactor system is shown in Figure 3.3.

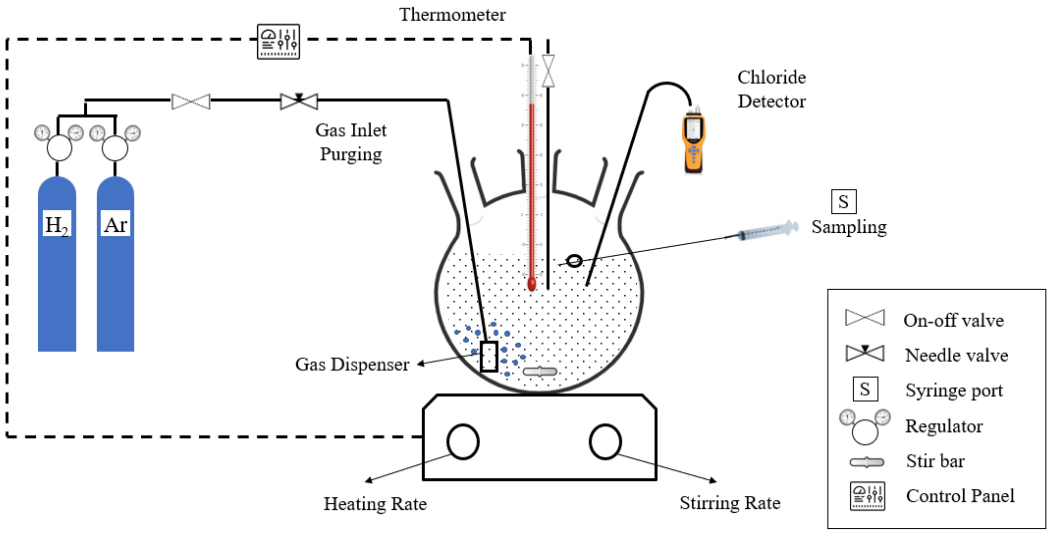

Figure 3.3 A schematic of reactor system

3.4.2 Catalytic Testing

Aqueous-phase HDC of TCE experiments were performed at 1 atm and 30 ^{o}C. In each experiment, the glass batch reactor was initially filled with a certain volume of ultrapure water. The stir bar was placed in the reactor. The reactor was then sealed with components by placing chloride detector, gas dispenser and two contact thermometer connections. At the beginning of the reaction, the stirrer was started,

and temperature was set to the reaction temperature. It took approximately 30 minutes for temperature to stabilize. Once the temperature is stable, the reactor was flushed with Ar to eliminate the presence of oxygen in the reactor. After Ar flushing, the reactor was also flushed with H_2 to fill the headspace with hydrogen atmosphere (1 atm). Before the addition of TCE to the reactor, TCE was dissolved in ethanol. Then, 1 ml of solution containing TCE and ethanol was injected to reactor from syringe port. The overall solution was stirred for at least 3 h to reach equilibrium, then 4 mL of Pt NP was injected into the reaction bottle at a set stirring rate 750 rpm. This is the time=0 sample which is used in kinetic calculations. At time zero, the concentration of TCE was calculated to be 20 ppm in liquid.

For 20 ppm TCE experiments, H_2 to TCE molar ratio is 4.8 (Appendix E), whereas the stoichiometric ratio of H_2 to TCE in HDC reaction is 4. In other words, 20 ppm TCE HDC reactions were carried under slightly excess hydrogen. Moreover, there is pure-H_2 headspace over the reaction solution forming a sufficient reservoir of H_2. As dissolved H_2 is consumed in the reactor as per the reaction, it is replenished by H_2 in the headspace. During the reaction, chloride concentration in liquid sample was detected using an ion selective chloride electrode and recorded using required software of the device (Hanna Instruments, HI92000 Software). According to working principle of the chloride detector, it was periodically calibrated by preparing 0.1, 1, 10 and 100 ppm NaCl standard solutions. A photograph of reactor system is shown in Figure 3.4.

The reactor was operated in both batch and semi-batch modes. After the addition of catalysis in batch mode, chloride concentration data was taken without any injection. HCl poisoning experiments were performed in semi-batch mode. In these experiments, TCE injection was continued until the catalysis was deactivated as the reaction ended.

Figure 3.4 A photograph of reactor system

CHAPTER 4

RESULTS & DISCUSSION

In this chapter, the results of the experiments carried out according to the research plan described in Chapter 3 and the discussions of these results are presented. This chapter consists of eight parts:

i. In Section 4.1, two types of reactor verification experiments are explained: HDC of TCE with catalyst without hydrogen and without catalyst with hydrogen.

ii. In Section 4.2, investigations of heat transfer limitations based on adiabatic temperature rise are described.

iii. In Section 4.3, investigations of mass transfer limitations based on stirring rate and stir bar types are explained.

iv. In Section 4.4, results of characterization studies are described.

v. In Section 4.5, results of aqueous phase HDC of TCE catalytic activity experiments with Pt NPs are shown.

vi. In Section 4.6, the effect of particle size on HDC of TCE are shown. The rate constants based on unit volume of reacting fluid, unit mass of solid in fluid-solid systems, unit interfacial surface in two fluid systems and initial turnover frequency (TOF) are calculated.

vii. In Section 4.7, the effect of TCE concentration HDC of TCE are shown. In addition to the rate constants calculated in Section 4.6, deactivation rate constant has been also calculated.

viii. In Section 4.8, results of HCl poisoning experiments, which is the main purpose of the research are shown. For each particle, these experiments are performed in cycles.

4.1 Reactor Validation

Since a new HDC reactor was built to perform the experiments of the present study, reactor validation experiments were performed. Catalytic activity studies were carried out to confirm that TCE conversion is a meaningful parameter that can be utilized to evaluate the catalytic activity of TCE HDC. As a result, two types of experiments were carried out.

The activity results were reported in the form of TCE conversion or chloride concentration with respect to time. These parameters can be related to each other. To ensure the system's mass balance, chloride balance was performed, assuming that no partially dechlorinated compounds formed in the reaction. This is a reasonable assumption considering that precious metals such as Pt and Pd hydrodechlorinates all partially chlorinated compounds [54].

4.1.1 HDC of TCE with Catalyst without Hydrogen

The experimental technique described in Section 3.4 was followed in these studies, with minor adjustments. The catalytic activity experiment was performed with Pt NPs in the presence of only argon and without hydrogen. The absence of hydrogen in the reactor eliminated the possibility of an HDC reaction. Figure 4.1 depicts the obtained chloride ion concentration with respect to reaction duration.

As it can be observed, the chloride ion concentration, and hence TCE conversion, was insignificant after 4 hours indicating that other routes for TCE elimination including TCE degradation are absent in our reactor. The results show that hydrogen is important for HDC to occur. In addition, the results also show that the experiment, sampling procedure as well as reactor components do not cause any chloride production.

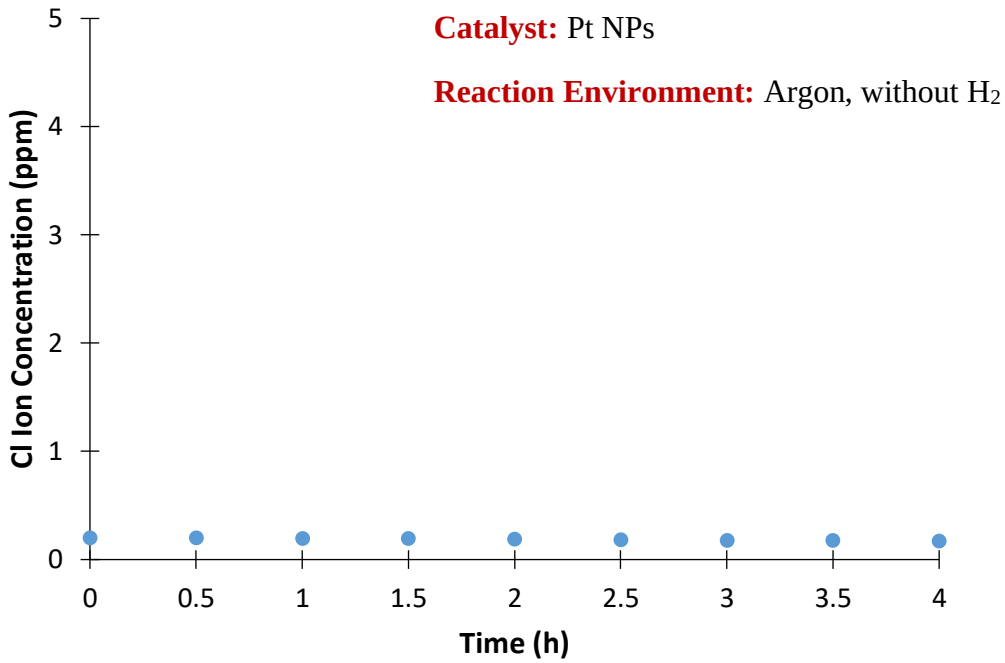

Figure 4.1 Catalytic activity data showing TCE conversion at ambient conditions (1 atm and 30^{o}C), with catalyst without H_2

4.1.2 HDC of TCE without Catalyst with Hydrogen

The reactor was operated without any catalyst sample under H_2 to assess the extent to which homogeneous HDC of TCE takes place. Figure 4.2 demonstrates that after 4 hours of reaction time, the chloride concentration was insignificant indicating that homogeneous TCE conversion does not occur appreciably under our reaction conditions.

It can be seen that the catalytic activity with 3 % TCE conversion under H_2 without catalyst is higher than the activity under Ar with catalyst. The difference can be attributed to homogeneous conversion of TCE, that cannot take place in the presence of Ar.

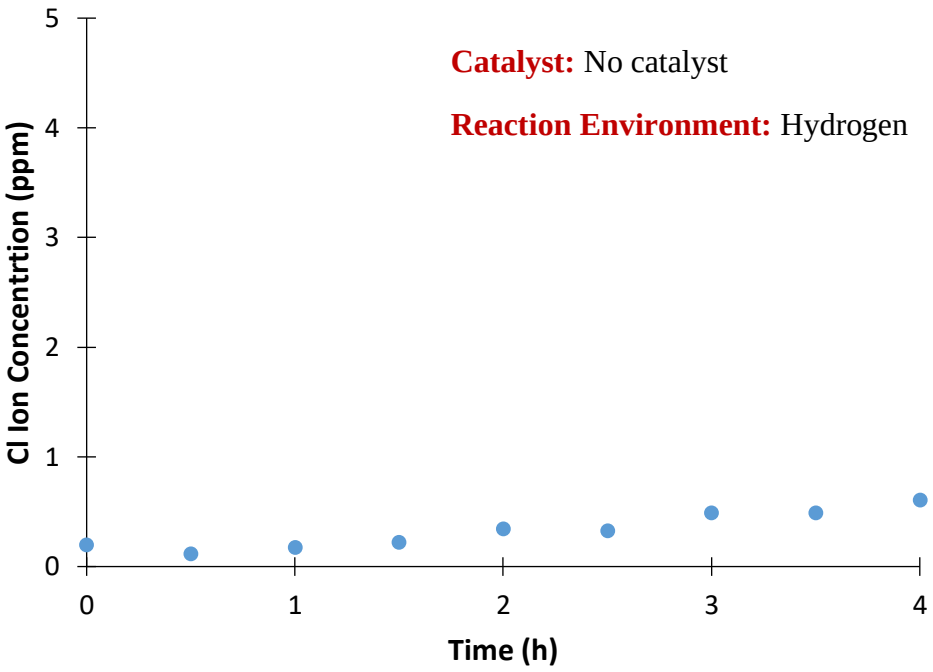

Figure 4.2 Catalytic activity data showing TCE conversion at ambient conditions (1 atm and 30°C) without catalyst with H_2

During this study, the glass reactor was cleaned after each usage to ensure that the activity produced was attributable to the performance of the catalyst.

4.2 Investigations of Heat-Transfer Limitations

The thermal effects of HDC of TCE were investigated for batch reactor operation. The heat of the HDC of the TCE reaction was calculated using the enthalpies of product and reactant formation [74]. The heat of the reaction was determined to be -309 kJ/mol at 25 °C and 1 atm.

At 100% conversion of TCE, 24 J of energy may be released for a given initial concentration of 20 ppm in a 510 mL liquid. The adiabatic temperature rise of 1.36 K can be calculated by Mathcad (Equation 4.1) taken the temperature dependence of heat capacity into account if the energy is exclusively used to heat the reaction media. The calculation of adiabatic temperature rise was shown in Appendix B. A procedure

with an adiabatic temperature rise of less than 50K is normally thought to offer no serious safety risks [75]. This implies that heat effects do not exist in our reaction system.

$$\Delta T_{ad} = \frac{-\Delta H_{rxn}}{C_p} \tag{4.1}$$

Where $-\Delta H_{rxn}$ is the reaction enthalpy (kJ/mol) and C_p is the specific heat capacity respective products (kJ/(mol.K)).

4.3 Investigations of Mass-Transfer Limitations

Catalytic reactors should be operated in such a way that mass transfer resistances are minimized as much as possible to assess true kinetics. The reactor system designed for HDC of TCE experiments faces numerous challenges related to transport phenomena because several phases (gas/liquid/solid) are present in the reactor during reaction. The effect of mass transfer was observed by considering general theory for spherical nonporous catalytic particles [81]. Figure 4.3 shows the TCE transport from the headspace through liquid phase and to the catalyst particle surface [82].

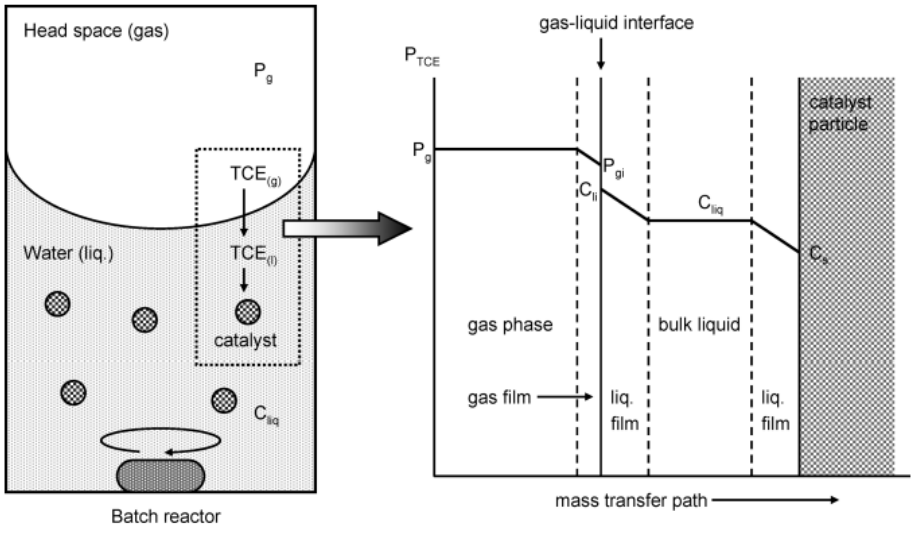

Figure 4.3 Mass Transfer Pathway of TCE in the Aqueous-Phase TCE HDC Reaction in a Batch Reactor [78]

HDC of TCE can be written as follows by letting the symbol A represent TCE, B hydrogen, C ethane, and D hydrogen chloride (Equation 4.2).

$$A + 4B \rightarrow C + 3D \tag{4.2}$$

Under our reaction conditions, $C_{B,S} \gg C_{A,S}$ (with hydrogen in excess). This also means that A is the limiting reactant. Then, the reaction rate expression can be written as Equation 4.3 & 4.4.

$$Reaction\ rate = ka_S C_{A,S} \tag{4.3}$$

$$Rate = ka_S C_S\ where\ C_S = C_{A,S} \tag{4.4}$$

The reaction rate is equal to the rate of the intermediate steps. These steps are formulated as Equation 4.5, 4.6 and 4.7.

$$Rate = k_{LS} a_S (C_{liq} - C_S) \rightarrow \quad C_{liq} - C_S = \frac{Rate}{k_{LS} a_s} \tag{4.5}$$

$$Rate = k_{GL} a_{GL} (C_{L,i} - C_{liq}) \rightarrow \quad C_{L,i} - C_{liq} = \frac{Rate}{k_{GL} a_{GL}} \tag{4.6}$$

$$Rate = k_G a_{GL} (P_g - P_{g,i}) = k_G a_{GL} (P_g - HC_{L,i}) \rightarrow P_g - HC_{L,i} = \frac{Rate}{k_G a_{GL}} \tag{4.7}$$

$a_{GL} and\ a_S$ are specific areas for gas-liquid interface and catalyst solid in overall batch reactor liquid volume. $C_{L,i}, C_{liq}\ and\ C_S$ are concentrations of TCE in liquid phase at gas-liquid interface, in liquid bulk, and at catalyst surface. H is Henry's law constant. k is rate constant for surface reaction. $k_G, k_{GL}\ and\ k_{LS}$ are mass transfer coefficients for gas, gas-liquid, and liquid-solid. $P_g\ and\ P_{g,i}$ are partial pressures of TCE in gas bulk and gas film at gas-liquid interface.

The above four equations 4.4-4.7 can be written as follows. After summation, the concentration terms of the left side of equations cancel each other.

$$C_S = \frac{Rate}{ka_s} \tag{4.8}$$

$$C_{liq} - C_S = \frac{Rate}{k_{LS}\, a_s} \tag{4.9}$$

$$C_{l,i} - C_{liq} = \frac{Rate}{k_{GL} a_{GL}} \tag{4.10}$$

$$\frac{P_g}{H} - C_{l,i} = \frac{Rate}{H\, k_G\, a_{GL}} \tag{4.11}$$

$$\frac{P_g}{H} = Rate\left(\frac{1}{ka_s} + \frac{1}{k_{LS}\, a_s} + \frac{1}{k_{GL} a_{GL}} + \frac{1}{H\, k_G\, a_{GL}}\right) \tag{4.12}$$

$$\boxed{Rate = \frac{P_g}{\frac{H}{ka_s} + \frac{H}{k_{LS}\, a_s} + \frac{H}{k_{GL} a_{GL}} + \frac{1}{k_G\, a_{GL}}}} \tag{4.13}$$

The overall rate expression (Equation 4.13) is shown above. The denominator is composed of resistances due to each transport limitation.

Gas-film resistance: It has been reported that the gas film resistance associated with reactant transfer from gas to liquid phase is negligible when compared to the liquid film resistance for solutions in contact with gases [76]–[78].

$$\frac{1}{k_G\, a_{GL}} \approx 0$$

Then, the overall rate expression becomes

$$Rate = \frac{P_g}{H\left(\frac{1}{ka_s} + \frac{1}{k_{LS}\, a_s} + \frac{1}{k_{GL} a_{GL}}\right)} \tag{4.14}$$

$$Rate = \frac{C_{liq}}{\frac{1}{ka_s} + \frac{1}{k_{LS}\, a_s} + \frac{1}{k_{GL} a_{GL}}} \tag{4.15}$$

$$\frac{C_{liq}}{Rate} = \frac{1}{ka_s} + \frac{1}{k_{LS}\, a_s} + \frac{1}{k_{GL} a_{GL}} \tag{4.16}$$

Gas-liquid interface: The liquid-film resistance is highly dependent on the hydrodynamics of the reactor. Because mass transfer coefficients are related to the hydrodynamic conditions of the batch reactor, mass transfer coefficients of the gas-liquid interface and liquid-solid interface ($k_{GL}a_{GL}$ and $k_{LS}\ a_s$) increase as the stirring rate increases [79].

As a result, an adequate stirring rate creates suitable hydrodynamic conditions for a uniform reaction rate throughout the reactor and eliminates gas-liquid and liquid-solid mass transfer resistances. Then, the observed reaction rate will only be limited by the true kinetics, which is desired.

The tests comprised of doing HDC of TCE experiments at different stirring speeds and with different stir bar types. It should be noted that, in our reaction system, Pt on alumina (nonporous) and Pt NPs were used. Therefore, pore diffusion in catalyst is not considered as a mass transfer limitation for both types of catalyst.

Stirring rate effect: The effect of stirring rate was studied experimentally while keeping kinetic parameters like catalyst amount, temperature, and reaction volume constant. TCE HDC studies were carried out at three different stirring speeds (500-625-750 rpm). Maximum stirring rate is 750 rpm for triangular stir bar. Increasing the stirring rate control above 750 rpm caused vortex formation and threw the stir bar.

Figure 4.4 shows the catalytic activity data of 1% Pt on nonporous alumina. As it can be observed, the maximum catalytic activity was attained with a stirring rate of 750 rpm but stirring rates of 500 and 625 rpm experienced severe external mass transfer restrictions. As a result, all kinetic analyses provided in this study were carried out at a mixing rate of 750 rpm to reduce external mass transfer resistances.

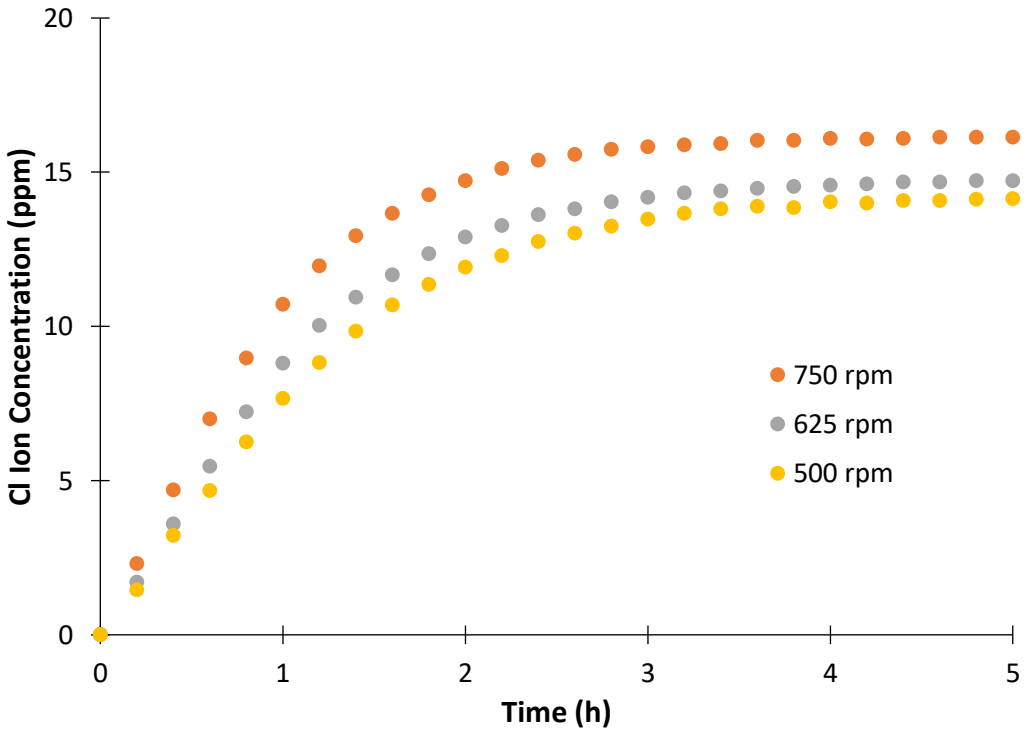

Figure 4.4 Effect of stirring rate on TCE conversion, reaction conditions: 1 atm and 30°C with 10 mg of 1%Pt/Al_2O_3

Stir bar effect: The effect of stir bars was studied experimentally while keeping kinetic parameters like catalyst amount, temperature, and reaction volume constant. Three different types of stir bar were used: standard, triangular, and cross stir bars (Figure 4.5).

Figure 4.5 Different stir bar types: standard, triangular and cross, respectively

The stirring rate was selected as 750 rpm, indicating the best catalytic activity as stirring rate. The catalytic activity data of 1% Pt on nonporous alumina are shown in Figure 4.6. As it can be observed, the maximum catalytic activity was attained with a triangular stir bar.

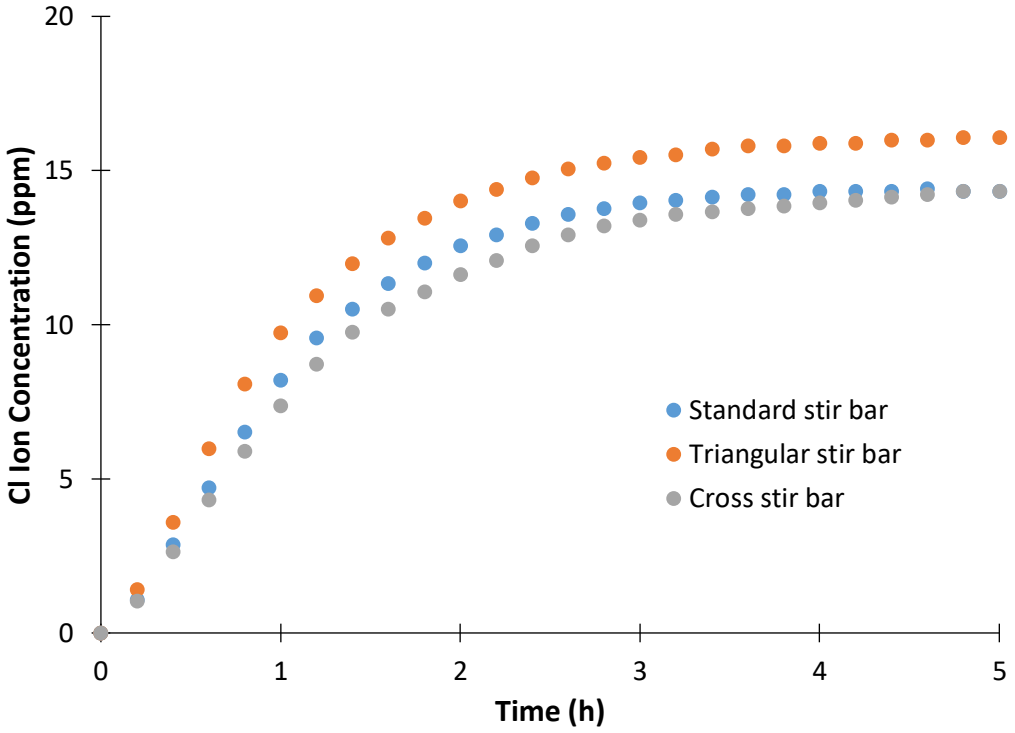

Figure 4.6 Effect of stir bar types on TCE conversion, reaction conditions: 1 atm and 30°C with 10 mg of 1%Pt/Al_2O_3

As a result, all kinetic analyses provided in this study were carried out at a mixing rate of 750 rpm with triangular stir bar to reduce external mass transfer resistances.

In addition, as it can be seen in Figure 3.4, chloride detector, gas dispenser and temperature probes in the reactor act as baffles. They control the liquid from the top to the bottom of the reactor, resulting in better and effective mixing.

The triangular stir bar is generally used for dissolving solids or mixing of colloids. The scraping action of the flat base disturbs colloidal particles. Thus, they're good for helping with dissolution or preventing sedimentation [80].

The mass transfer coefficients in gas-liquid and liquid-solid interface were also investigated with general rate equation. Rate equation 4.16 can be written as:

$$\frac{1}{Rate_{initial}} = C_1 + \frac{C_2}{W_s} \tag{4.17}$$

Where

$$W_s = a_s \left(\frac{R}{3}\right)\left(\frac{\rho_p}{\rho_{liq}}\right) \tag{4.18}$$

$$C_1 = \left(\frac{1}{k_{GL}a_{GL}}\right)\left(\frac{1}{C_{liq}}\right) \tag{4.19}$$

$$C_2 = \left(\frac{1}{k} + \frac{1}{k_{LS}}\right)\left(\frac{1}{C_{liq}}\right)\left(\frac{R}{3}\right)\left(\frac{\rho_p}{\rho_{liq}}\right) \tag{4.20}$$

ρ_p is density of catalyst particle, R is mean radius of catalyst particle, and ρ_{liq} is density of liquid. W_s is mass fraction of catalyst with respect to total liquid (g_{Pt}/g_{liq}). Specific area, a_s, is a property of solids defined as the total surface area of a material per unit of mass, (with units of m^2/g) or solid or bulk volume (units of m^2/m^3).

Equation 4.17 indicates that initial reaction rate varies with catalyst loading (W_s) which determines the liquid-catalyst surface interfacial area. It also indicates how mixing within the batch reactor affects the reaction rate. A stirring rate which is high enough for gas-liquid mass transfer to be negligible would give $C_1 \sim 0$, meaning $k_{GL}a_{GL}$ is very large. A low stirring rate decreases the gas-liquid interfacial area (a_{GL}). The effect of stirring can be quantified in this manner. This mass transfer analysis is applicable to spherical nonporous catalytic particles of any size [78].

The $1/rate_0$ vs $1/W_s$ plot was collected for the Pt NPs with particle size 3.0 nm in diameter (Figure 4.7). Mass transfer experiments were carried out with the smallest particle because the fastest reaction is obtained with the smallest Pt nanoparticle. Smaller particle size leads to higher mass transfer rate.

Each data point corresponds to a separate catalyst run at a specific catalyst weight at 750 rpm, with higher catalyst amounts leading to higher initial reaction rate. In this way we can see if 750 rpm eliminates the external mass transfer effect. Three different catalyst weight (2, 4, and 6 mL of Pt NPs) was selected for this experiment. The initial TCE concentration is 20 ppm in all experiments.

The intercept C_1 is equal to 0.2198 and is nearly zero at 750 rpm. This means $k_{GL}a_{GL}$ is very large from Equation 4.19, indicating the reaction system almost reached the condition of zero gas-liquid mass transfer resistance.

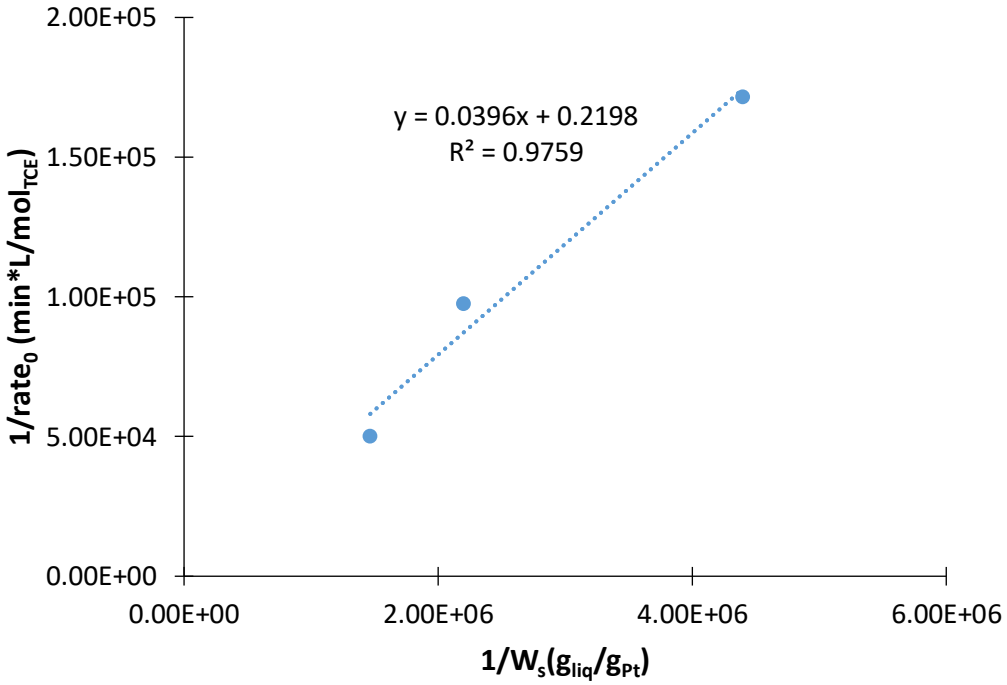

Figure 4.7 The relationship between $1/rate_0$ and $1/W_s$ for the mass transfer analysis of catalytic NPs, reaction conditions: 1 atm and 30°C at 750 rpm

Then, rate equation 4.15 simplifies to:

$$Rate = \frac{C_{liq}}{\frac{1}{ka_s} + \frac{1}{k_{LS}\, a_s}} \tag{4.21}$$

Liquid-solid interface: The liquid-solid mass transfer coefficient k_{LS} toward a spherical particle could be estimated by the Ranz-Marshall correlation (Equation 4.22) [83], [84].

$$Sh = 2 + 0.6Re_P^{1/2}Sc^{1/3} \tag{4.22}$$

Equation 4.22 is valid for

$$2 \leq Re_P \leq 200 \qquad 0.6 \leq Sc \leq 2.7$$

However, Reynolds number is lower than 2 because of nano size particles for our catalytic colloid system. Schmidt number is higher than 2.7. In this case, the analytical solution for steady-state diffusion is possible when a sphere is immersed in an infinite stagnant fluid, and the result is represented in the form $Sh = 2$ [83].

From the definition of Sherwood number:

$$Sh = \frac{k_{LS}R}{2D_{TCE}} \tag{4.23}$$

Where D_{TCE} is the diffusivity of TCE in water and it is equal to 1.04×10^{-5} cm^2/s at 25°C [85]. k_{LS} was calculated to be 0.689 m/s for 3.0 nm particles. a_s can be found by considering total surface area per unit of mass, and it is calculated as 90.9 m^2/g_{cat}.

For 2 mL catalyst loading experiment, a_s is also calculated as 0.048 m^{-1} from Equation 4.18, giving the corresponding liquid-solid mass transfer resistance $1/k_{LS}a_s$ value is 0.505 min. For this experiment, observed reaction rate constant is found as 0.0382 min^{-1}, indicating $1/ka_s$ value is 26.2 min. $1/ka_s$, the surface reaction resistance was found to be much greater than $1/k_{LS}a_s$, indicating the mass transfer effect through the diffusion layer can be neglected.

Finally, rate equation can be written as:

$$Rate = \frac{C_{liq}}{\frac{1}{ka_s}} \tag{4.24}$$

4.4 Characterization of Pt NPs

4.4.1 Transmission Electron Microscopy (TEM) Analysis

TEM images and particle size distributions provided particle size information for Pt nanoparticles in Figure 4.8, 4.9 and 4.10. Other images of these particle sizes are shown in Appendix C. Orange curves are Gaussian curve fits to the particle size histograms. The mean particle sizes and relative standard deviations were determined, and it was found that these values were similar for every particle size.

For first particle (Figure 4.8), it is observed that particle diameters vary between 1.9 and 4.3 nm. For this particle, approximately 150 particles have been investigated and measured using the *ImageJ* program. The average of these 150 particles was calculated as 3.0 nm and the standard deviation was calculated as 0.5. This standard deviation corresponds to approximately 16.2 %.

For second particle (Figure 4.9), it is observed that particle diameters vary between 4.8 and 8.1 nm. For this particle, again approximately 150 particles have been investigated and measured. The average of these 150 particles was calculated as 5.8 nm and the standard deviation was calculated as 0.8. This standard deviation corresponds to approximately 13.3 %.

For third particle (Figure 4.10), it is observed that particle diameters vary between 46.1 and 75.6 nm. For this particle, approximately 90 particles have been investigated and measured. The average of these 90 particles was calculated as 60.9 nm and the standard deviation was calculated as 8.6. This standard deviation corresponds to approximately 14.1 %.

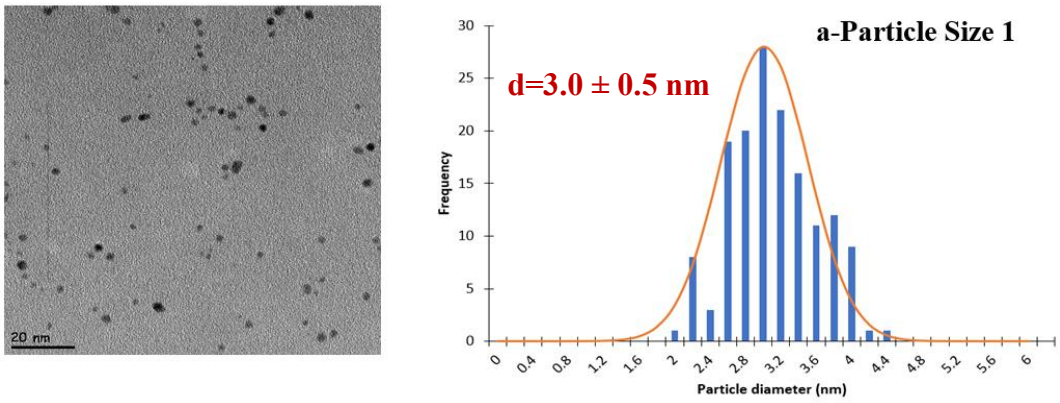

Figure 4.8 TEM image and particle size distribution of Pt NPs - Particle Size 1

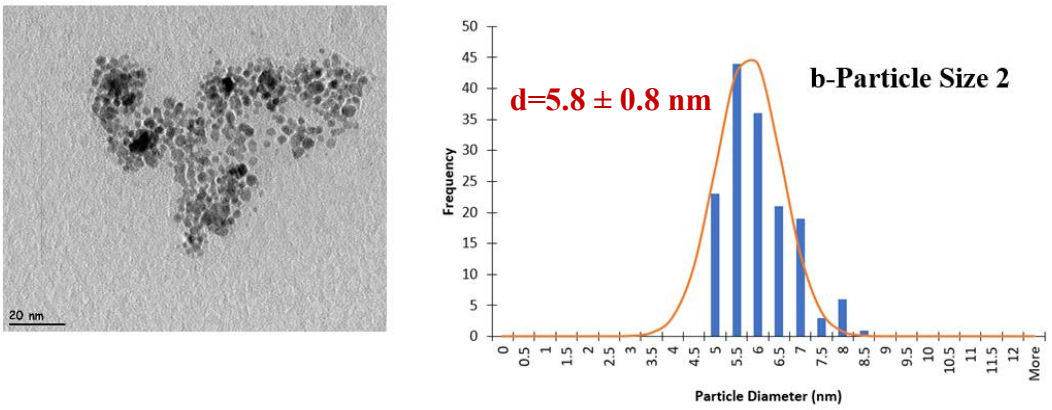

Figure 4.9 TEM image and particle size distribution of Pt NPs - Particle Size 2

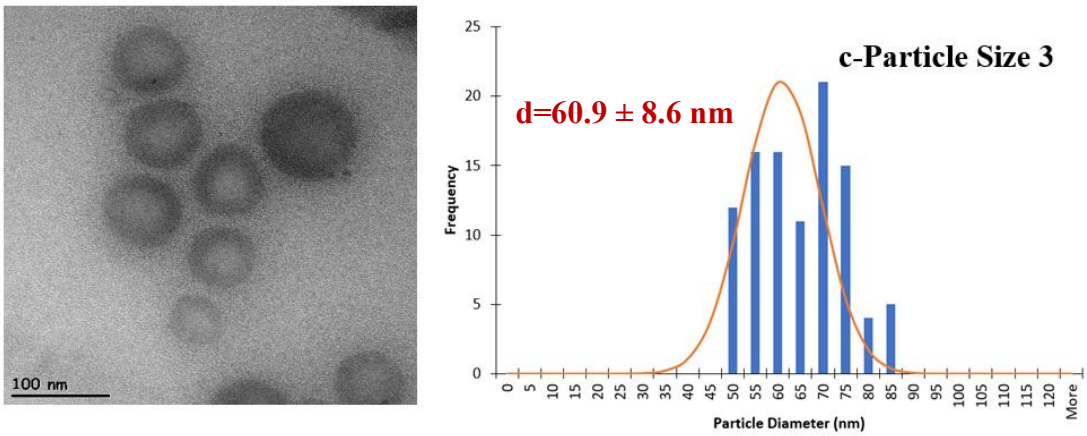

Figure 4.10 TEM images and particle size distributions of Pt NPs - Particle Size 3

4.4.2 Malvern Particle Size Analyzer

Malvern particle size analyzer also provided particle size information for Pt nanoparticles in Figure 4.11, 4.12 and 4.13. The mean particle sizes were determined, and relative standard deviations were calculated based on particle size distributions. The particle size and standard deviation results obtained from the particle size analyzer were very similar to the TEM.

For first particle (Figure 4.11), it is observed that particle diameters vary between 2.8 and 4.3 nm. The average of these particles was found as 3.5 nm and the standard deviation was calculated as 0.4. This standard deviation corresponds to approximately 11.4 %.

For second particle (Figure 4.12), it is observed that particle diameters vary between 4.5 and 8.3 nm. The average of these particles was found as 6.1 nm and the standard deviation was calculated as 0.9. This standard deviation corresponds to approximately 14.8 %.

For third particle (Figure 4.13), it is observed that particle diameters vary between 49.3 and 75 nm. The average of these particles was found as 60.8 nm and the standard deviation was calculated as 6.7. This standard deviation corresponds to approximately 11 %.

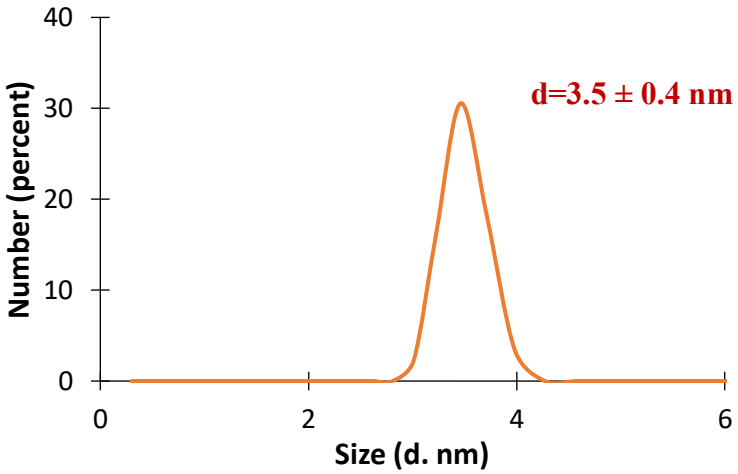

Figure 4.11 Particle size distribution of particle size 1 (Malvern analyzer)

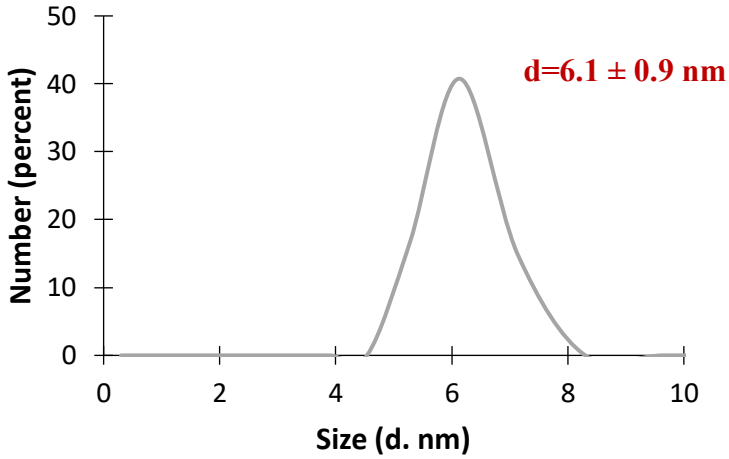

Figure 4.12 Particle size distribution of particle size 2 (Malvern analyzer)

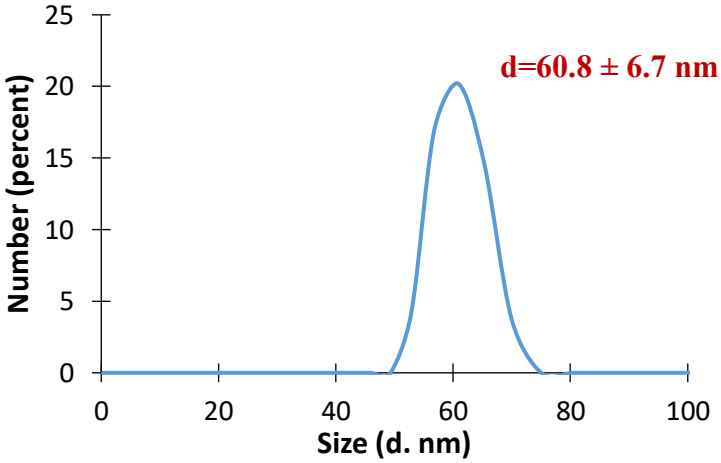

Figure 4.13 Particle size distribution of particle size 3 (Malvern analyzer)

4.4.3 Ultraviolet-Visible (UV-Vis) Spectroscopy

One of the most significant techniques for determining the formation of metal nanoparticles in aqueous solution is UV–Visible spectroscopy. Thus, the synthesized samples were characterized with aforementioned spectroscopy. Firstly, UV-Visible spectra of the chloroplatinic acid (H_2PtCl_6) are checked for Pt (before synthesis). There is a single maximum absorption band at 260 nm (Figure 4.14). This band corresponds to the absorption of Pt^{4+} ions [86], [87].

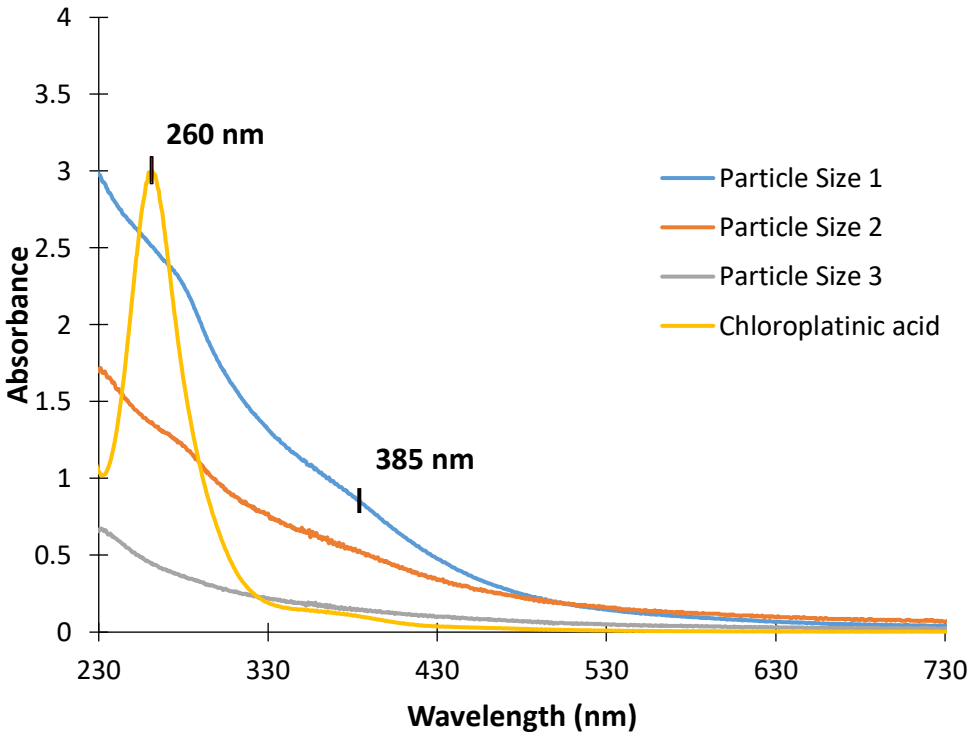

Figure 4.14 UV-Vis spectra of chloroplatinic acid and Pt NPs for each particle size

Before measuring the absorbance of synthesized Pt NP sols, the solutions were mixed for half an hour, and they were diluted with ultrapure water at 1:4 ratio. The UV–Visible spectra of the synthesized platinum nanoparticles are also shown in Figure 4.14. After the reduction of Pt^{4+}, the peak at 260 nm is negligible while a continuum which dominates near 230 nm are observed. This situation shows that Pt^{4+} ions were reduced to Pt^{0} nanoparticles. The absence of this peak indicates the reduction of Pt ions [86]. The weak peak obtained at 385 nm indicates the surface plasmonic resonance. Surface plasmonic resonance occurs when nanoparticles absorb light at different UV-Vis wavelengths and are excited due to charge density [88].

The proportion of light that is absorbed is determined by the number of molecules with which it interacts, according to UV principles. Concentrated solutions have a greater number of molecules that interact with the light that enters, enhancing absorbance [89].

Pt NPs concentration of particle size 1 (small-3.0 nm), 2 (medium-5.8 nm) and 3 (large-60.9 nm) were calculated as $1.87x10^{14}$ NP/ml, $2.65x10^{13}$ NP/ml and $2.28x10^{10}$ NP/ml, respectively (Table 4.1). Thus, high absorbance value was achieved with smallest particle size which was the more concentrated sol as shown in Figure 4.14. Concentration calculation of Pt NPs was shown in Appendix D in detail.

Table 4.1 Concentration of Pt NPs for different particle sizes

	Concentration (NP/mL)
Particle Size 1 (Small-3.0 nm)	$1.87x10^{14}$
Particle Size 2 (Medium-5.8 nm)	$2.65x10^{13}$
Particle Size 3 (Large-60.9 nm)	$2.28x10^{10}$

4.4.4 Malvern Concentration Analyzer

Concentration of Pt NPs were also confirmed by taking measurements from the Malvern concentration analyzer in Figure 4.15, 4.16 and 4.17.

Concentration measurements obtained from the Malvern concentration analyzer were quite similar to the calculated concentration data (Table 4.1).

The concentration of first particle (small-3.0 nm) was found as $2.21x10^{14}$ particles/ml. The concentration of second particle (medium-5.8 nm) was found as $1.98x10^{13}$ particles/ml. The concentration of third particle (large-60.9 nm) was found as $2.17x10^{10}$ particles/ml.

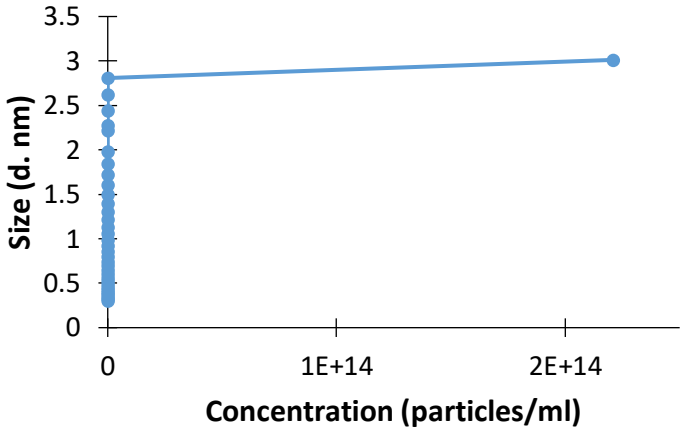

Figure 4.15 Concentration of particle size 1 (small-3.0 nm)-Malvern analyzer

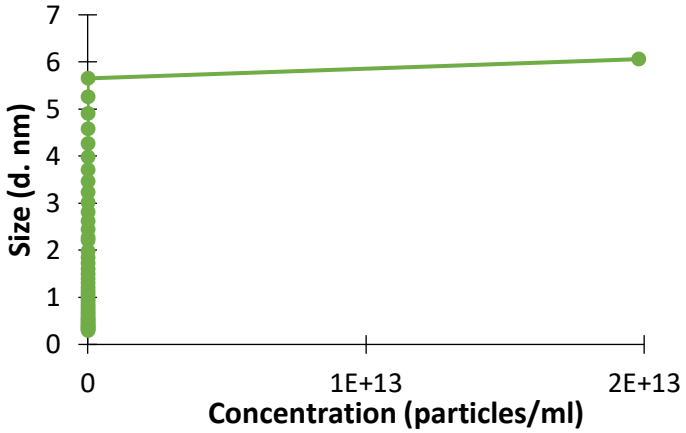

Figure 4.16 Concentration of particle size 2 (medium-5.8 nm)-Malvern analyzer

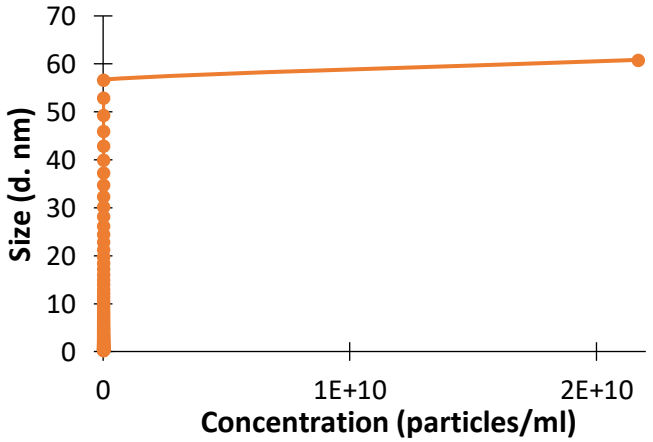

Figure 4.17 Concentration of particle size 3 (large-60.9 nm)-Malvern analyzer

4.5 Aqueous-phase HDC of TCE with Pt NPs: Catalytic Activity

Batch reactor studies were done for every particle size using 20 ppm initial TCE concentration at 30 ^{o}C and 1 atm. As expected from reaction scheme, HCl concentration increased with respect to time. When HCl concentration stayed constant, the reaction is completed. Chloride concentration was measured with the help of chloride detector. For 20 ppm initial TCE concentration, the maximum Cl ion concentration to be obtained at the end of the experiment is 16.17 ppm from reaction stoichiometry. Assuming no chloride induced deactivation under these conditions, the chloride concentration values were normalized. Almost 100% conversion was achieved in all experiments (Figure 4.18, Figure 4.20 and Figure 4.22). Catalytic activity tests for each particle size were run multiple times to check consistency. Conversion calculations were shown in Appendix E. To obtain a rate constant while performing the kinetic study, these data were averaged and plotted with the error bars based on standard deviation (Figure 4.19, Figure 4.21 and Figure 4.23). Particle 1 (smallest one) reached 100% conversion in approximately 1 hour.

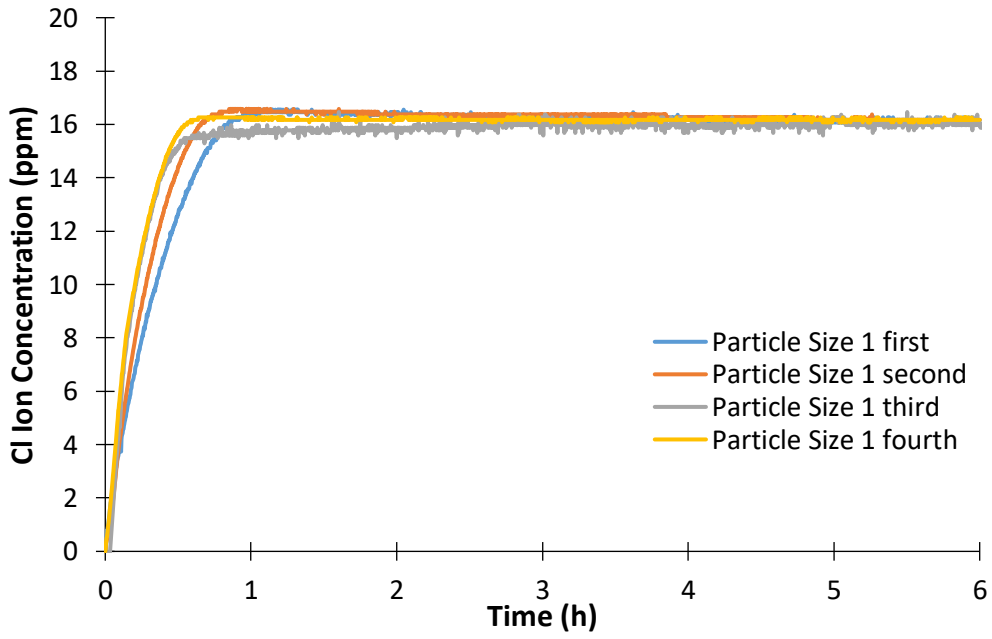

Figure 4.18 Catalytic activity test of particle size 1 (small-3.0 nm), reaction conditions: 1 atm and 30^{o}C with 4 mL Pt NPs

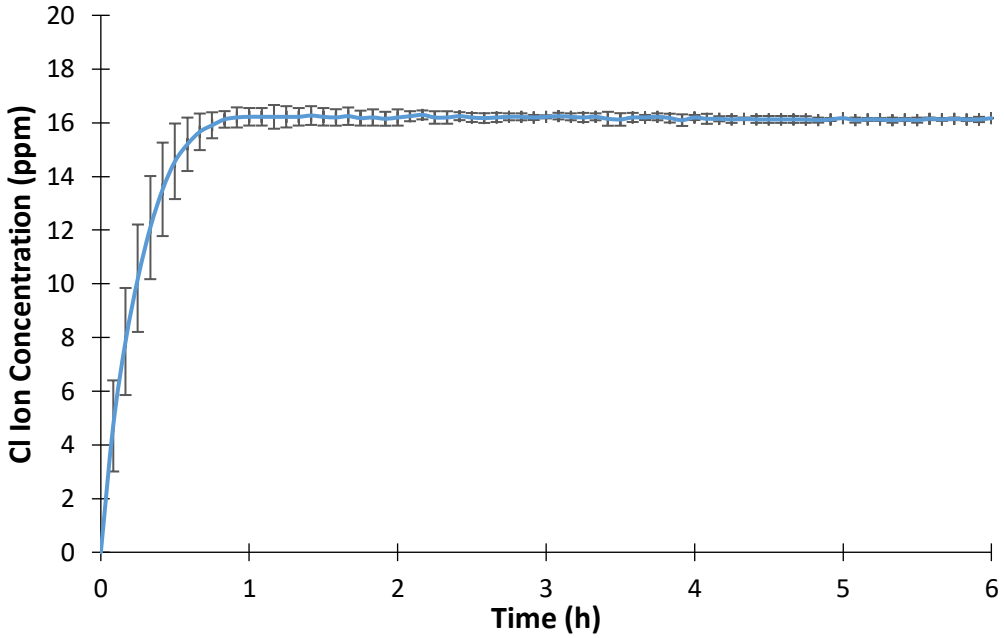

Figure 4.19 Catalytic activity test of particle size 1 (small-3.0 nm) with error bars

Particle 2 reached 100% conversion in approximately 3-4 hours later.

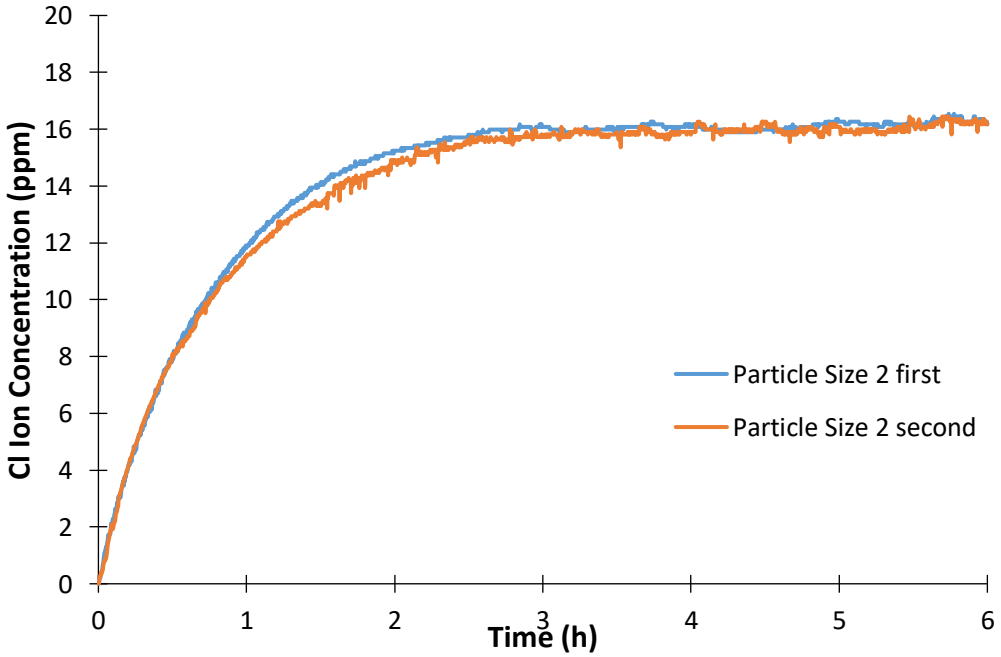

Figure 4.20 Catalytic activity test of particle size 2 (medium-5.8 nm), reaction conditions: 1 atm and 30^{o}C with 4 mL Pt NPs

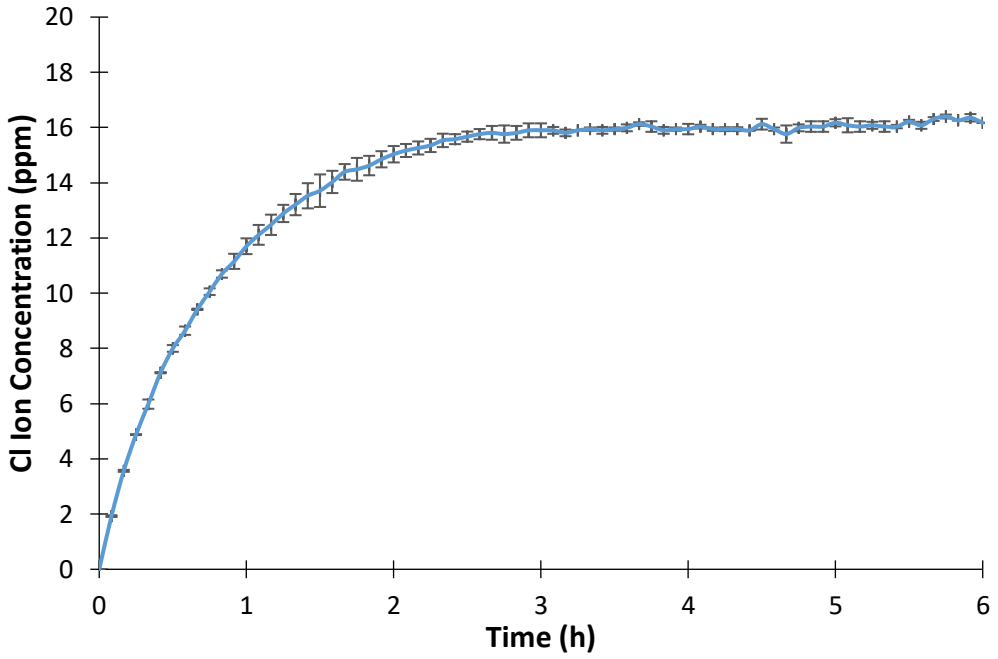

Figure 4.21 Catalytic activity test of particle size 2 (medium-5.8 nm) with error bars

Particle 3 reached 100% conversion in approximately 9 hours later.

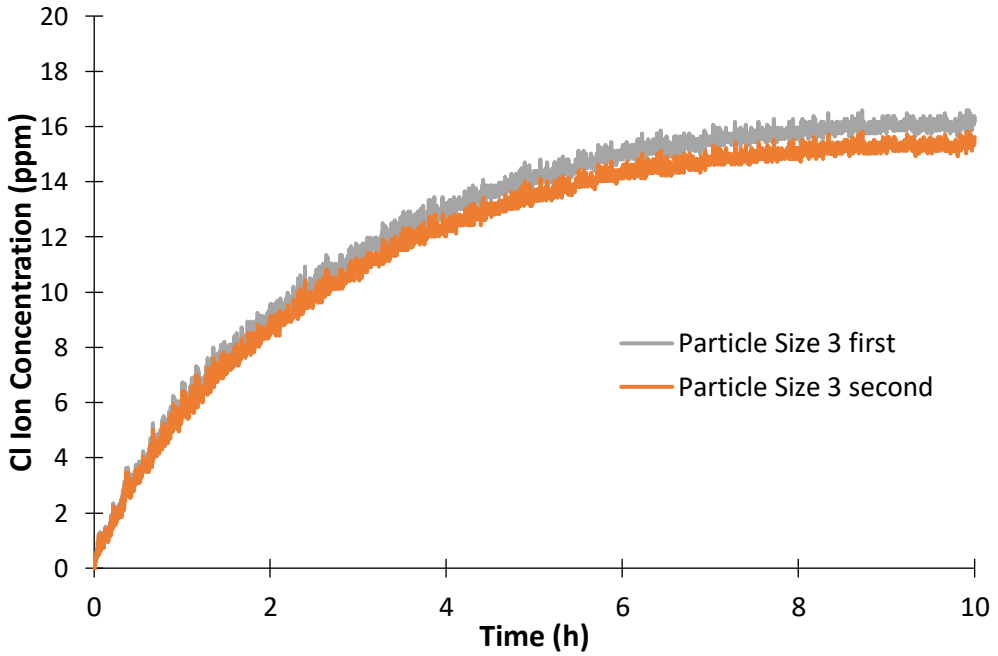

Figure 4.22 Catalytic activity test of particle size 3 (large-60.9 nm), reaction conditions: 1 atm and 30^{o}C with 4 mL Pt NPs

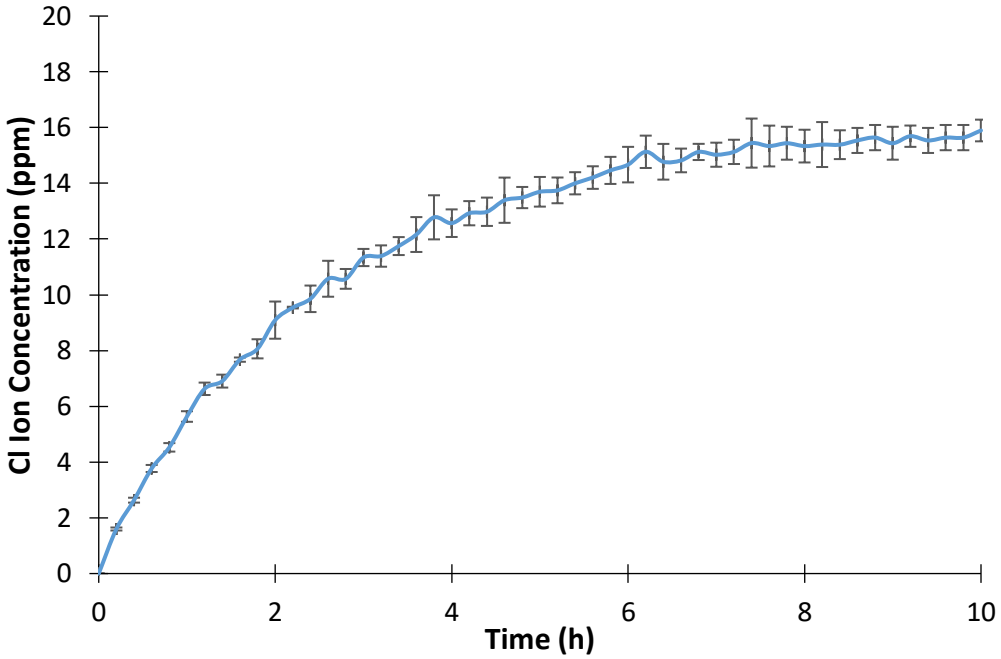

Figure 4.23 Catalytic activity test of particle size 3 (large-60.9 nm) with error bars

A first-order reaction such as HDC of TCE should reach complete conversion in a batch-reactor unless there is a deactivation and/or an inhibition effect [20], [33], [35], indicating a complete loss of activity over this catalyst. It has been reported in the literature that Pt/Al_2O_3 catalysis is not resistant to deactivation in hydrodechlorination and therefore the conversion is low [29], [30]. However, 100% conversion was achieved with Pt nanoparticles in all three different particle sizes.

4.6 Effect of Particle Size on TCE HDC Catalytic Activity of Pt NPs

Batch reactor kinetic studies showed that the TCE HDC activity of the Pt NP sols varied with Pt NP size, as shown in Figure 4.24. The activity experiments show that concentration on Cl ion with respect to time. As expected, the fastest reaction kinetic was observed at the smallest particle size.

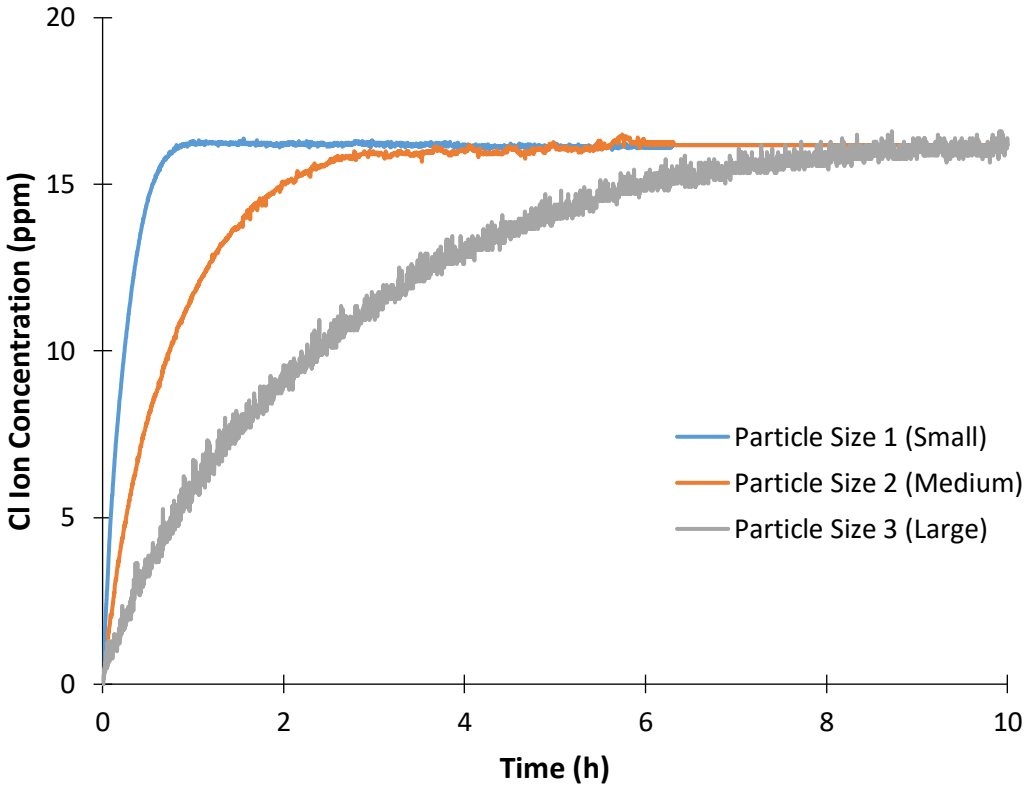

Figure 4.24 Catalytic activity test for different particle sizes (3.0, 5.8 and 60.9 nm), $C_{TCE,0}$=20 ppm, reaction conditions: 1 atm and 30°C

To understand kinetic structure of this reaction, rate calculations were done. Initially, rate constant (k) of each particle size was determined (Figure 4.25, Figure 4.26 and Figure 4.27). Rate constant calculations were shown in Appendix E and F. Slope of graphs gave us a rate constant based on a unit volume of reacting fluid (Equation 4.25).

Based on unit volume of reacting fluid:

$$r_{TCE} = \frac{1}{V}\frac{dN_{TCE}}{dt} = \frac{moles\ TCE\ reacted}{(volume\ of\ fluid)(time)} = -kC_{TCE} \qquad (4.25)$$

Where r_{TCE} is rate of reaction, k is reaction rate constant, and C_{TCE} is concentration of TCE.

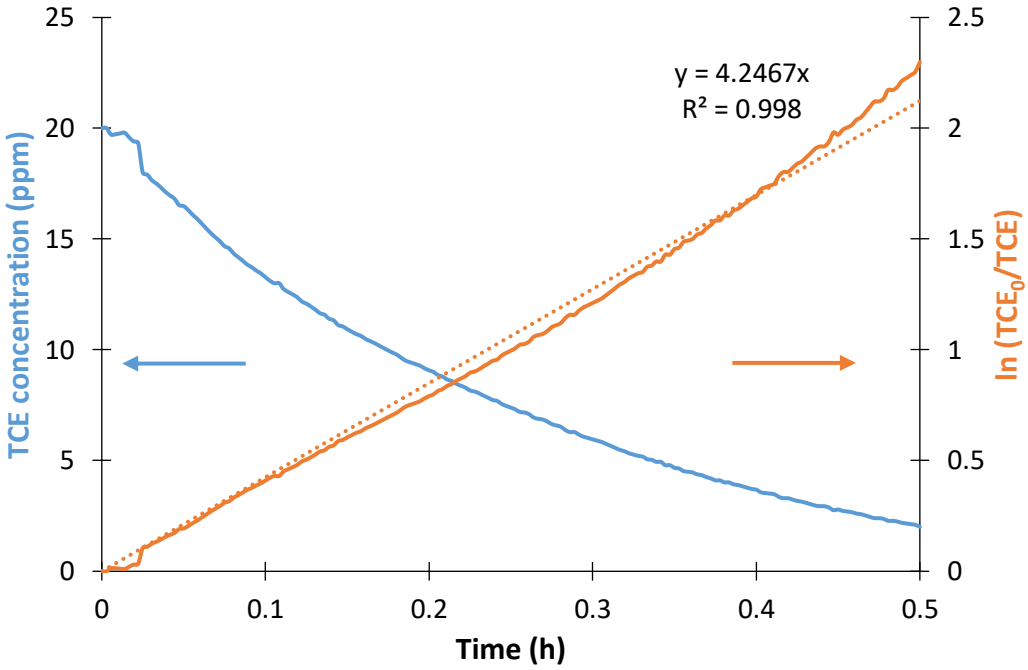

Figure 4.25 Rate constant determination of particle size 1 (small-3.0 nm), reaction conditions: 1 atm and 30°C with 4 mL Pt NPs

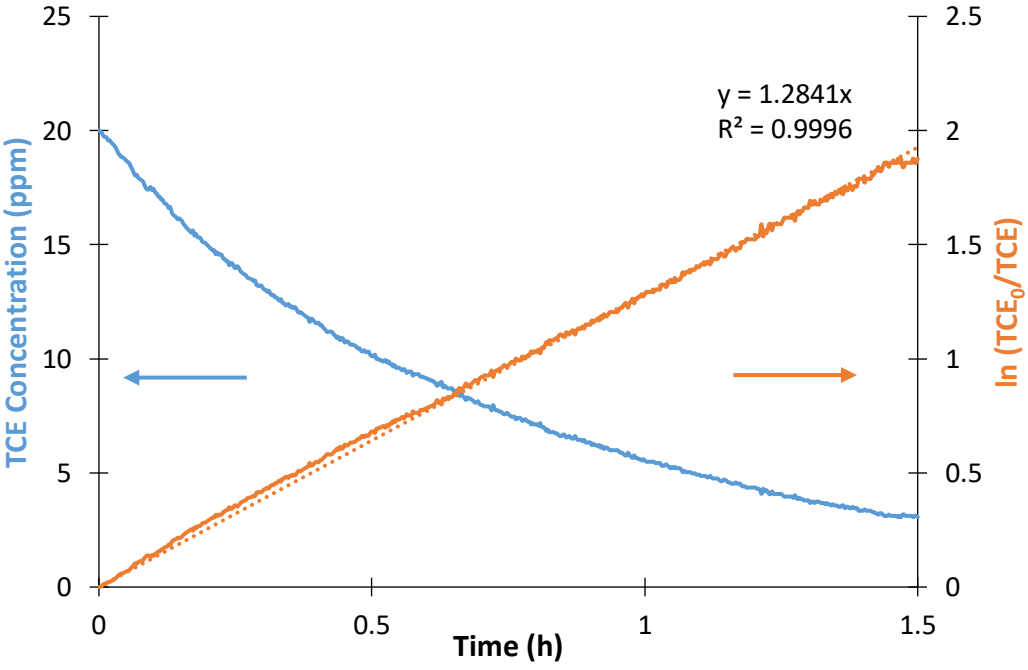

Figure 4.26 Rate constant determination of particle size 2 (medium-5.8 nm), reaction conditions: 1 atm and 30°C with 4 mL Pt NPs

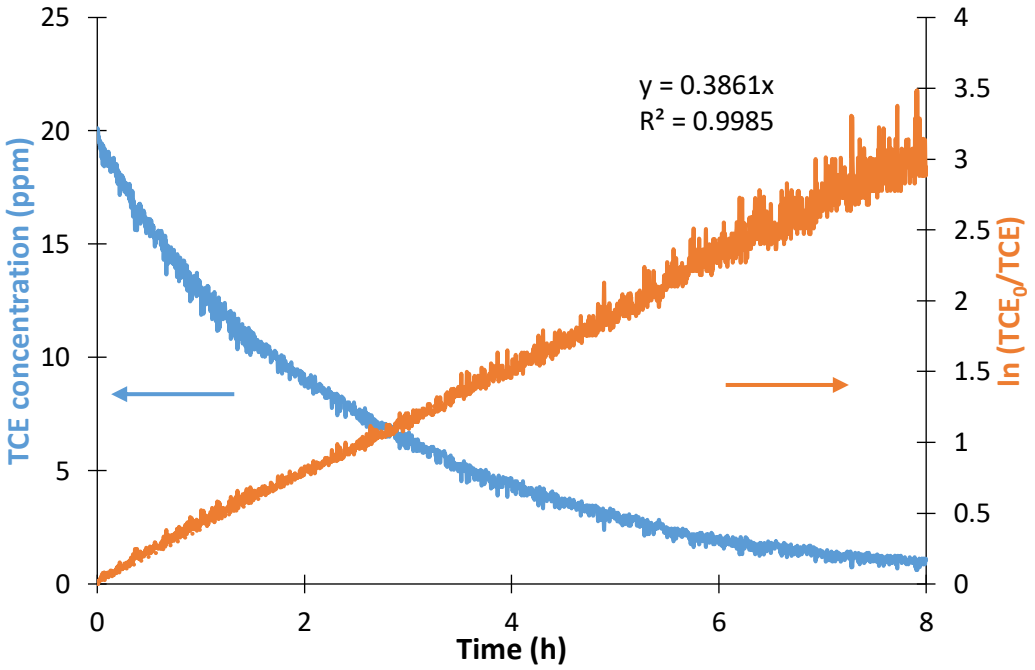

Figure 4.27 Rate constant determination of particle size 3 (large-60.9 nm), reaction conditions: 1 atm and 30°C with 4 mL Pt NPs

Rate constants were found as 4.2 h^{-1}, 1.3 h^{-1} and 0.4 h^{-1} for Particle size 1, 2 and 3, respectively. Rate constants (k) were also calculated based on unit mass of solid in fluid-solid system (k') and unit interfacial surface in two fluid systems (k") (Equations 4.26-4.28). Based on total Pt atoms, initial turnover frequency (TOF) values were also calculated. Necessary equations were given in Appendix F, and summary of results was shown in Table 4.2.

Based on unit mass of solid in fluid – solid systems:

$$r'_{TCE} = \frac{1}{W}\frac{dN_{TCE}}{dt} = \frac{moles\ TCE\ formed}{(mass\ of\ catalyst)(time)} = -k'C_{TCE} \qquad (4.26)$$

Based on unit interfacial surface in two fluid systems:

$$r''_{TCE} = \frac{1}{S}\frac{dN_{TCE}}{dt} = \frac{moles\ TCE\ formed}{(surface\ of\ catalyst)(time)} = -k''C_{TCE} \qquad (4.27)$$

$$r_{TCE}.V = r'_{TCE}.W = r''_{TCE}.S \qquad (4.28)$$

Table 4.2 Summary of rate constants for each particle size, $C_{TCE,0}$=20 ppm

	k (h^{-1})	k' $(\frac{L}{g\ Pt.min})$	k'' $(\frac{L}{m_{surf\ Pt}^2.min})$	**Initial TOF** $(\frac{mol\ TCE}{mol\ Pt.s})$
Particle Size 1 (Small-3.0 nm)	4.2	156.3	1.7	0.077
Particle Size 2 (Medium-5.8 nm)	1.3	47.3	1.0	0.023
Particle Size 3 (Large-60.9 nm)	0.4	14.2	3.1	0.007

As shown in Table 4.2, reaction rate constant based on unit volume of reacting fluid, k, decreased with increasing of particle size. Same volume of fluid (0.510 L) was used in all experiments. Decreasing the particle size increases the number of particles represented by the same volume of fluid. Because the surface area of the reactant has been increased as particle size decreases, the rate of reaction increases. The more the accessible surface area for particles to collide, the faster reaction occurs. The reaction rate constant based on unit mass of fluid-solid systems, k', also decreased with increasing of particle size. Same weight of catalyst (0.231 mg Pt) was used in all experiments. Decreasing the particle size increases the number of particles represented by the same catalyst weight. The reaction rate constant based on unit interfacial surface in two fluid systems, k'', decreased when increasing particle size from 3.0 nm to 5.8 nm. However, this rate constant was calculated as highest at largest particle (60.9 nm) because of larger diameter.

The initial turnover frequency (TOF) was calculated based on initial rate and molar concentration of Pt in the batch reactor. TOF is a measure of the instantaneous efficiency of a catalyst, and it is calculated as the derivative of the number of turnovers of the catalytic cycle with respect of the time per active site. As shown in Figure 4.28 and Table 4.2, TOF data decreased with increasing particle size. These results demonstrated that HDC of TCE is a structure sensitive reaction.

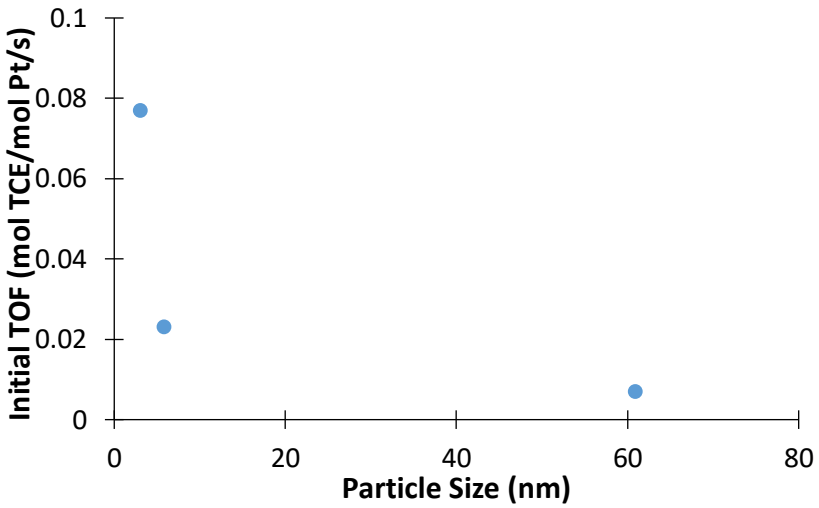

Figure 4.28 Initial TOF data with respect to particle size, $C_{TCE,0}$=20 ppm, reaction conditions: 1 atm and 30^{o}C

4.7 Effect of TCE Concentration on TCE HDC Catalytic Activity of Pt NPs

To check TCE concentration effect on TCE HDC catalytic activity, batch reactor studies were also done with 1000 ppm initial TCE concentration for every particle size (Figure 4.29). Same experimental procedure was applied as mentioned Section 3.4.2.

For 1000 ppm initial TCE concentration, the maximum Cl ion concentration to be obtained at the end of the experiment is 808.5 ppm from reaction stoichiometry. For this time, while higher catalytic activity (55% conversion) was achieved with Particle 1 (smallest), conversion of TCE was lower with 48% and 35% for Particle Size 2 and 3, respectively.

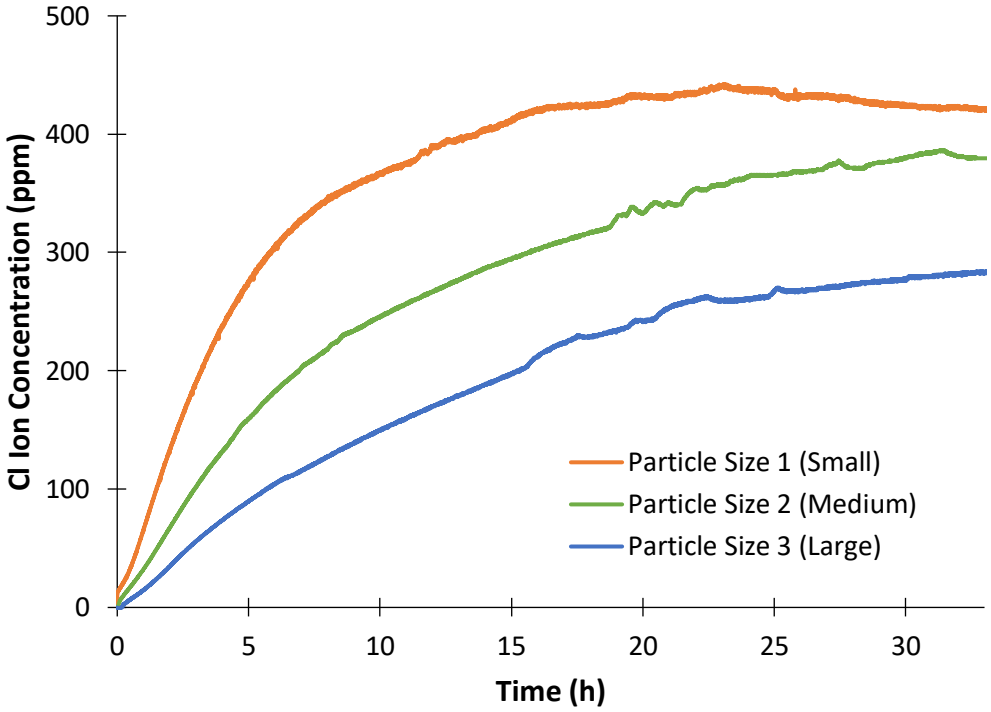

Figure 4.29 Catalytic activity test for different particle sizes (3.0, 5.8 and 60.9 nm), $C_{TCE,0}$=1000 ppm), reaction conditions: 1 atm and 30°C with 4 mL Pt NPs

TCE HDC could not achieve 100 % conversion because of deactivation phenomena. Thus, deactivation parameter "a" and deactivation rate constant (k_d) are considered for kinetic studies (Equation 4.29)[79]. Since the deactivation parameter is an activity coefficient, a_0=1 at time=0 was assumed indicating that fresh catalyst was not deactivated. Necessary rate derivations were shown in Appendix G.

$$ln\left(ln\frac{(1-X_{TCE})}{(1-X_{TCE_\infty})}\right) = ln\left(\frac{k'W/V}{k_d}\right) - k_d t \qquad (4.29)$$

Rate calculations were done, and deactivation rate constant (k_d) were found for Particle size 1, 2 and 3 from the slope of graphs (Figure 4.30, 4.31 and 4.32) as 0.18 h^{-1}, 0.08 h^{-1} and 0.06 h^{-1}, respectively. Then, rate constants based on a unit volume of reacting fluid, mass of solid in fluid-solid system, unit interfacial surface in two fluid systems an initial turnover frequency (TOF) were also calculated (Appendix G).

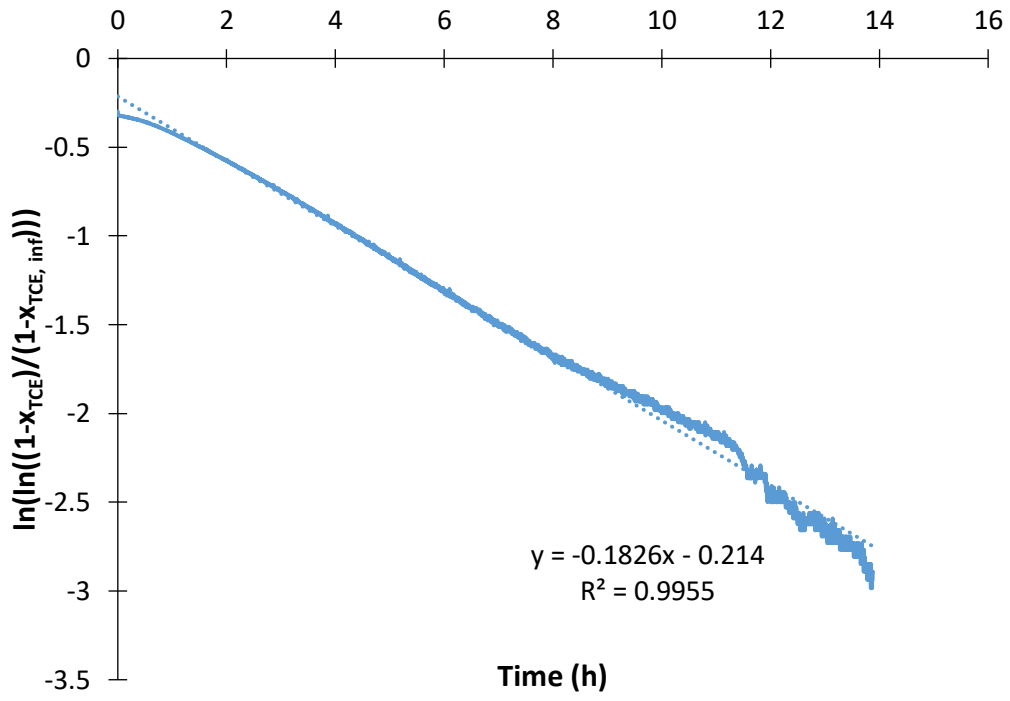

Figure 4.30 Deactivation rate constant determination of particle size 1 (small-3.0 nm)

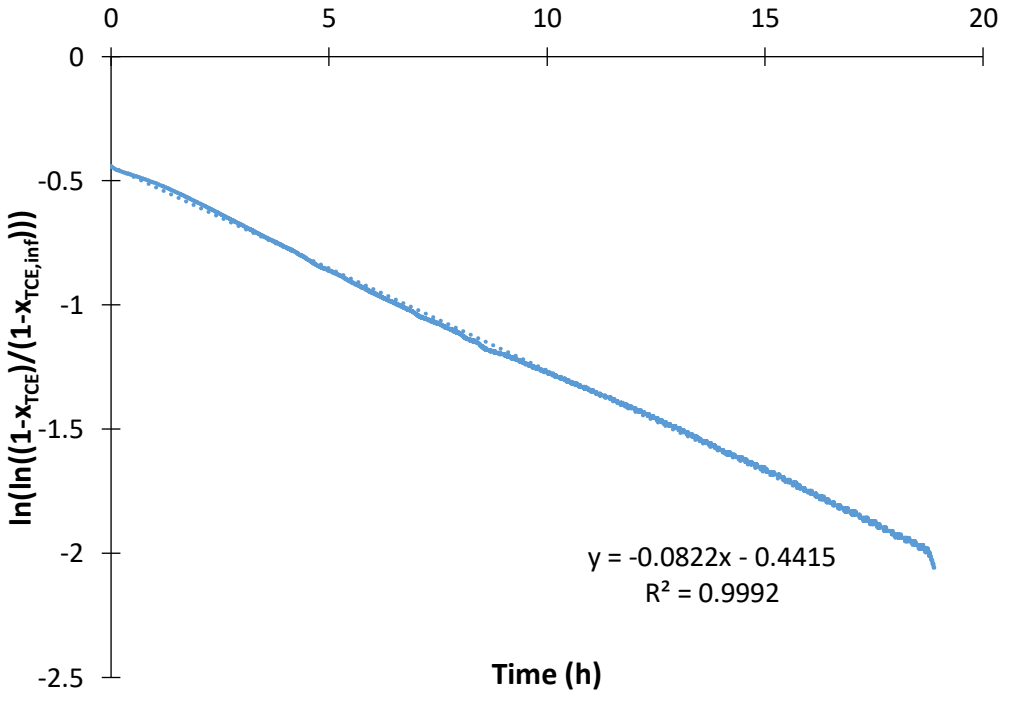

Figure 4.31 Deactivation rate constant determination of particle size 2 (medium-5.8 nm)

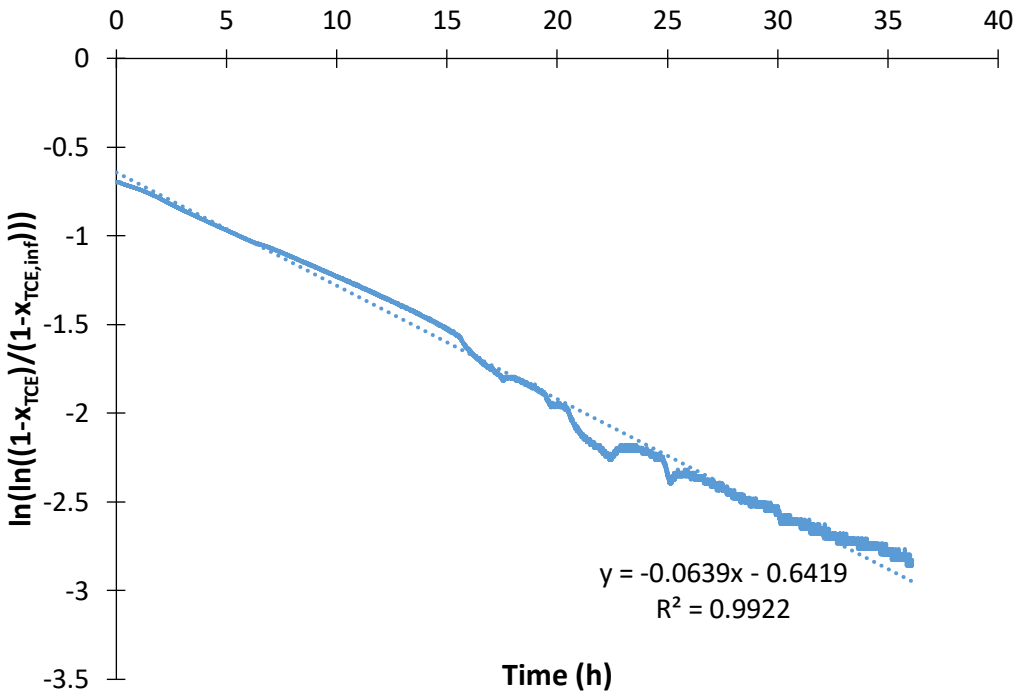

Figure 4.32 Deactivation rate constant determination of particle size 3 (large-60.9 nm)

Summary of results was shown in Table 4.3.

Table 4.3 Summary of rate constants for each particle size, $C_{TCE,0}$=1000 ppm

	k_d (h^{-1})	k (h^{-1})	k' $(\frac{L}{g\ Pt.min})$	$k''(\frac{L}{m_{surf\ Pt}{}^2.min})$	Initial TOF $(\frac{mol\ TCE}{mol\ Pt.s})$
Particle Size 1 (Small)	0.18	0.15	5.41	0.06	0.13
Particle Size 2 (Medium)	0.08	0.05	1.95	0.04	0.05
Particle Size 3 (Large)	0.06	0.03	1.25	0.27	0.03

As shown in Table 4.3, deactivation rate constant decreased with increasing particle size. That is, smallest particle deactivates faster at 1000 ppm initial TCE concentration. However, if we consider the k_d to k ratios, this deactivation ratio is the smallest in the smallest particle.

Other rate constants (k, k' and k'') provide the same situation with 20 ppm initial TCE concentration. The reaction rate constant based on unit mass of fluid-solid systems, k', decreased with increasing of particle size. The reaction rate constant based on unit interfacial surface in two fluid systems, k'', decreased when increasing particle size from 3.0 nm to 5.8 nm. However, this rate constant was calculated as highest at largest particle (60.9 nm) because of larger diameter.

At a higher initial liquid-phase TCE concentration of 1000 ppm, the rate constants were lower. Pt NPs lost their first-order dependence on TCE concentration because hydrogen was not excess in this case.

As shown in Figure 4.33 and Table 4.3, TOF data also decreased with increasing particle size. These results demonstrated that HDC of TCE is a structure sensitive reaction.

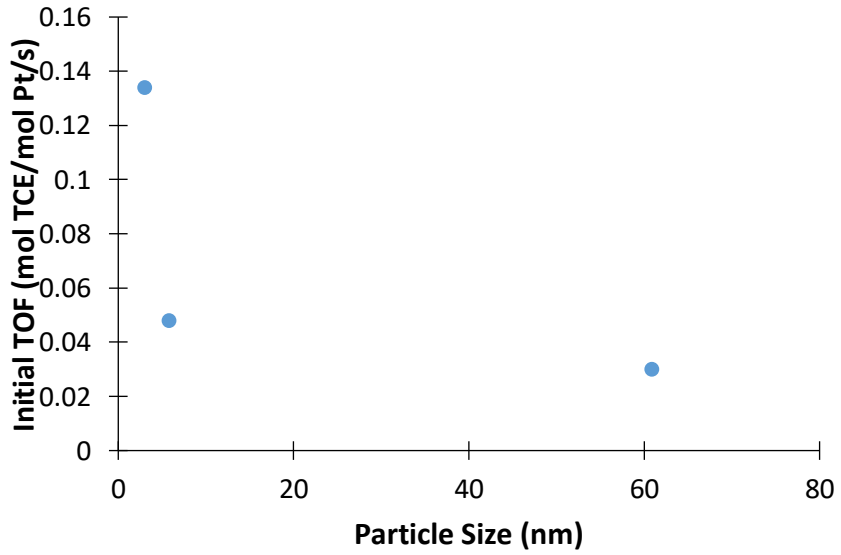

Figure 4.33 Initial TOF data with respect to particle size, $C_{TCE,0}$=1000 ppm, reaction conditions: 1 atm and 30°C with 4 mL Pt NPs

4.8 HCl Poisoning Experiments

As the aim of this study, the effect of particle size of catalysis on chloride resistance were investigated. The deactivation resistance test was planned as follows:

i. Increase in HCl concentration was expected as a result of our HDC of TCE reaction).
ii. The reaction was completed when the HCl concentration stays constant.
iii. When HCl concentration was constant, the reaction was forced to start by injection of TCE.
iv. Changes of HCl concentration with respect to repeated doses of TCE indicated the resistance to deactivation.

To check HCl poisoning, semi-batch reactor studies were done with 20 ppm initial TCE concentration for every particle size (Figure 4.34, 4.35 and 4.36). Same experimental procedure was applied as mentioned Section 3.4.2. 20 ppm TCE was injected at the end of each cycle. This shows that it works in a semi-batch procedure.

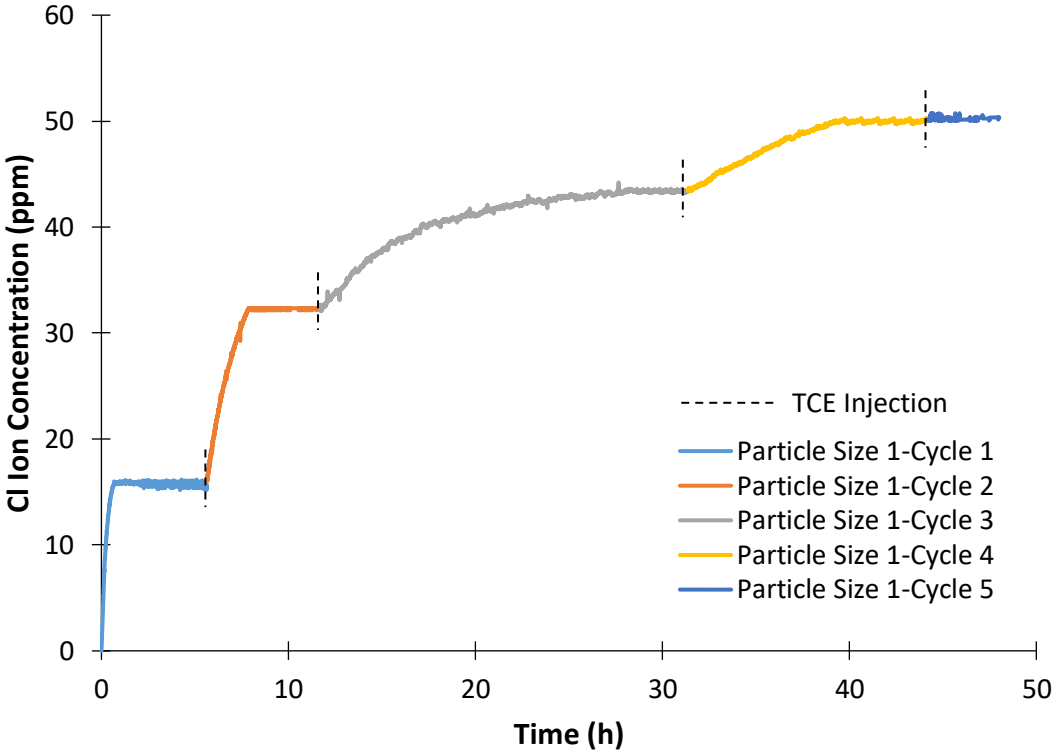

Figure 4.34 HCl poisoning experiment-Particle 1 (small-3.0 nm), reaction conditions: 1 atm and 30°C with 4 mL Pt NPs

For particle size 1, there are 5 cycles, and total reaction time is approximately 50 hours (Figure 4.34). At the end of these 5 cycles, chloride concentration is found as approximately 50 ppm. 100% conversion was achieved in the first two cycles, but in the second cycle the rate of the reaction starts to decrease. It takes about 1 hour to reach 100% conversion in the first cycle, while it takes about 3 hours to reach 100% conversion in the second cycle. After second cycle, catalyst begins to deactivate and does not reach 100% conversion. In the third cycle, it takes about 17 hours for the chloride concentration to stabilize, and the conversion was approximately 72%. In the fourth cycle, it takes approximately 9 hours for the chloride concentration to stabilize, and the conversion decreased to 37%. As the activity still continued, TCE injection was done for the fifth time. However, since no increase was observed in the chloride concentration after injection. For this reason, it was understood that the catalyst was completely deactivated.

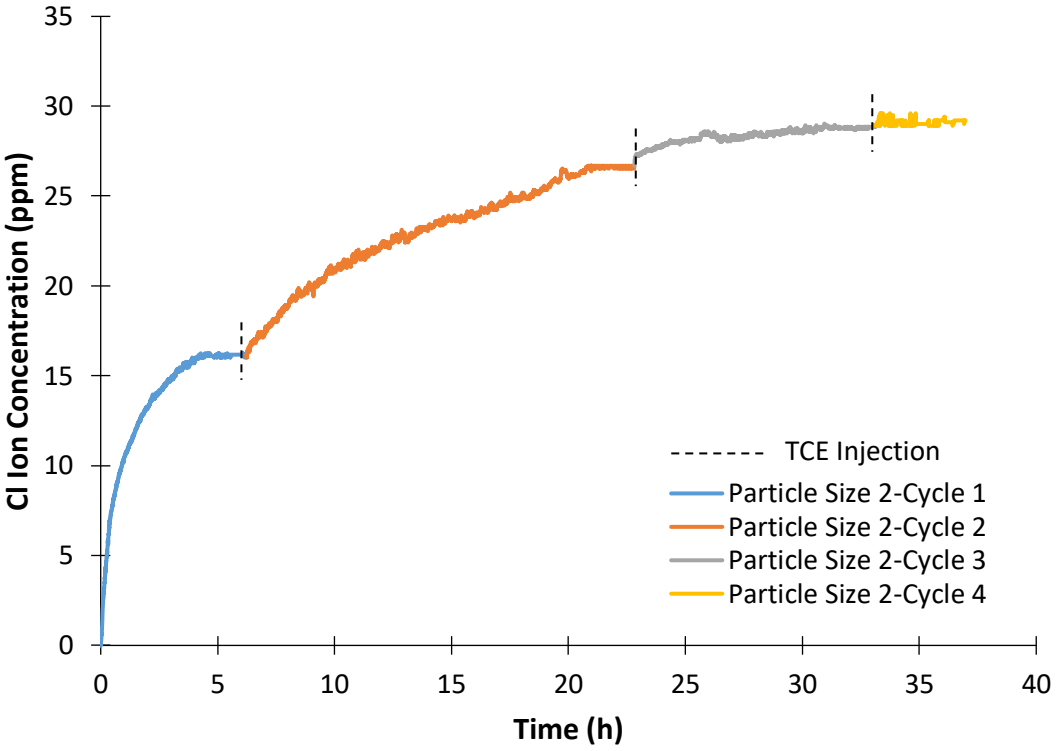

Figure 4.35 HCl poisoning experiment-Particle 2 (medium-5.8 nm), reaction conditions: 1 atm and 30^{o}C with 4 mL Pt NPs

For particle size 2, there are 4 cycles, and total reaction time is approximately 36 hours (Figure 4.35). At the end of these 4 cycles, chloride concentration is found as approximately 30 ppm. 100% conversion was only achieved in first cycle. It takes about 4 hours to reach 100% conversion in the first cycle. After first cycle, catalyst begins to deactivate and does not reach 100% conversion. In the second cycle, it takes about 15 hours for the chloride concentration to stabilize, and the conversion was approximately 67%. In the third cycle, it takes about 5 hours for the chloride concentration to stabilize, and the conversion was approximately 14%. As the activity still continued, TCE injection was done for the fourth time. However, since no increase was observed in the chloride concentration after injection. For this reason, it was understood that the catalyst was completely deactivated.

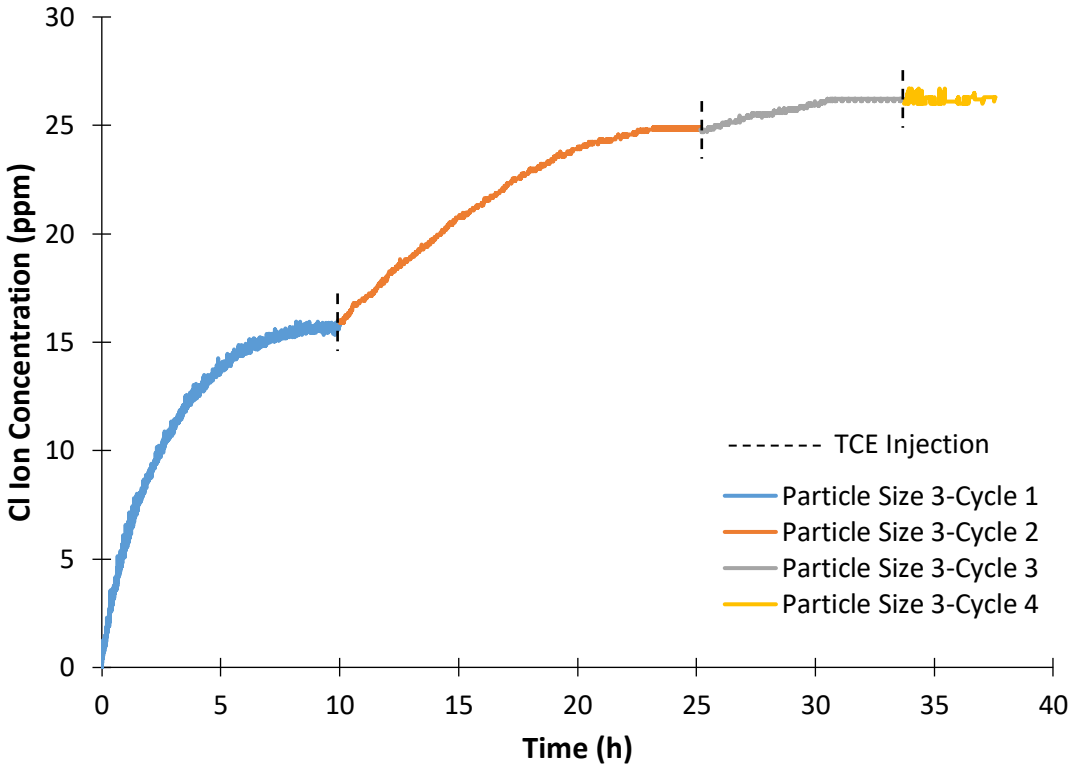

Figure 4.36 HCl poisoning experiment-Particle 3 (large-60.9 nm), reaction conditions: 1 atm and 30°C with 4 mL Pt NPs

For particle size 3, there are 4 cycles, and total reaction time is approximately 38 hours (Figure 4.36). At the end of these 4 cycles, chloride concentration is found as approximately 27 ppm. 100% conversion was only achieved in first cycle. It takes about 10 hours to reach 100% conversion in the first cycle. After first cycle, catalyst begins to deactivate and does not reach 100% conversion. In the second cycle, it takes about 14 hours for the chloride concentration to stabilize, and the conversion was approximately 54%. After second cycle, the reaction rate is greatly reduced. In the third cycle, it takes about 5 hours for the chloride concentration to stabilize, and the conversion was approximately 12%. As the activity still continued, TCE injection was done for the fourth time. However, since no increase was observed in the chloride concentration after injection. It was understood that the catalyst was completely deactivated. HCl poisoning experiments show us highest resistance to chloride poisoning were observed at the smallest particle size.

CHAPTER 5

CONCLUSIONS AND RECOMMENDATIONS

In this study, the effect of particle size of Pt nanoparticles on resistance to chloride poisoning was investigated for HDC of TCE in water. It has been shown that chloride poisoning caused by HCl can be prevented by designing the system.

For this experimental system, three different sizes of Pt nanoparticles were successfully synthesized with modified Slot-Geuze colloidal synthesis method. The size distribution of these particles was examined with transmission electron microscopy, and about 100-150 particles were measured for all of them. Accordingly, particle sizes were measured as 3.0, 5.8 and 60.9 nm in diameters, respectively. Malvern particle size analyzer was also used for particle size distribution and these results support the TEM results. The formation and reduction of these particles was confirmed by UV-Vis spectroscopy.

Reactor verification was done in the experimental system before starting the experiments. For this, two experiments were carried out: (i) in the absence of hydrogen in the presence of catalyst, (ii) in the presence of hydrogen in the absence of catalyst. TCE conversion has been confirmed to be a meaningful parameter that can be used to evaluate the catalytic activity of TCE HDC. The presence of hydrogen and catalyst is important for this experiment.

Heat and mass transfer limitations were investigated in the experimental system. For HDC of TCE, which is an exothermic reaction, the adiabatic temperature rise was calculated as 1.36 K and it was shown that there was no heat effect in the system. Since there is more than one phase in the reactor system, mass transfer effects were tried to be minimized as much as possible to achieve the most accurate kinetics. The tests comprised of doing HDC of TCE experiments at different stirring speeds (500, 625, 750 rpm) and with different stir bar types (standard, triangular, cross).

The maximum catalytic activity was attained with a 750 rpm stirring rate and triangular stir bar. As a result, all kinetic analyses provided in this study were carried out at a mixing rate of 750 rpm with triangular stir bar to reduce external mass transfer resistances. In addition to this, the gas-liquid, liquid-solid mass transfer coefficients, and the surface reaction for each NP catalyst were experimentally quantified. A 750 rpm stirring rate which was found high enough for gas-liquid mass transfer to be negligible, indicating that $k_{GL}a_{GL}$ is very large. Moreover, $1/ka_s$, the surface reaction resistance was found to be much greater than $1/k_{LS}a_s$, indicating the mass transfer effect through the diffusion layer can also be neglected.

Catalytic activity tests were performed after the mass transfer effects were minimized. Firstly, the effect of particle size on TCE HDC catalytic activity of Pt NPs was investigated. For 20 ppm initial TCE concentration, almost 100% conversion was achieved in all experiments. As expected, the fastest reaction kinetic was observed at the smallest particle size. Rate constants were found as 4.2 h^{-1}, 1.3 h^{-1} and 0.4 h^{-1} for Particle size 1, 2 and 3, respectively. Rate constants (k) were also calculated based on unit mass of solid in fluid-solid system (k') and unit interfacial surface in two fluid systems (k"). The initial turnover frequency (TOF) was calculated based on initial rate and molar concentration of Pt in the batch reactor. TOF data decreased with increasing particle size. These results demonstrated that HDC of TCE is a structure sensitive reaction.

Secondly, batch reactor studies were also done with 1000 ppm initial TCE concentration for every particle size to check TCE concentration effect on TCE HDC catalytic activity. For this time, while higher catalytic activity (55% conversion) was achieved with Particle 1 (smallest), conversion of TCE was lower with 48% and 35% for Particle Size 2 and 3, respectively. TCE HDC could not achieved 100 % conversion because of deactivation phenomena. Deactivation rate constant (k_d) were found as 0.18 h^{-1}, 0.08 h^{-1} and 0.06 h^{-1} for Particle size 1, 2 and 3, respectively. Deactivation rate constant decreased with increasing particle size. That is, smallest particle deactivates faster at 1000 ppm initial TCE concentration. However, if we

consider the k_d to k ratios, this deactivation ratio is the smallest in the smallest particle. At a higher initial liquid-phase TCE concentration of 1000 ppm, the rate constants were lower. Pt NPs lost their first-order dependence on TCE concentration because hydrogen was not excess in this case. Initial TOF data also decreased with increasing particle size in this case.

Finally, the effect of particle size of catalysis on chloride resistance were investigated as the purpose of this study. Increase in HCl concentration was expected as a result of our HDC of TCE reaction. The reaction was completed when the HCl concentration stays constant. When HCl concentration was constant, the reaction was forced to start by injection of TCE. Changes of HCl concentration with respect to repeated doses of TCE indicated the resistance to deactivation.

For particle size 1, there were 5 cycles, and total reaction time was approximately 50 hours. At the end of these 5 cycles, chloride concentration was found as approximately 50 ppm. 100% conversion was achieved in the first two cycles, but in the second cycle the rate of the reaction started to decrease. After second cycle, catalyst begins to deactivate and the conversion was found as 72% and 37% in the third and fourth cycles, respectively. Since no increase was observed in the chloride concentration after fifth injection, it was understood that the catalyst was completely deactivated.

For particle size 2, there were 4 cycles, and total reaction time was approximately 36 hours. At the end of these 4 cycles, chloride concentration was found as approximately 30 ppm. 100% conversion was only achieved in first cycle. After first cycle, the conversion was found as 67% and 14% in the second and third cycles, respectively. No increase in chloride concentration was observed after fourth injection, indicating deactivation.

For particle size 3, there were 4 cycles, and total reaction time is approximately 38 hours. At the end of these 4 cycles, chloride concentration was found as approximately 27 ppm. 100% conversion was only achieved in first cycle. In the

second and third cycles, the conversion was found as 54% and 12% in the third and fourth cycles, respectively. No increase was observed in the chloride concentration after fourth injection, indicating deactivation. This shows us highest chloride poisoning resistance due to HCl were observed at the smallest particle size.

A smaller particle around 10 nm for a third particle can be synthesized. In this way, the interval between particle sizes is closer and effect of particle size can be seen better.

The potential of Pt NPs as a groundwater remediation technology can be improved by immobilizing them on a solid support.

REFERENCES

[1] T. C. Kalkinma Bakanliği Özel İhtisas Komisyonu Raporu, “Su Kaynakları Yönetimi ve Güvenliği Ankara 2014.”

[2] C. E. Clark and J. A. Veil, “Produced water volumes and management practices in the United States.,” United States, 2009. doi: 10.2172/1007397.

[3] M. Moran, Occurrence and Implications of Selected Chlorinated Solvents in Ground Water and Source Water in the Occurrence and Implications of Selected Chlorinated Solvents in Ground Water and Source Water in the United States and in Drinking Water in 12 Northeast a. 2006.

[4] R. E. Doherty, “A History of the Production and Use of Carbon Tetrachloride, Tetrachloroethylene, Trichloroethylene and 1,1,1-Trichloroethane in the United States: Part 1—Historical Background; Carbon Tetrachloride and Tetrachloroethylene,” *Environ. Forensics*, vol. 1, no. 2, pp. 69–81, Jun. 2000, doi: 10.1006/ENFO.2000.0010.

[5] P. J. Squillace and C. V Price, “Urban land-use study plan for the National Water-Quality Assessment Program,” 1996. doi: 10.3133/ofr96217.

[6] “National Primary Drinking Water Regulations Contaminant MCL or TT 1 (mg/L) 2 Potential health effects from long-term 3 exposure above the MCL Common sources of contaminant in drinking water Public Health Goal (mg/L) 2.”

[7] “European Union Risk Assessment Report.”

[8] “Summary Data for 2013 Priority List of Hazardous Substances ATSDR, Division of Toxicology & Human Health Sciences 1.”

[9] M. O. Nutt, J. B. Hughes, and M. S. Wong, “Designing Pd-on-Au bimetallic nanoparticle catalysts for trichloroethene hydrodechlorination,” *Environ. Sci. Technol.*, vol. 39, no. 5, pp. 1346–1353, Mar. 2005, doi: 10.1021/es048560b.

[10] “OPPT Trichloroethylene (TCE) Draft Risk Assessment Final Comments of 9 Member Peer Review Panel,” 2013, Accessed: Jun. 22, 2022. [Online].

Available: http://www.epa.gov/opptintr/exposure/pubs/efast.htm.

[11] M. S. Wong *et al.*, “Cleaner water using bimetallic nanoparticle catalysts,” *J. Chem. Technol. Biotechnol.*, vol. 84, no. 2, pp. 158–166, Feb. 2009, doi: 10.1002/jctb.2002.

[12] “World Health Organization Regional Offi ce for Europe Selected Pollutants,” Accessed: Jun. 22, 2022. [Online]. Available: www.euro.who.int.

[13] H. H. Russell, J. E. Matthews, G. W. Sewell, R. S. Kerr Environmental, and W. W. Kovalick, “Ground Water Issue EPA TCE Removal from Contaminated Soil and Ground Water Superfund Technology Support Center for Ground Water,” 1992.

[14] “Hydrodehalogenation of 1-to 3-Carbon Halogenated Organic Compounds in Water Using a Palladium Catalyst and Hydrogen Gas,” 1999, doi: 10.1021/es980963m.

[15] Z. Zhao, Y.-L. Fang, P. J. J. Alvarez, and M. S. Wong, “Degrading perchloroethene at ambient conditions using Pd and Pd-on-Au reduction catalysts,” *Appl. Catal. B-Environmental*, vol. 140, pp. 468–477, 2013, doi: 10.1016/j.apcatb.2013.04.032.

[16] A. Elola, E. Díaz, and S. Ordoñez, “A New Procedure for the Treatment of Organochlorinated Off-Gases Combining Adsorption and Catalytic Hydrodechlorination,” *Environ. Sci. Technol.*, vol. 43, no. 6, pp. 1999–2004, Mar. 2009, doi: 10.1021/es803226v.

[17] C. G. Schreier and M. Reinhard, “Catalytic hydrodehalogenation of chlorinated ethylenes using palladium and hydrogen for the treatment of contaminated water,” *Chemosphere*, vol. 31, no. 6, pp. 3475–3487, 1995, doi: 10.1016/0045-6535(95)00200-R.

[18] M. Martino, R. Rosal, H. Sastre, and F. V. Díez, “Hydrodechlorination of dichloromethane, trichloroethane, trichloroethylene and tetrachloroethylene over a sulfided Ni/Mo-γ-alumina catalyst,” *Appl. Catal. B Environ.*, vol. 20,

no. 4, pp. 301–307, Apr. 1999, doi: 10.1016/S0926-3373(98)00120-9.

[19] C. Schüth, S. Disser, F. Schüth, and M. Reinhard, “Tailoring catalysts for hydrodechlorinating chlorinated hydrocarbon contaminants in groundwater,” *Appl. Catal. B Environ.*, vol. 28, no. 3–4, pp. 147–152, Dec. 2000, doi: 10.1016/S0926-3373(00)00171-5.

[20] G. V Lowry and M. Reinhard, “Hydrodehalogenation of 1- to 3-Carbon Halogenated Organic Compounds in Water Using a Palladium Catalyst and Hydrogen Gas,” *Environ. Sci. Technol.*, vol. 33, no. 11, pp. 1905–1910, Jun. 1999, doi: 10.1021/es980963m.

[21] C. Schüth and M. Reinhard, “Hydrodechlorination and hydrogenation of aromatic compounds over palladium on alumina in hydrogen-saturated water,” *Appl. Catal. B Environ.*, vol. 18, no. 3–4, pp. 215–221, Oct. 1998, doi: 10.1016/S0926-3373(98)00037-X.

[22] X. Ding, Z. Yao, Y. Xu, B. Liu, Q. Liu, and Y. She, “Aqueous-phase hydrodechlorination of 4-chlorophenol on palladium nanocrystals: Identifying the catalytic sites and unraveling the reaction mechanism,” *J. Catal.*, vol. 368, pp. 336–344, Dec. 2018, doi: 10.1016/j.jcat.2018.10.008.

[23] G. V Lowry and M. Reinhard, “Pd-Catalyzed TCE Dechlorination in Groundwater: Solute Effects, Biological Control, and Oxidative Catalyst Regeneration,” *Environ. Sci. Technol.*, vol. 34, no. 15, pp. 3217–3223, Aug. 2000, doi: 10.1021/es991416j.

[24] S. Kovenklioglu *et al.*, “United States Patent (19) Kovenklioglu et al. 54 Method of Hydrodehalogenating Halogenated Organic Compounds in Aqueous Environmental Sources.”

[25] E. N. Balko, J. B. Hoke, N. Brunswick, and G. A. Gramiccioni, “United States Patent (19) Balko et al. 54 Hydrodehalogenation of Aromatic Compounds,” 1992.

[26] “III IIHIII III US005490941A 11 Patent Number: 45 Date of Patent:

5,490,941 54 Method of Treatment of a Fluid Containing Volatile Organic Halogenated Compounds," 1996.

[27] S. Ordóñez, H. Sastre, and F. V Díez, "Hydrodechlorination of aliphatic organochlorinated compounds over commercial hydrogenation catalysts," *Appl. Catal. B Environ.*, vol. 25, no. 1, pp. 49–58, 2000, doi: https://doi.org/10.1016/S0926-3373(99)00119-8.

[28] S. Ordóñez, H. Sastre, and F. V. Díez, "Hydrodechlorination of organochlorinated aliphatic compounds over nickel catalysts," *React. Kinet. Catal. Lett.*, vol. 70, no. 1, pp. 61–66, 2000, doi: 10.1023/A:1010302413567.

[29] S. Ordóez, F. V Díez, and H. Sastre, "Characterisation of the deactivation of platinum and palladium supported on activated carbon used as hydrodechlorination catalysts," *Appl. Catal. B Environ.*, vol. 31, no. 2, pp. 113–122, 2001, doi: 10.1016/S0926-3373(00)00270-8.

[30] S. Ordóñez, H. Sastre, and F. V. Díez, "Thermogravimetric determination of coke deposits on alumina-supported noble metal catalysts used as hydrodechlorination catalysts," *Thermochim. Acta*, vol. 379, no. 1–2, pp. 25–34, Nov. 2001, doi: 10.1016/S0040-6031(01)00598-6.

[31] E. López, S. Ordóñez, and F. V Díez, "Deactivation of a Pd/Al2O3 catalyst used in hydrodechlorination reactions: Influence of the nature of organochlorinated compound and hydrogen chloride," *Appl. Catal. B Environ.*, vol. 62, no. 1–2, pp. 57–65, 2006, doi: 10.1016/j.apcatb.2005.06.014.

[32] S. Ordóñez, F. V Díez, and H. Sastre, "Hydrodechlorination of tetrachloroethylene over vanadium-modified Pt/Al 2 O 3 catalysts," *Catal. Letters*, vol. 72, no. 4, 2001.

[33] M. O. Nutt, K. N. Heck, P. Alvarez, and M. S. Wong, "Improved Pd-on-Au bimetallic nanoparticle catalysts for aqueous-phase trichloroethene hydrodechlorination," *Applied Catalysis B: Environmental*, vol. 69, no. 1–2. pp. 115–125, 2006, doi: 10.1016/j.apcatb.2006.06.005.

[34] Y.-L. Fang, J. T. Miller, N. Guo, K. N. Heck, P. J. J. Alvarez, and M. S. Wong, "Structural analysis of palladium-decorated gold nanoparticles as colloidal bimetallic catalysts," *Catal. TODAY*, vol. 160, no. 1, pp. 96–102, Feb. 2011, doi: 10.1016/j.cattod.2010.08.010.

[35] L. A. Pretzer *et al.*, "Hydrodechlorination catalysis of Pd-on-Au nanoparticles varies with particle size," *J. Catal.*, vol. 298, pp. 206–217, Feb. 2013, doi: 10.1016/j.jcat.2012.11.005.

[36] H. Hildebrand, K. Mackenzie, and F. D. Kopinke, "Pd/Fe3O4 nano-catalysts for selective dehalogenation in wastewater treatment processes-Influence of water constituents," *Appl. Catal. B Environ.*, vol. 91, no. 1–2, pp. 389–396, Sep. 2009, doi: 10.1016/J.APCATB.2009.06.006.

[37] B. P. Chaplin *et al.*, "Critical Review of Pd-Based Catalytic Treatment of Priority Contaminants in Water," 2012, doi: 10.1021/es204087q.

[38] H. C. Choi, S. H. Choi, O. B. Yang, J. S. Lee, K. H. Lee, and Y. G. Kim, "Hydrodechlorination of carbon tetrachloride over Pt/MgO," *J. Catal.*, vol. 161, no. 2, pp. 790–797, 1996, doi: 10.1006/JCAT.1996.0242.

[39] E. J. A. X. Van De Sandt, A. Wiersma, M. Makkee, H. Van Bekkum, and J. A. Moulijn, "Selection of activated carbon for the selective hydrogenolysis of CCl2F2 (CFC-12) into CH2F2 (HFC-32) over palladium-supported catalysts," *Appl. Catal. A Gen.*, vol. 173, no. 2, pp. 161–173, Oct. 1998, doi: 10.1016/S0926-860X(98)00176-8.

[40] V. I. Kovalchuk and J. L. D'Itri, "Catalytic chemistry of chloro- and chlorofluorocarbon dehalogenation: From macroscopic observations to molecular level understanding," *Appl. Catal. A Gen.*, vol. 271, no. 1–2, pp. 13–25, Sep. 2004, doi: 10.1016/J.APCATA.2004.02.042.

[41] E. López, S. Ordóñez, and F. V. Díez, "Deactivation of a Pd/Al2O3 catalyst used in hydrodechlorination reactions: Influence of the nature of organochlorinated compound and hydrogen chloride," *Appl. Catal. B Environ.*, vol. 62, no. 1–2, pp. 57–65, 2006, doi:

10.1016/j.apcatb.2005.06.014.

[42] A. Gampine and D. P. Eyman, “Catalytic hydrodechlorination of chlorocarbons. 2. Ternary oxide supports for catalytic conversions of 1,2-dichlorobenzene,” *J. Catal.*, vol. 179, no. 1, pp. 315–325, 1998, doi: 10.1006/JCAT.1998.2223.

[43] D. J. Moom, M. J. Chung, K. Y. Park, and S. I. Hong, “Deactivation of Pd catalysts in the hydrodechlorination of chloropentafluoroethane,” *Appl. Catal. A Gen.*, vol. 168, no. 1, pp. 159–170, Mar. 1998, doi: 10.1016/S0926-860X(97)00352-9.

[44] K. Van Gorp, E. Boerman, C. V. Cavenaghi, and P. H. Berben, “Catalytic hydrogenation of fine chemicals: Sorbitol production,” *Catal. Today*, vol. 52, no. 2–3, pp. 349–361, Sep. 1999, doi: 10.1016/S0920-5861(99)00087-5.

[45] M. Besson and P. Gallezot, “Deactivation of metal catalysts in liquid phase organic reactions,” *Catal. Today*, vol. 81, no. 4, pp. 547–559, Jul. 2003, doi: 10.1016/S0920-5861(03)00153-6.

[46] G. Yuan and M. A. Keane, “Catalyst deactivation during the liquid phase hydrodechlorination of 2,4-dichlorophenol over supported Pd: Influence of the support,” *Catal. Today*, vol. 88, no. 1–2, pp. 27–36, Dec. 2003, doi: 10.1016/J.CATTOD.2003.08.004.

[47] G. Yuan and M. A. Keane, “Liquid phase hydrodechlorination of chlorophenols over Pd/C and Pd/Al2O3: a consideration of HCl/catalyst interactions and solution pH effects,” *Appl. Catal. B Environ.*, vol. 52, no. 4, pp. 301–314, 2004, doi: https://doi.org/10.1016/j.apcatb.2004.04.015.

[48] D. Fritsch, K. Kuhr, K. Mackenzie, and F. D. Kopinke, “Hydrodechlorination of chloroorganic compounds in ground water by palladium catalysts: Part 1. Development of polymer-based catalysts and membrane reactor tests,” *Catal. Today*, vol. 82, no. 1–4, pp. 105–118, Jul. 2003, doi: 10.1016/S0920-5861(03)00208-6.

[49] S. Ordóñez, H. Sastre, and F. V. Díez, “Hydrodechlorination of tetrachloroethylene over modified red mud: Deactivation studies and kinetics,” *Appl. Catal. B Environ.*, vol. 34, no. 3, pp. 213–226, Nov. 2001, doi: 10.1016/S0926-3373(01)00217-X.

[50] B. Coq, G. Ferrat, and F. Figueras, “Conversion of chlorobenzene over palladium and rhodium catalysts of widely varying dispersion,” *J. Catal.*, vol. 101, no. 2, pp. 434–445, 1986, doi: 10.1016/0021-9517(86)90271-X.

[51] J. W. Bozzelli, Y. M. Chen, and S. S. C. Chuang, “Catalytic hydrodechlorination of 1,2-Dichloroethane and trichloroethylene over Rh/SiO2 catalysts,” *Chem. Eng. Commun.*, vol. 115, no. 1, pp. 1–11, Apr. 1992, doi: 10.1080/00986449208936024.

[52] N. Munakata and M. Reinhard, “Palladium-catalyzed aqueous hydrodehalogenation in column reactors: Modeling of deactivation kinetics with sulfide and comparison of regenerants,” *Appl. Catal. B Environ.*, vol. 75, no. 1–2, pp. 1–10, Aug. 2007, doi: 10.1016/J.APCATB.2007.03.005.

[53] W. G. Davie, Hefachen and N. A. Lebron, and Martin Reinhard, “Implementing Heterogeneous Catalytic Dechlorination Technology for Remediating TCE-Contaminated Groundwater,” doi: 10.1021/es8014919.

[54] G. Celik, S. A. Ailawar, S. Gunduz, J. T. Miller, P. L. Edmiston, and U. S. Ozkan, “Aqueous-phase hydrodechlorination of trichloroethylene over Pd-based swellable organically-modified silica (SOMS): Catalyst deactivation due to chloride anions,” *Appl. Catal. B-Environmental*, vol. 239, pp. 654–664, Dec. 2018, doi: 10.1016/j.apcatb.2018.08.065.

[55] G. Yuan and M. A. Keane, “Role of base addition in the liquid-phase hydrodechlorination of 2,4-dichlorophenol over Pd/Al2O3 and Pd/C,” *J. Catal.*, vol. 225, no. 2, pp. 510–522, Jul. 2004, doi: 10.1016/J.JCAT.2004.05.003.

[56] K. Mackenzie, H. Frenzel, and F. D. Kopinke, “Hydrodehalogenation of halogenated hydrocarbons in water with Pd catalysts: Reaction rates and

surface competition," *Appl. Catal. B Environ.*, vol. 63, no. 3–4, pp. 161–167, Mar. 2006, doi: 10.1016/J.APCATB.2005.10.004.

[57] G. Celik, S. A. Ailawar, S. Gunduz, J. T. Miller, P. L. Edmiston, and U. S. Ozkan, "Aqueous-Phase Hydrodechlorination of Trichloroethylene over Pd-Based Swellable Organically Modified Silica: Catalyst Deactivation Due to Sulfur Species," *Ind. Eng. Chem. Res.*, vol. 58, no. 10, pp. 4054–4064, Mar. 2019, doi: 10.1021/acs.iecr.8b05979.

[58] S. Ordóñez, B. P. Vivas, and F. V. Díez, "Minimization of the deactivation of palladium catalysts in the hydrodechlorination of trichloroethylene in wastewaters," *Appl. Catal. B Environ.*, vol. 95, no. 3–4, pp. 288–296, 2010, doi: 10.1016/j.apcatb.2010.01.006.

[59] C. Schüth, N. A. Kummer, C. Weidenthaler, and H. Schad, "Field application of a tailored catalyst for hydrodechlorinating chlorinated hydrocarbon contaminants in groundwater," *Appl. Catal. B Environ.*, vol. 52, no. 3, pp. 197–203, Sep. 2004, doi: 10.1016/J.APCATB.2004.03.018.

[60] F. D. Kopinke, D. Angeles-Wedler, D. Fritsch, and K. Mackenzie, "Pd-catalyzed hydrodechlorination of chlorinated aromatics in contaminated waters-Effects of surfactants, organic matter and catalyst protection by silicone coating," *Appl. Catal. B Environ.*, vol. 96, no. 3–4, pp. 323–328, Jun. 2010, doi: 10.1016/J.APCATB.2010.02.028.

[61] R. Navon, S. Eldad, K. Mackenzie, and F. D. Kopinke, "Protection of palladium catalysts for hydrodechlorination of chlorinated organic compounds in wastewaters," *Appl. Catal. B Environ.*, vol. 119–120, pp. 241–247, May 2012, doi: 10.1016/J.APCATB.2012.03.002.

[62] D. Comandella, S. Woszidlo, A. Georgi, F. D. Kopinke, and K. Mackenzie, "Efforts for long-term protection of palladium hydrodechlorination catalysts," *Appl. Catal. B Environ.*, vol. 186, pp. 204–211, Jun. 2016, doi: 10.1016/J.APCATB.2015.12.043.

[63] C. R. Henry, C. Chapon, S. Giorgio, and C. Goyhenex, "Size Effects in

Heterogeneous Catalysis," *Chemisorpt. React. Support. Clust. Thin Film.*, pp. 117–152, 1997, doi: 10.1007/978-94-015-8911-6_5.

[64] M. Che and C. O. Bennett, "The Influence of Particle Size on the Catalytic Properties of Supported Metals," *Adv. Catal.*, vol. 36, no. C, pp. 55–172, Jan. 1989, doi: 10.1016/S0360-0564(08)60017-6.

[65] R. M. Rioux, H. Song, J. D. Hoefelmeyer, P. Yang, and G. A. Somorjai, "High-surface-area catalyst design: Synthesis, characterization, and reaction studies of platinum nanoparticles in mesoporous SBA-15 silica," *J. Phys. Chem. B*, vol. 109, no. 6, pp. 2192–2202, Feb. 2005, doi: 10.1021/jp048867x/asset/ımages/large/jp048867xf00015.jpeg.

[66] R. M. Rioux, A. B. B. Hsu, A. M. E. Grass, A. H. Song, and A. G. A. Somorjai, "Influence of Particle Size on Reaction Selectivity in Cyclohexene Hydrogenation and Dehydrogenation over Silica-Supported Monodisperse Pt Particles," doi: 10.1007/s10562-008-9637-8.

[67] W. W. McNab and R. Ruiz, "Palladium-catalyzed reductive dehalogenation of dissolved chlorinated aliphatics using electrolytically-generated hydrogen," *Chemosphere*, vol. 37, no. 5, pp. 925–936, Jul. 1998, doi: 10.1016/S0045-6535(98)00095-2.

[68] M. A. Álvarez-Montero, L. M. Gómez-Sainero, A. Mayoral, I. Diaz, R. T. Baker, and J. J. Rodriguez, "Hydrodechlorination of chloromethanes with a highly stable Pt on activated carbon catalyst," *J. Catal.*, vol. 279, no. 2, pp. 389–396, Apr. 2011, doi: 10.1016/J.JCAT.2011.02.009.

[69] "Platinum - The chemical element, its science, properties, and uses." https://www.explainthatstuff.com/platinum.html (accessed Jul. 25, 2022).

[70] C. Bock, H. Halvorsen, and B. Macdougall, "Catalyst Synthesis Techniques," 2009.

[71] J. T. Miller, M. Schreier, A. J. Kropf, and J. R. Regalbuto, "A fundamental study of platinum tetraammine impregnation of silica 2. The effect of method

of preparation, loading, and calcination temperature on (reduced) particle size," *J. Catal.*, vol. 225, no. 1, pp. 203–212, Jul. 2004, doi: 10.1016/j.jcat.2004.04.007.

[72] P. Gélin and M. Primet, "Complete oxidation of methane at low temperature over noble metal based catalysts: A review," *Appl. Catal. B Environ.*, vol. 39, no. 1, pp. 1–37, Nov. 2002, doi: 10.1016/S0926-3373(02)00076-0.

[73] J. W. Slot and H. J. Geuze, "A new method of preparing gold probes for multiple-labeling cytochemistry.," *Eur. J. Cell Biol.*, vol. 38 1, pp. 87–93, 1985.

[74] S. I. Sandler, "Chemical, biochemical and engineering thermodynamics," p. 1007.

[75] W. Dermaut, "1 Process Safety and Reaction Hazard Assessment."

[76] M. A. (Mark A. . Donelan, "Gas transfer at water surfaces," p. 383, 2002.

[77] W. Brutsaert, G. H. Jirka, American Chemical Society., and International Symposium on Gas Transfer at Water Surfaces (1983 : Cornell University), "Gas transfer at water surfaces," p. 639, 1984.

[78] Y.-L. Fang, K. N. Heck, P. J. J. Alvarez, and M. S. Wong, "Kinetics Analysis of Palladium/Gold Nanoparticles as Colloidal Hydrodechlorination Catalysts," *ACS Catal.*, vol. 1, no. 2, pp. 128–138, Feb. 2011, doi: 10.1021/cs100067k.

[79] O. Levenspiel, "Chemical Reaction Engineering, 3rd Edition | Wiley," *New York*, p. 704, 1998.

[80] "How do I choose a magnetic stirring bar / magnetic flea? - The Laboratory People." https://camblab.info/how-do-i-choose-a-magnetic-stirring-bar-magnetic-flea/ (accessed Aug. 07, 2022).

[81] C. H. Bartholomew and R. J. Farrauto, "Fundamentals of industrial catalytic processes," p. 966, 2006.

[82] N. Chen, R. M. Rioux, L. A. M. M. Barbosa, and F. H. Ribeiro, "Kinetic and

theoretical study of the hydrodechlorination of CH 4- xClx (x = 1-4) compounds on palladium," *Langmuir*, vol. 26, no. 21, pp. 16615–16624, 2010, doi: 10.1021/la1020753.

[83] I. Tosun, "Modeling in Transport Phenomena, Second Edition: A Conceptual Approach," 2007, Accessed: Aug. 07, 2022. [Online]. Available: http://www.amazon.com/exec/obidos/redirect?tag=citeulike07-20&path=ASIN/0444530215.

[84] A. S. L. Frank P. Incropera, David P. DeWitt, Theodore L. Bergman, "Fundamentals of Heat and Mass Transfer - 6th Edition Incropera .pdf," p. 999, 2007.

[85] D. M. I. René P. Schwarzenbach, Philip M. Gschwend, "Environmental Organic Chemistry Appendix C," *Environ. Org. Chem.*, pp. 0–7, 2016.

[86] D. S. Sheny, D. Philip, and J. Mathew, "Synthesis of platinum nanoparticles using dried anacardium occidentale leaf and its catalytic and thermal applications," *Spectrochim. Acta - Part A Mol. Biomol. Spectrosc.*, vol. 114, pp. 267–271, 2013, doi: 10.1016/J.SAA.2013.05.028.

[87] R. Dobrucka, "Biofabrication of platinum nanoparticles using Fumariae herba extract and their catalytic properties," *Saudi J. Biol. Sci.*, vol. 26, no. 1, pp. 31–37, Jan. 2019, doi: 10.1016/J.SJBS.2016.11.012.

[88] P. Yugandhar and N Savithramma, "Biosynthesis, characterization and antimicrobial studies of green synthesized silver nanoparticles from fruit extract of Syzygium alternifolium (Wt.) Walp. an endemic, endangered medicinal tree taxon," doi: 10.1007/s13204-015-0428-4.

[89] J. Räty, K.-E. Peiponen, and T. Asakura, "UV-Visible Reflection Spectroscopy of Liquids," vol. 92, 2004, doi: 10.1007/978-3-540-45093-1.

APPENDICES

A. Synthesis Route of Colloidal Pt Nanoparticles

Colloidal Slot-Geuze synthesis method is for Au NPs. The procedure for other metal NPs was almost same as for Au NPs, except that metal salt solution was substituted for the gold salt solution. In the literature, this method has been applied for Pd and has given successful results [33]. While applying for Pd, moles of gold salt solution ($HAuCl_4$) and palladium gold solution (H_2PdCl_4) were kept equal.

For $HAuCl_4$, 100 μL, 0.296 M

$$100\ \mu L\ x\ \frac{0.296\ mol}{L}\ x\ \frac{1\ L}{10^6\ \mu L} = 2.96\ x\ 10^{-5}\ mol\ HAuCl_4$$

- For H_2PdCl_4, 12 mL, 2.47 mM

$$12\ mL\ x\ \frac{2.47\ mmol}{L}\ x\ \frac{1\ L}{1000\ mL}\ x\ \frac{1\ mol}{1000\ mmol} = 2.964\ x\ 10^{-5}\ mol\ H_2PdCl_4$$

As it can be seen here, the moles of metal salt solutions of both metals are the same. This method was applied for Pt in this study and calculations were made for it.

We have chloroplatinic acid (8 wt % solution in water). Convert it to molarity:

Density:1.05 gr/mL, MW:409.81 gr/mol

$$\frac{8\ gr\ H_2PtCl_6}{100\ gr\ solution\ in\ water} x \frac{1\ mol\ H_2PtCl_6}{409.81\ gr\ H_2PtCl_6} x \frac{1.05\ gr}{1\ mL} x \frac{1000\ mL}{1\ L}$$
$$= 0.205\ M$$

For approximately. 2.96x10^{-5} mol H_2PtCl_6

$$\frac{2.96\ x\ 10^{-5}\ mol}{\frac{0.205\ mol}{L}} = 1.444\ x\ 10^{-4}\ L = 144.4\ \mu L$$

Total volume is 100 mL,

- 80 mL for first solution
- 20 mL for second solution

First Solution: According to calculations, a platinum salt solution is prepared by diluting 144.4 μL of a H_2PtCl_6 solution (0.205 M) in 79.86 mL of ultrapure water (80-0.1444=79.86 mL). That is approximately 80 mL.

Second Solution: 0.04 g trisodium citrate, 0.05 g tannic acid, and 0.018 g potassium carbonate dissolved in 20 mL of nanopure water.

Trisodium citrate was used in literature [33], [35], we have trisodium citrate dihydrate. Thus, the amount of trisodium citrate dihydrate to be used was calculated.

Trisodium citrate MW: 258.06 g/mol

$$0.04\ g\ trisodium\ citrate\ x\ \frac{1\ mol}{258.06\ g} = 1.55\ x10^{-4}\ mol$$

Trisodium citrate dihydrate MW: 294.1 g/mol

$$1.55\ x10^{-4}\ mol\ x\ \frac{294.1\ g}{1\ mol} = 0.0456\ g\ trisodium\ citrate\ dihydrate$$

B. Adiabatic Temperature Rise Calculation

ORIGIN := 1

$$CA(T) := 8.314 \cdot \left[1.131 + \left(19.225 \cdot 10^{-3} \cdot \frac{T}{K}\right) - \left[5.561 \cdot 10^{-6} \cdot \left(\frac{T}{K}\right)^{2}\right]\right] \frac{J}{mol \cdot K}$$

$$CB(T) := 8.314 \cdot \left[3.156 + \left(0.623 \cdot 10^{-3} \cdot \frac{T}{K}\right) + \left[0.151 \cdot 10^{5} \cdot \left(\frac{T}{K}\right)^{-2}\right]\right] \cdot \frac{J}{mol \cdot K}$$

kJ := 1000J

$$\Delta H := -309 \frac{kJ}{mol}$$

Guess

T := 150K

Given

$$\int_{298K}^{T} CA(T)\, dT + 3 \cdot \int_{298K}^{T} CB(T)\, dT - \Delta H = 0$$

Find(T) = 1.361 K

C. TEM Images

Particle 1 (Small-3.0 nm)

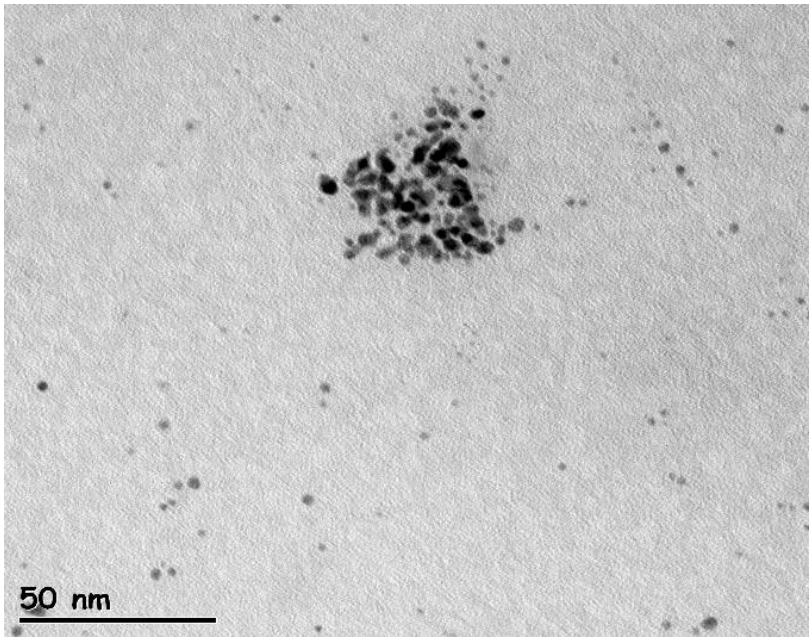

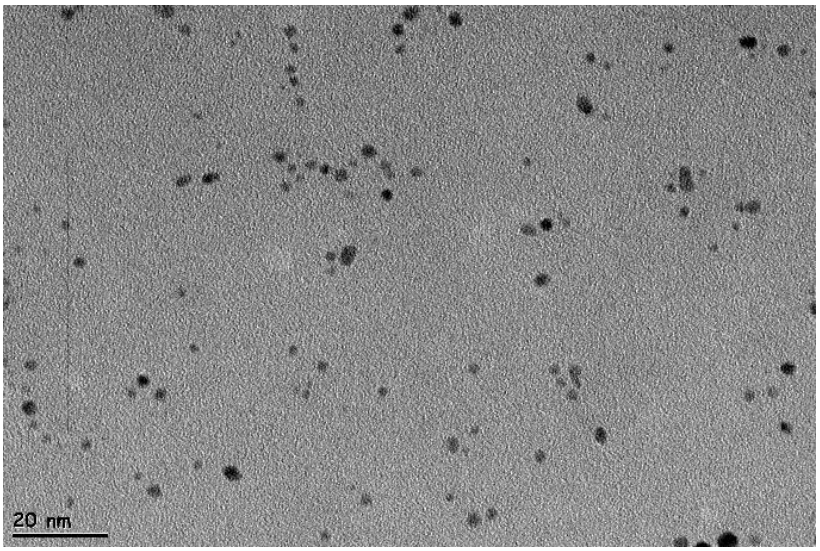

Figure B.1 TEM Images of Particle 1 (Small-3.0 nm)

Particle 2 (Medium-5.8 nm)

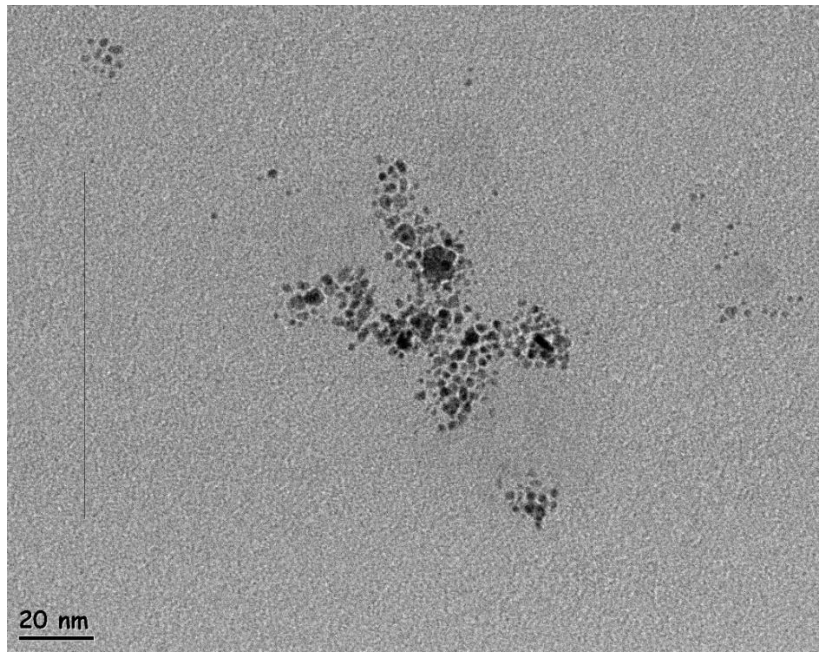

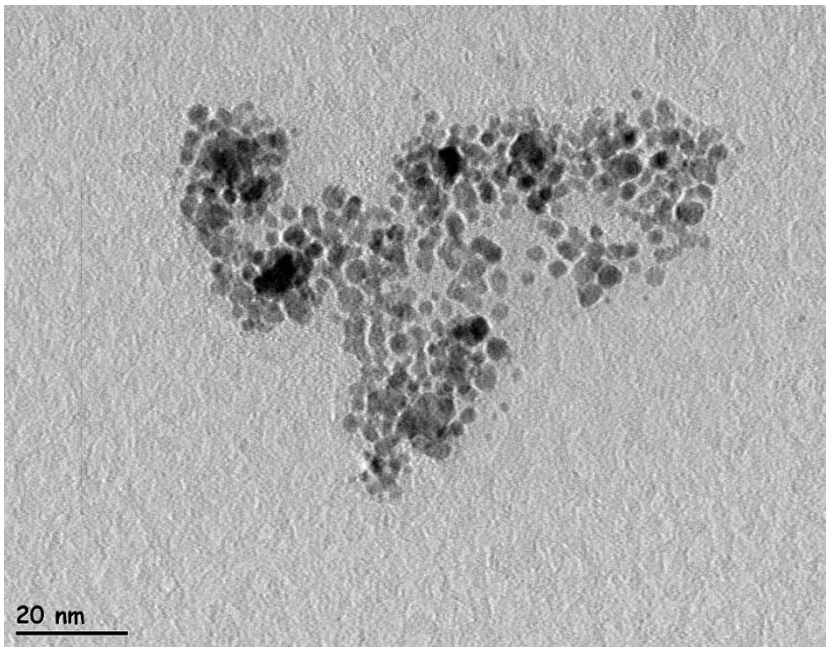

Figure B.2 TEM Images of Particle 2 (Medium-5.8 nm)

Particle 3 (Large 60.9 nm)

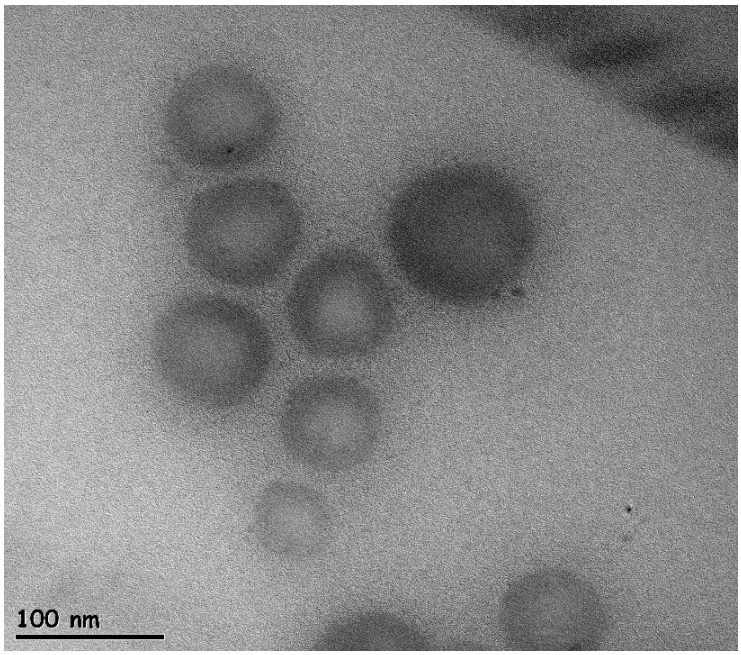

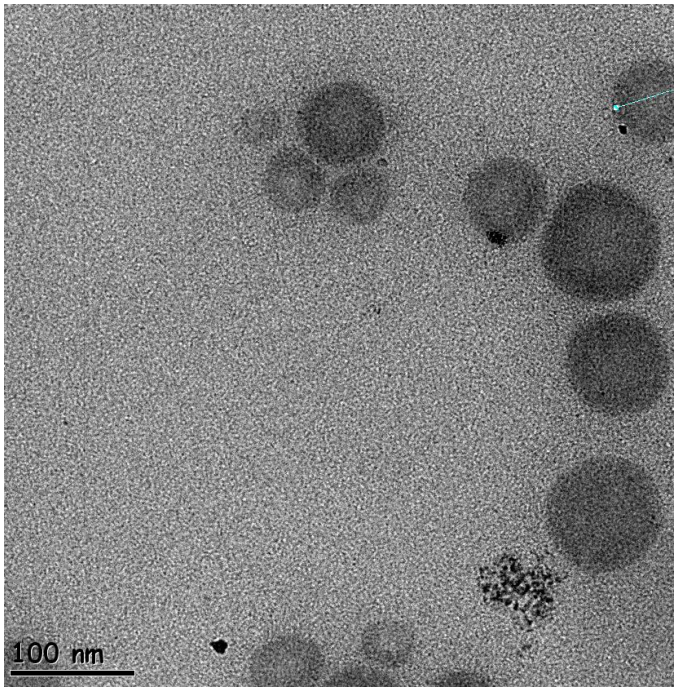

Figure B.3 TEM Images of Particle 3 (Large-60.9 nm)

D. Concentration Calculation of Pt NPs

- Weight of metal taken for NP synthesis (metal only, not metal salt), W
- Density of metal, $\rho = 21.45\ g/cm^3$ for Pt nanoparticle
- Calculate the volume of metal taken, W/ρ
- Average size of NPs using TEM (NPs are monodispersed, 2R)
- Volume of a single NP, by assuming sphere (V=4/3πR^3)
- Number of particles in colloidal solution, N= (W/ρ)/V
- Calculate the concentration of NP (N/final volume of colloidal solution)

During synthesis, we use 2.96x10^{-5} mol H_2PtCl_6, corresponding to 2.96x10^{-5} mol Pt.

$$2.96x10^{-5}\ mol\ Pt\ x\ \frac{195.084\ g}{1\ mol} = 0.00577\ g\ Pt$$

- **Particle 1-Small: D=3.0 nm, R=1.5 nm**

$$V = \frac{4}{3}\pi R^3 = \frac{4}{3}\pi(1.5x10^{-7}\ cm)^3 = 1.44x10^{-20}\ cm^3$$

$$N = \frac{W/\rho}{V} = \frac{0.00577\ g\ Pt}{21.45\frac{g}{cm^3}x1.44x10^{-20}\ cm^3} = 1.87x10^{16}\ NP$$

$$final\ volume\ of\ colloidal\ sol = 100\ mL$$

$$Concentration = \frac{1.87x10^{16}\ NP}{100\ mL} = 1.87x10^{14}\frac{NP}{mL}$$

- **Particle 2-Medium: D=5.8 nm, R=2.9 nm**

$$V = \frac{4}{3}\pi R^3 = \frac{4}{3}\pi(2.9x10^{-7}\ cm)^3 = 1.02x10^{-19}\ cm^3$$

$$N = \frac{W/\rho}{V} = \frac{0.00577\ g\ Pt}{21.45\frac{g}{cm^3}x1.02x10^{-19}\ cm^3} = 2.65x10^{15}\ NP$$

$$Concentration = \frac{2.65x10^{15}\ NP}{100\ mL} = 2.65x10^{13}\frac{NP}{mL}$$

- **Particle 3-Large: D=60.9 nm, R=30.5 nm**

$$V = \frac{4}{3}\pi R^3 = \frac{4}{3}\pi(30.5x10^{-7}\ cm)^3 = 1.18x10^{-16}\ cm^3$$

$$N = \frac{W/\rho}{V} = \frac{0.00577\ g\ Pt}{21.45\frac{g}{cm^3}x1.18x10^{-16}\ cm^3} = 2.28x10^{12}\ NP$$

$$Concentration = \frac{2.28x10^{12}\ NP}{100\ mL} = 2.28x10^{10}\frac{NP}{mL}$$

E. Rate Constant Expression and Conversion Calculation of TCE HDC

For HDC of TCE (represented by A) reaction,

$$C_2HCl_3 + 4H_2 \rightarrow C_2H_6 + 3HCl$$

Assumptions:

- First order
- Constant volume batch reactor (no in, no out)
- Well-mixed

$$F_{A,0} - F_A + \int r_A dV = \frac{dN_A}{dt}$$

$$F_{A,0} - F_A + r_A V = \frac{dN_A}{dt}$$

$$r_A V = \frac{dN_A}{dt}$$

$$r_A = \frac{d(N_A/V)}{dt} = \frac{dC_A}{dt}$$

Assumption: *For 20 ppm TCE, H_2 is in excess. We can check* $\frac{n_{H_{2(aq)}}}{n_{TCE}}$.

Batch Reactor Total Volume	800 mL
Liquid Phase Volume	510 mL
Gas Phase Volume	290 mL

- **290 mL H_2 in gas phase**

$$\rho_{H_2} = 0.0799\ kg/m^3\ (at\ 1\ atm, 30°C)$$

$$290\ mL\ H_2\ x\ 0.0799\ \frac{kg}{m^3}\ x\ \frac{10^{-6}\ m^3}{1\ mL}\ x\ \frac{1\ mol}{2.016\ g\ H_2}\ x\ \frac{1000\ g}{1\ kg}$$

$$= 0.012\ mol\ H_2\ (gas\ phase)$$

- **510 mL H_2 in gas phase**

$$\rho_{water} = 996\ kg/m^3\ (at\ 1\ atm, 30℃)$$

$$510\ mL\ water\ x\ 997\ \frac{kg}{m^3}\ x\ \frac{10^{-6}\ m^3}{1\ mL}\ x\ \frac{1000\ g}{1\ kg} = 507.96\ g\ water$$

H_2 solubility in water (1 atm, 30°C): 0.00147 g H_2 dissolved in 1 kg water

$$\frac{0.00147\ g\ H_2}{1000\ g\ water}\ x\ 507.96\ g\ water\ x\ \frac{1\ mol}{2.016\ g\ H_2} = 3.7\ x\ 10^{-4}\ mol\ H_2$$

20 ppm TCE in 0.510 L

$$\frac{20\ mg\ TCE}{L}\ x\ 0.510\ L\ x\ \frac{1\ mol}{131.4\ g\ TCE}\ x\ \frac{1\ g}{1000\ mg} = 7.762\ x\ 10^{-5}\ mol\ TCE$$

$$\frac{n_{H_{2(aq)}}}{n_{TCE}} = \frac{3.7\ x\ 10^{-4}\ mol\ H_2}{7.762\ x\ 10^{-5}\ mol\ TCE} = \mathbf{4.8}$$

$$C_B \cong C_{B,0}$$

$$r_A = -kC_A$$

$$C_A = \frac{N_A}{V} = \frac{N_{A,0}(1 - x_A)}{V} = C_{A,0}(1 - x_A)$$

$$r_A = \frac{dC_A}{dt} = -kC_A$$

$$-kC_{A,0}(1 - x_A) = \frac{d\left(C_{A,0}(1 - x_A)\right)}{dt}$$

$$\frac{-d(x_A)}{1 - x_A} = -kdt$$

$$\ln(1 - x_A) = -kt$$

For integration, at time=0 $x_A = 0$. Slope of ln(1-x_A) vs. time graph gives -k, or slope of ln($C_{A,0}/C_A$) vs. time graph gives k.

In order to calculate conversion:

$$C_{TCE} = C_{TCE,0}(1 - x_A)$$

$$C_{Cl} = C_{Cl,0} + 3C_{TCE,0}x_A$$

$$C_{Cl,0} = 0$$

$$C_{TCE,0} = 20\ ppm$$

20 ppm TCE to molarity (M)

$$\frac{20\ mg}{L} x \frac{1\ mol}{131.4\ g} x \frac{1\ g}{1000\ mg} = 0.1522\ mM$$

From our reaction expression,

$$C_{Cl} = 3C_{TCE,0}x_A$$

$$x_A = \frac{C_{Cl}}{3C_{TCE,0}}$$

For final TCE concentration,

$$C_{TCE} = C_{TCE,0}\left(1 - \frac{C_{Cl}}{3C_{TCE,0}}\right)$$

$$C_{TCE} = C_{TCE,0} - \frac{C_{Cl}}{3}$$

Then, convert chloride concentration from ppm to M.

F. Rate Constant Calculation of TCE HDC

Particle Size 1 (Small-3.0 nm)

$$k = 4.2\ h^{-1}$$

$$k' = \frac{kV}{W}$$

$$V = Volume\ of\ fluid = 0.510\ L$$

$$W = mass\ of\ solid$$

There is 0.00577 g Pt in 100 mL of colloidal sol. We add 4 mL of this solution to reactor during HDC reaction.

$$W = \frac{0.00577\ g\ Pt}{100\ mL} x\ 4\ mL = 2.31x10^{-4}\ g\ Pt$$

$$k' = \frac{kV}{W} = \frac{4.2\ h^{-1}\ x\ 0.510\ L}{2.31x10^{-4}\ g\ Pt} x \frac{1\ h}{60\ min}$$

$$k' = 156.3\ \frac{L}{g\ Pt.min}$$

$$k'' = \frac{k'W}{S}$$

$$\frac{W}{S} = \frac{4/3\pi R^3 \rho N}{4\pi R^2 N} = \frac{\rho R}{3}$$

$$Diameter = 3.0\ nm$$

$$\rho = density\ of\ Pt\ NPs = 21.45\ g/cm^3$$

$$\frac{W}{S} = \frac{\rho R}{3} = \frac{21.45\ g/cm^3 x (1.5x10^{-7} cm)}{3} x \frac{(100\ cm)^2}{1\ m^2} = 0.011 \frac{g\ Pt}{{m_{surf\ Pt}}^2}$$

$$k'' = \frac{k'W}{S} = 156.3\ \frac{L}{g\ Pt.min}\ x\ 0.011 \frac{g\ Pt}{{m_{surf\ Pt}}^2} = 1.7 \frac{L}{{m_{surf\ Pt}}^2.min}$$

Initial TOF (TOF_0) Calculation

$$\frac{-dC_{TCE}}{dt} = k_{meas} C_{TCE}$$

$$TOF_0 = \frac{initial\ rate}{[Pt]} = \frac{C_{TCE,0}}{[Pt]}\ x\ k_{meas}$$

$$k_{meas} = 4.2\ h^{-1}$$

$$C_{TCE,0} = 20\ ppm$$

$$[Pt] = Molar\ concentration\ of\ Pt\ in\ the\ batch\ reactor$$

$$[Pt] = \frac{\frac{0.00577\ g\ Pt}{100\ mL}\ x\ 4\ mL\ x\ \frac{1\ mol}{195.084\ g\ Pt}}{0.510\ L} = \frac{2.32x10^{-6} mol\ Pt}{L}$$

$$TOF_0 = \frac{\frac{20\ mg\ TCE}{L}\ x\ \frac{1\ mol\ TCE}{131.4\ g\ TCE}\ x\ \frac{1\ g}{1000\ mg}}{\frac{2.32x10^{-6} mol\ Pt}{L}}\ x\ \frac{4.2}{h}\ x\ \frac{1\ h}{3600\ s}$$

$$TOF_0 = 0.077\ \frac{mol\ TCE}{mol\ Pt.s}$$

Particle Size 2 (Medium-5.8 nm)

$$k = 1.3\ h^{-1}$$

$$k' = \frac{kV}{W}$$

$$V = Volume\ of\ fluid = 0.510\ L$$

$$W = mass\ of\ solid$$

There is 0.00577 g Pt in 100 mL of colloidal sol. We add 4 mL of this solution to reactor during HDC reaction.

$$W = \frac{0.00577\ g\ Pt}{100\ mL} x\ 4\ mL = 2.31x10^{-4}\ g\ Pt$$

$$k' = \frac{kV}{W} = \frac{1.3\ h^{-1}\ x\ 0.510\ L}{2.31x10^{-4}\ g\ Pt} x \frac{1\ h}{60\ min}$$

$$k' = 47.3\ \frac{L}{g\ Pt.min}$$

$$k'' = \frac{k'W}{S}$$

$$\frac{W}{S} = \frac{4/3\pi R^3 \rho N}{4\pi R^2 N} = \frac{\rho R}{3}$$

$$Diameter = 5.8\ nm$$

$$\rho = density\ of\ Pt\ NPs = 21.45\ g/cm^3$$

$$\frac{W}{S} = \frac{\rho R}{3} = \frac{21.45\ g/cm^3 x (2.9x10^{-7} cm)}{3} x \frac{(100\ cm)^2}{1\ m^2} = 0.021\ \frac{g\ Pt}{m_{surf\ Pt}{}^2}$$

$$k'' = \frac{k'W}{S} = 47.3\ \frac{L}{g\ Pt.min}\ x\ 0.021 \frac{g\ Pt}{m_{surf\ Pt}{}^2} = 1.0\ \frac{L}{m_{surf\ Pt}{}^2.min}$$

Initial TOF (TOF_0) Calculation

$$\frac{-dC_{TCE}}{dt} = k_{meas} C_{TCE}$$

$$TOF_0 = \frac{initial\ rate}{[Pt]} = \frac{C_{TCE,0}}{[Pt]}\ x\ k_{meas}$$

$$k_{meas} = 1.3\ h^{-1}$$

$$C_{TCE,0} = 20\ ppm$$

$$[Pt] = Molar\ concentration\ of\ Pt\ in\ the\ batch\ reactor$$

$$[Pt] = \frac{\frac{0.00577\ g\ Pt}{100\ mL}\ x\ 4\ mL\ x\ \frac{1\ mol}{195.084\ g\ Pt}}{0.510\ L} = \frac{2.32x10^{-6} mol\ Pt}{L}$$

$$TOF_0 = \frac{\frac{20\ mg\ TCE}{L}\ x\ \frac{1\ mol\ TCE}{131.4\ g\ TCE}\ x\ \frac{1\ g}{1000\ mg}}{\frac{2.32x10^{-6} mol\ Pt}{L}}\ x\ \frac{1.3}{h}\ x\ \frac{1\ h}{3600\ s}$$

$$TOF_0 = 0.023\ \frac{mol\ TCE}{mol\ Pt.s}$$

Particle Size 3 (Large-60.9 nm)

$$k = 0.4\ h^{-1}$$

$$k' = \frac{kV}{W}$$

$$V = Volume\ of\ fluid = 0.510\ L$$

$$W = mass\ of\ solid$$

There is 0.00577 g Pt in 100 mL of colloidal sol. We add 4 mL of this solution to reactor during HDC reaction.

$$W = \frac{0.00577\ g\ Pt}{100\ mL} x\ 4\ mL = 2.31x10^{-4}\ g\ Pt$$

$$k' = \frac{kV}{W} = \frac{0.4\ h^{-1}\ x\ 0.510\ L}{2.31x10^{-4}\ g\ Pt} x \frac{1\ h}{60\ min}$$

$$k' = 14.2\ \frac{L}{g\ Pt.min}$$

$$k'' = \frac{k'W}{S}$$

$$\frac{W}{S} = \frac{4/3\pi R^3 \rho N}{4\pi R^2 N} = \frac{\rho R}{3}$$

$$Diameter = 60.9\ nm$$

$$\rho = density\ of\ Pt\ NPs = 21.45\ g/cm^3$$

$$\frac{W}{S} = \frac{\rho R}{3} = \frac{21.45\ g/cm^3 x (30.5x10^{-7} cm)}{3} x \frac{(100\ cm)^2}{1\ m^2} = 0.218\ \frac{g\ Pt}{{m_{surf\ Pt}}^2}$$

$$k'' = \frac{k'W}{S} = 14.2\ \frac{L}{g\ Pt.min}\ x\ 0.218 \frac{g\ Pt}{{m_{surf\ Pt}}^2} = 3.1\ \frac{L}{{m_{surf\ Pt}}^2.min}$$

Initial TOF (TOF_0) Calculation

$$\frac{-dC_{TCE}}{dt} = k_{meas} C_{TCE}$$

$$TOF_0 = \frac{initial\ rate}{[Pt]} = \frac{C_{TCE,0}}{[Pt]}\ x\ k_{meas}$$

$$k_{meas} = 0.4\ h^{-1}$$

$$C_{TCE,0} = 20\ ppm$$

$$[Pt] = Molar\ concentration\ of\ Pt\ in\ the\ batch\ reactor$$

$$[Pt] = \frac{\frac{0.00577\ g\ Pt}{100\ mL} x\ 4\ mL\ x\ \frac{1\ mol}{195.084\ g\ Pt}}{0.510\ L} = \frac{2.32x10^{-6} mol\ Pt}{L}$$

$$TOF_0 = \frac{\frac{20\ mg\ TCE}{L}\ x\ \frac{1\ mol\ TCE}{131.4\ g\ TCE}\ x\ \frac{1\ g}{1000\ mg}}{\frac{2.32x10^{-6} mol\ Pt}{L}}\ x\ \frac{0.4}{h}\ x\ \frac{1\ h}{3600\ s}$$

$$TOF_0 = 0.007\ \frac{mol\ TCE}{mol\ Pt.s}$$

G. Deactivation Parameter Calculation

Assumption: first order, constant volume batch reactor (no in, no out), well-mixed.

HDC of TCE is an elementary reaction with the parameter "a" included to take deactivation into account.

$$\frac{dC_A}{dt} = r_A \; where \; A = TCE$$

$$-r_A = kC_AC_Ba = k'C_Aa$$

$$k' = kC_B$$

$$-\frac{da}{dt} = k_d a$$

Since the deactivation parameter is an activity coefficient, we can assume that a_0=1 at time=0 indicating that fresh catalyst is not deactivated.

$$a = a_0 \, exp(-k_d t) = exp(-k_d t)$$

$$-r_A = k'C_A exp(-k_d t) = k' \, C_{A_0}(1 - X_A) exp(-k_d t)$$

$$r_A \frac{W}{V} = \frac{dC_A}{dt}$$

$$-k' \, C_{A_0}(1 - X_A) exp(-k_d t) \frac{W}{V} = \frac{d\left(C_{A_0}(1 - X_A)\right)}{dt} = -C_{A_0} \frac{dX_A}{dt}$$

$$\frac{dX_A}{(1 - X_A)} = \frac{k'W}{V} exp(-k_d t) dt$$

At time is infinity, TCE conversion is the plateau conversion.

$$ln\left(ln\frac{(1 - X_A)}{\left(1 - X_{A_\infty}\right)}\right) = ln\left(\frac{k'W/V}{k_d}\right) - k_d t$$

If our rate form assumption is valid, then the plot of $ln\left(ln\frac{(1-X_A)}{(1-X_{A_\infty})}\right)$ vs. t should be linear with a slope of -k_d and with an intercept of $ln\left(\frac{k'W/V}{k_d}\right)$.

In order to calculate conversion:

$$C_{TCE} = C_{TCE,0}(1 - x_A)$$

$$C_{Cl} = C_{Cl,0} + 3C_{TCE,0}x_A$$

$$C_{Cl,0} = 0$$

$$C_{TCE,0} = 1000\,ppm$$

1000 ppm TCE to molarity (M)

$$\frac{1000\,mg}{L}x\frac{1\,mol}{131.4\,g}x\frac{1\,g}{1000\,mg} = 7.61\,mM$$

From our reaction expression,

$$C_{Cl} = 3C_{TCE,0}x_A$$

$$x_A = \frac{C_{Cl}}{3C_{TCE,0}}$$

For final TCE concentration,

$$C_{TCE} = C_{TCE,0}\left(1 - \frac{C_{Cl}}{3C_{TCE,0}}\right)$$

$$C_{TCE} = C_{TCE,0} - \frac{C_{Cl}}{3}$$

Then, convert chloride concentration from ppm to M.

Particle Size 1 (Small-3.0 nm):

$$Slope = k_d = 0.18\ h^{-1}$$

$$From\ a = exp(-k_d t)\ equation, a\ can\ be\ found\ with\ respect\ to\ time.$$

$$Intercept = ln\left(\frac{k'W/V}{k_d}\right) = -0.214$$

$$\frac{k'W/V}{k_d} = 0.807$$

$$k = k'W/V = 0.15\ h^{-1}$$

$$k' = \frac{kV}{W}$$

$$V = Volume\ of\ fluid = 0.510\ L$$

$$W = mass\ of\ solid$$

There is 0.00577 g Pt in 100 mL of colloidal sol. We add 4 mL of this solution to reactor during HDC reaction.

$$W = \frac{0.00577\ g\ Pt}{100\ mL}\ x\ 4\ mL = 2.31x10^{-4}\ g\ Pt$$

$$k' = \frac{kV}{W} = \frac{0.15\ h^{-1}\ x\ 0.510\ L}{2.31x10^{-4}\ g\ Pt}\ x\ \frac{1\ h}{60\ min}$$

$$k' = 5.41\ \frac{L}{g\ Pt.min}$$

$$k'' = \frac{k'W}{S}$$

$$\frac{W}{S} = \frac{4/3\pi R^3 \rho N}{4\pi R^2 N} = \frac{\rho R}{3}$$

$$Diameter = 3.0\ nm$$

$$\rho = density\ of\ Pt\ NPs = 21.45\ g/cm^3$$

$$\frac{W}{S} = \frac{\rho R}{3} = \frac{21.45\ g/cm^3 x (1.5x10^{-7} cm)}{3} x \frac{(100\ cm)^2}{1\ m^2} = 0.011 \frac{g\ Pt}{{m_{surf\ Pt}}^2}$$

$$k'' = \frac{k'W}{S} = 5.41\ \frac{L}{g\ Pt.min}\ x\ 0.011 \frac{g\ Pt}{{m_{surf\ Pt}}^2} = 0.06 \frac{L}{{m_{surf\ Pt}}^2.min}$$

Initial TOF (TOF_0) Calculation

$$\frac{-dC_{TCE}}{dt} = k_{meas} C_{TCE}$$

$$TOF_0 = \frac{initial\ rate}{[Pt]} = \frac{C_{TCE,0}}{[Pt]}\ x\ k_{meas}$$

$$k_{meas} = 0.15\ h^{-1}$$

$$C_{TCE,0} = 1000\ ppm$$

$$[Pt] = Molar\ concentration\ of\ Pt\ in\ the\ batch\ reactor$$

$$[Pt] = \frac{\frac{0.00577\ g\ Pt}{100\ mL} x\ 4\ mL\ x\ \frac{1\ mol}{195.084\ g\ Pt}}{0.510\ L} = \frac{2.32x10^{-6} mol\ Pt}{L}$$

$$TOF_0 = \frac{\frac{1000\ mg\ TCE}{L}\ x\ \frac{1\ mol\ TCE}{131.4\ g\ TCE}\ x\ \frac{1\ g}{1000\ mg}}{\frac{2.32x10^{-6} mol\ Pt}{L}}\ x\ \frac{0.15}{h}\ x\ \frac{1\ h}{3600\ s}$$

$$TOF_0 = 0.13\ \frac{mol\ TCE}{mol\ Pt.s}$$

Particle Size 2 (Medium-5.8 nm):

$$Slope = k_d = 0.08\ h^{-1}$$

$$From\ a = exp(-k_d t)\ equation, a\ can\ be\ found\ with\ respect\ to\ time.$$

$$Intercept = ln\left(\frac{k'W/V}{k_d}\right) = -0.4415$$

$$\frac{k'W/V}{k_d} = 0.643$$

$$k = k'W/V = 0.05\ h^{-1}$$

$$k' = \frac{kV}{W}$$

$$V = Volume\ of\ fluid = 0.510\ L$$

$$W = mass\ of\ solid$$

There is 0.00577 g Pt in 100 mL of colloidal sol. We add 4 mL of this solution to reactor during HDC reaction.

$$W = \frac{0.00577\ g\ Pt}{100\ mL}\ x\ 4\ mL = 2.31x10^{-4}\ g\ Pt$$

$$k' = \frac{kV}{W} = \frac{0.05\ h^{-1}\ x\ 0.510\ L}{2.31x10^{-4}\ g\ Pt}\ x\ \frac{1\ h}{60\ min}$$

$$k' = 1.95\ \frac{L}{g\ Pt.min}$$

$$k'' = \frac{k'W}{S}$$

$$\frac{W}{S} = \frac{4/3\pi R^3 \rho N}{4\pi R^2 N} = \frac{\rho R}{3}$$

$$Diameter = 5.8\ nm$$

$$\rho = density\ of\ Pt\ NPs = 21.45\ g/cm^3$$

$$\frac{W}{S} = \frac{\rho R}{3} = \frac{21.45\ g/cm^3 x (2.9x10^{-7} cm)}{3} x \frac{(100\ cm)^2}{1\ m^2} = 0.021\ \frac{g\ Pt}{{m_{surf\ Pt}}^2}$$

$$k'' = \frac{k'W}{S} = 1.95\ \frac{L}{g\ Pt.min}\ x\ 0.021 \frac{g\ Pt}{{m_{surf\ Pt}}^2} = 0.04\ \frac{L}{{m_{surf\ Pt}}^2.min}$$

Initial TOF (TOF_0) Calculation

$$\frac{-dC_{TCE}}{dt} = k_{meas} C_{TCE}$$

$$TOF_0 = \frac{initial\ rate}{[Pt]} = \frac{C_{TCE,0}}{[Pt]}\ x\ k_{meas}$$

$$k_{meas} = 0.05\ h^{-1}$$

$$C_{TCE,0} = 1000\ ppm$$

$$[Pt] = Molar\ concentration\ of\ Pt\ in\ the\ batch\ reactor$$

$$[Pt] = \frac{\frac{0.00577\ g\ Pt}{100\ mL} x\ 4\ mL\ x\ \frac{1\ mol}{195.084\ g\ Pt}}{0.510\ L} = \frac{2.32x10^{-6} mol\ Pt}{L}$$

$$TOF_0 = \frac{\frac{1000\ mg\ TCE}{L}\ x\ \frac{1\ mol\ TCE}{131.4\ g\ TCE}\ x\ \frac{1\ g}{1000\ mg}}{\frac{2.32x10^{-6} mol\ Pt}{L}}\ x\ \frac{0.05}{h}\ x\ \frac{1\ h}{3600\ s}$$

$$TOF_0 = 0.05\ \frac{mol\ TCE}{mol\ Pt.s}$$

Particle Size 3 (Large-60.9 nm):

$$Slope = k_d = 0.06\ h^{-1}$$

$$From\ a = exp(-k_d t)\ equation, a\ can\ be\ found\ with\ respect\ to\ time.$$

$$Intercept = ln\left(\frac{k'W/V}{k_d}\right) = -0.6419$$

$$\frac{k'W/V}{k_d} = 0.526$$

$$k = k'W/V = 0.03\ h^{-1}$$

$$k' = \frac{kV}{W}$$

$$V = Volume\ of\ fluid = 0.510\ L$$

$$W = mass\ of\ solid$$

There is 0.00577 g Pt in 100 mL of colloidal sol. We add 4 mL of this solution to reactor during HDC reaction.

$$W = \frac{0.00577\ g\ Pt}{100\ mL}\ x\ 4\ mL = 2.31x10^{-4}\ g\ Pt$$

$$k' = \frac{kV}{W} = \frac{0.034\ h^{-1}\ x\ 0.510\ L}{2.31x10^{-4}\ g\ Pt}\ x\frac{1\ h}{60\ min}$$

$$k' = 1.25\ \frac{L}{g\ Pt.min}$$

$$k'' = \frac{k'W}{S}$$

$$\frac{W}{S} = \frac{4/3\pi R^3 \rho N}{4\pi R^2 N} = \frac{\rho R}{3}$$

$$Diameter = 60.9\ nm$$

$$\rho = density\ of\ Pt\ NPs = 21.45\ g/cm^3$$

$$\frac{W}{S} = \frac{\rho R}{3} = \frac{21.45\ g/cm^3 x (30.5x10^{-7} cm)}{3} x \frac{(100\ cm)^2}{1\ m^2} = 0.218\ \frac{g\ Pt}{{m_{surf\ Pt}}^2}$$

$$k'' = \frac{k'W}{S} = 1.25\ \frac{L}{g\ Pt.min}\ x\ 0.218 \frac{g\ Pt}{{m_{surf\ Pt}}^2} = 0.27\ \frac{L}{{m_{surf\ Pt}}^2.min}$$

Initial TOF (TOF_0) Calculation

$$\frac{-dC_{TCE}}{dt} = k_{meas} C_{TCE}$$

$$TOF_0 = \frac{initial\ rate}{[Pt]} = \frac{C_{TCE,0}}{[Pt]}\ x\ k_{meas}$$

$$k_{meas} = 0.034\ h^{-1}$$

$$C_{TCE,0} = 1000\ ppm$$

$$[Pt] = Molar\ concentration\ of\ Pt\ in\ the\ batch\ reactor$$

$$[Pt] = \frac{\frac{0.00577\ g\ Pt}{100\ mL} x\ 4\ mL\ x\ \frac{1\ mol}{195.084\ g\ Pt}}{0.510\ L} = \frac{2.32x10^{-6} mol\ Pt}{L}$$

$$TOF_0 = \frac{\frac{1000\ mg\ TCE}{L}\ x\ \frac{1\ mol\ TCE}{131.4\ g\ TCE}\ x\ \frac{1\ g}{1000\ mg}}{\frac{2.32x10^{-6} mol\ Pt}{L}}\ x\ \frac{0.034}{h}\ x\ \frac{1\ h}{3600\ s}$$

$$TOF_0 = 0.03\ \frac{mol\ TCE}{mol\ Pt.s}$$